ANALYSIS OF ELECTROPHORESIS PERFORMANCE

Final Report
RAI-88-EL2-4

Period Covered: 2/21/85 - 6/30/88

Contract: NAS8-36042

Prepared for:

George C. Marshall Space Flight Center

MSFC, AL 35812

Prepared by:

Glyn O. Roberts

Date: 6/30/88

Roberts Associates, Incorporated

1729 Pine Valley Drive

Vienna, VA 22180

TABLE OF CONTENTS

LIST OF FIGURES

LIST OF TABLES

SUMMARY

We are developing a flexible efficient computer code to simulate electrophoretic separation phenomena, in either a cylindrical or a rectangular geometry. The code will compute the evolution in time (or in distance down a separation chamber) of the concentrations of an arbitrary number of chemical species, and of the temperature, pH distribution, conductivity, electric field, and fluid motion. Use of nonuniform meshes and fast accurate implicit time-stepping will yield accurate answers at economical cost.

The biggest problem in recent space and ground tests of free-flow electrophoresis separation equipment has been excessive sample spreading in the field direction, and consequent loss of resolution. Prior theories attributed the spreading (in space experiments where gravity could not be blamed) to two crescent-forming effects:

increased residence time near the walls; and

the electroosmosis flow in the chamber driven by the slip velocity at the walls.

But the observed spreading is too great for this explanation, unless the sample is first spread towards the walls by some other effect.

Using the model in its rectangular-geometry mode, we sought to explain the observed results as due to a combination of three additional effects:

electrokinetic spreading;

sample spreading towards the wall along diverging field lines associated with the non-uniform conductivity; and

sample spreading towards the walls due to the transverse flows associated with the nonuniform wall slip velocity produced by field variations.

The model runs were successful, and confirmed the significance of the phenomena, but the effects were still too small to explain the observations.

We therefore reached the conclusion that the effect was caused by electric and dielectric body forces. The suggestion has been confirmed by preliminary analysis and experiments.

We are now including such forces in the computer model, under a separate contract. We will develop experimental parameters for a definitive analysis of electrohydrodynamic phenomena in electrophoresis, and for their accurate simulation in the model. This will require carefully chosen experiments, to isolate the phenomena and their relative magnitude. Once this has been done, an upgraded code can be applied in the determination of designs and parameters for successful operational separation processes.

In summary, electrophoretic purification of biochemical products is likely to be the first major commercial application of the zero-gravity environment of space. Terrestrial and space experiments and model simulations have shown significant problems due to electrokinetic and electrohydrodynamic phenomena. The code will be a significant factor in overcoming these problems, and in the design and operation of commercial separation devices.

Chapter 1
BACKGROUND

Electrophoretic separation exploits the varying electrokinetic mobilities of different species in aqueous solution, as a function of the pH (or acidity). There are two techniques important for bulk free-flow separation.

1. In zone electrophoresis, the sample is injected into a uniform buffer of fixed pH, and the components separate in the direction of the electric field.

2. In isoelectric focusing, a mixture of ampholytes is electrolyzed, establishing a pH gradient in which the ampholytes (including the proteins and other substances of interest) focus at their isoelectric point (where the mean ionization and mobility become zero.

For diagnostic separations, gels and porous films are used, in order to eliminate undesired flows. There is still a flow through the porous medium due to electroosmosis (see below), unless it is canceled by the flow due to a pressure gradient.

For bulk separations, continuous flow devices have been developed, using both principles (zone electrophoresis and isoelectric focusing). In continuous flow electrophoresis (CFE), a uniform buffer flows between parallel plates, and an electric field is applied in the transverse direction. A mixture is injected into the center of the gap, and the components separate and are withdrawn through collection ports at the end of the chamber. In recirculating isoelectric focusing (RIEF), all the components are continuously withdrawn at one end of the chamber, and recycled to the other end, until the desired product is sufficiently pure in the appropriate collection port.

These free-flow devices allow large throughput. But their operation is hindered by undesired flow components. For example, there are flows driven by terrestrial gravity, since density differences due to concentration and temperature (from ohmic heating) cause undesired convection currents. Also in cell analyses the cells themselves settle under gravity. This is the reason for NASA's involvement in electrophoresis.

1.1 HYDRODYNAMICS

The flow field and pressure distribution in free-flow electrophoresis are determined by a balance of the following effects,

external boundary conditions on the flow or pressure,
viscosity,
momentum (normally a weak effect),
convection, due to horizontal variations in density,
wall electroosmosis,
electric field body force on the mean charge density,
dielectric body force.

Ideally, the flow would be a simple balance between the imposed pressure gradient and viscosity, implying a Poiseuille flow profile in a separation chamber. This profile is modified by the other effects. The more significant of these effects are discussed below.

1.1.1 Convection

Horizontal density gradients, caused either by temperature differences due to ohmic heating or by variations in the concentrations, lead to convection currents. Such currents are negligible in space. They can normally be kept down to manageable levels in the laboratory by efficient cooling at the sides and by using small dimensions (which unfortunately decreases throughput).

Ellerbroek and Kolin (1979), Rhodes and Snyder (1981, 1982), Saville (1978), and Lynch and Saville (1981) have studied convection models for continuous flow electrophoresis chambers. These computations used simplified models for the ohmic heating. McDonnell Douglas Astronautics Corporation has a similar hydrodynamic model (Richman, 1984).

For convection due to heating, the rate of heating is proportional to the square of the applied field, and to the conductivity. The separation rate is typically proportional to the field and to the conductivity. Decreasing the concentration of the buffer does not help, because the sample concentration must generally be decreased in proportion.

1.1.2 Wall Electroosmosis

Wall electroosmosis is caused by charge separation at the wall. The solid becomes charged, usually negatively, by the passage of ions into solution. The solution becomes positively charged in a thin layer against the wall, called the Debye layer. Its thickness L is of order microns or less, depending inversely on the square root of the ion concentration in the fluid. The charge Q per unit area, and the so-called zeta potential QL/k (where k is the dielectric constant), depend on the materials, the temperature, and the pH.

When a tangential electric field is applied, the force on the ions in the fluid results in motion through the fluid, and the species migrate as the current passes. In the fluid interior, charge neutrality prevails, so there is no net electric force on the fluid. In the Debye layer there is a large net electric force on the fluid, producing motion. The force is balanced by the viscous stresses associated with the motion.

The net effect outside the infinitesimally thin Debye layer is a slip velocity

$$\underline{U} = \underline{E}QL/\mu .$$

Here $\underline{E}$ is the electric field, L is the Debye layer thickness described above, and μ is the viscosity. The stress $\underline{E}Q$ is balanced by the viscous stress $-\mu\underline{U}/L$ at the wall. Like the rate of separation, electroosmosis is linear in the applied field.

In a plane-walled separation chamber, the flow field distribution resulting from this slip velocity is a superposed Poiseuille flow profile in the opposite direction. A pressure gradient is established to maintain this flow.

Wall electroosmosis can be effectively eliminated by the use of gels or by using a sugar solution with a strong vertical density gradient. These methods restrict the separation throughput. It can be controlled by the use of micropore screens. Wall baffles and special coatings have also been tested. Percy Rhodes of MSFC has suggested the use of separation cells with moving boundaries, to cancel the electroosmosis and to give a uniform flow profile along the chamber.

Dewey and Graham (1983) (under the guidance of Saville) computed the flow driven by wall electroosmosis in a segmented tube. Roberts (1984a) generalized their computation to include the effects of rotation.

1.1.3 Electric Field Body Force on the Mean Charge Density

The electric force on the charged ions causes them to move steadily through the water against the viscous drag. If the mean charge density is not zero, there is a net force on the fluid. The mean charge density is always negligible compared with its positive and negative components, but the body force may not be negligible. The body force density can be written, using electrostatic units, as

$$\underline{E}q = \sigma\underline{E}[\underline{E}.\nabla(k/4\pi\sigma)] ,$$

where q is the charge density, k is the dielectric constant, and σ is the conductivity. Thus the force is significant when there are sharp variations of the conductivity or the dielectric constant in the direction of the field. Note that the effect is quadratic in the applied field, so that its relative importance compared with the rate of separation can be reduced by reducing the field.

1.1.4 Dielectric Body Force

Water has a high dielectric constant of about 80. This reflects the polarization of the molecules into dipoles by an electric field. If the field is not uniform, there is a resulting body force distribution. Physically, the two ends of the dipole are at locations with differing fields, and thus experience different forces. The Geophysical Fluid Flow Cell (GFFC) in Spacelab 3 used this effect in silicone oil, and so does NASA's planned Atmospheric General Circulation Experiment (AGCE).

If the dielectric constant of the fluid does not vary with position, then the dielectric body force can be expressed as the gradient of a scalar, and can therefore be canceled out by a pressure gradient. Variations in the dielectric constant with temperature or with concentrations may therefore play an important role. The dielectric constant is reduced by the presence of ions.

This effect is also proportional to the square of the applied field.

1.2 ELECTROKINETICS

Electrokinetics is concerned with the evolution of the concentration and the degree of ionization of each species, together with the pH and conductivity, as the ions move in response to an electric field.

For low concentrations of sample species in a uniform buffer of relatively high concentration, the conductivity and field strength remain uniform, so do the pH and degree of ionization, and species of differing mobilities separate in the field direction in a straightforward manner.

However, useful separation devices require higher concentrations, and the phenomena involved are more complicated. The changes in pH and conductivity with the local concentrations lead to variations in the degrees of ionization and in the local field strength.

With samples including significant concentrations of large protein molecules, a phenomenon analogous to electrodialysis results in the establishment of a region of low conductivity on the side of the sample toward which the protein ions are migrating, and in a high conductivity region on the other side, as the different concentration distributions evolve in time.

The coupled equations describing these phenomena are strongly nonlinear and not amenable to analytic solution. Numerical models are the only practical method of study. The models need only operate in one spatial dimension, plus time, to clarify the main phenomena.

Bier et al. (1983) and Roberts (1984b) independently developed electrokinetic models, which predict the evolution of the species concentrations, the pH distribution, and the conductivity and current and field distributions. Bier's one-dimensional code was applied to seven cases, involving zone electrophoresis, moving boundary electrophoresis, isotachophoresis, isoelectric focusing, and electrodialysis. Our code was two-dimensional (with one dimension as an option depending on parameter input at compilation); it is now being upgraded to allow the option of three dimensions, with a Cartesian or cylindrical geometry. Using the one-dimensional capability, we reproduced Bier's results. Our code differs from Bier's in the following respects:

Bier confines attention to single ionizations, and cannot handle proteins;

Bier computes fluxes of each ion separately instead of averaging over the degrees of ionization;

Bier neglects bulk fluid motion;

Bier is currently limited to five species; and

We use fast implicit methods and flexible nonuniform meshes.

Further details of our own SAMPLE code are given below.

1.3 The SAMPLE Code

Our report (1984b) described the current status of the code. Many modifications have been made since then, under other programs and in this program (Roberts, 1985, 1986, Rhodes et al., 1988), and more are planned.

Briefly, the code computes the evolution in time (or distance down a continuous flow electrophoresis chamber or recirculating isoelectric focusing chamber) of the concentrations of N species such as hemoglobin, sulfate, sodium, phosphate, histidine or ammonium. There are six stages in each time step:

1. Get the pH distribution from charge neutrality, using appropriate models for the mean ionization of each species as a function of pH, and including hydrogen and hydroxyl ions.

2. Get the conductivity distribution by adding the species contributions, and get the ion diffusion potential.

3. Solve a Poisson-like equation for the current distribution and voltage distribution, using charge continuity.

4. Get the flow field from a simplified model of the hydrodynamics. Current options are
   no motion,

   uniform Poiseuille flow down a chamber,

   electroosmosis slip profile in the direction of the local field at the wall, and proportional to the field, and with a flow in the thickness direction determined by the divergence of the electroosmosis flow, and

   added flow components due to moving walls, as in the planned apparatus of Rhodes (1985).

   In addition, a full electrohydrodynamic model has been implemented in two dimensions, as part of a separate continuing contract.

5. Get the species fluxes, adding contributions from the mean flow, electric field, and diffusion.

6. Update the concentrations of the N species, using the flux divergence.

The code has been validated using pH and conductivity measurements, and using analytic solutions for the dispersion of low-concentration samples. It has been used to reproduce the seven sets of one-dimensional results reported by Bier et al. (1983), and to simulate two series of cellulose acetate experiments performed with hemoglobin in a barbital buffer at MSFC in 1983 and 1984 (Roberts, 1985, Rhodes et al., 1988). It has also been used to simulate low-concentration CFE with uniform electroosmosis; the results agree with analytic results. Finally, our simulations of electroosmosis effects on isoelectric focusing in two dimensions were reported by Roberts (1984c,d).

This is a powerful tool with great flexibility in simulating a wide range of situations. Prior applications include:

steady three-dimensional continuous flow electrophoresis solutions;

steady three-dimensional moving-wall continuous flow electrophoresis solutions;

steady two-dimensional moving-wall continuous flow electrophoresis solutions;

time-dependent two-dimensional channel electrophoresis;

time-dependent two-dimensional channel isoelectric focusing with uniform electroosmosis;

time-dependent two-dimensional acetate film experiments;

time-dependent one-dimensional acetate film experiments;

time-dependent one-dimensional isotachophoresis; and

time-dependent one-dimensional moving boundary electrophoresis.

However, in its form as used for this contract, the code had the following limitations.

1. Salts were neglected. Thus sodium sulfate and hemoglobin barbiturate do not occur either as molecules or ions. There is no chemistry apart from simple reactions with water and hydrogen and hydroxyl ions. For many situations this is a good approximation. Eliminating this limitation would be a major undertaking, and we have no such plans at present.

2. Activity effects were neglected. In reality, each ion is statistically surrounded by a Debye cloud of ions with opposite charge, with radius of order the Debye thickness. This cloud modifies the ion motion and thus also the conductivity. We plan to implement an activity effects formulation in the near future.

3. Temperature effects were neglected. They include variations in the ionizations, the diffusivities, the conductivities, the viscosity, the buoyancy (if gravity is present), the electroosmosis, and the activity. Our long-term plans include temperature effects modeling.

4. The hydrodynamics was oversimplified, as described above, and was inadequate to explain some of the observed phenomena. Electrohydrodynamic effects play a dominant role in many situations, and are included in the new version of the model under current development.

5. Time-dependent three-dimensional cases are excluded, although such phenomena are frequently observed in electrophoresis. This deficiency is being addressed under the separate program.

The appendix summarizes the equations and numerical methods as used in the SAMPLE code for this contract.

Chapter 2
PROGRAM RESULTS

2.1 OBJECTIVES

The main objective of this program was to analyze and model the sample spreading phenomena which are observed in laboratory and space-based electrophoresis, and which have not been previously explained. The success of future tests depends on a better understanding of these phenomena. This required analytic studies, model development, model studies, and parallel laboratory studies.

2.2 TASKS

The program required us to upgrade the computer model, to apply it to experiments chosen to validate the electrokinetics, and to apply it to cases where electroosmosis is significant. Support of critical validation experiments performed at MSFC was also required.

We have implemented all the planned code upgrades except for activity effects. These do not seem to play a dominant role, at any practical concentration.

We supported a series of porous medium experiments in acetate film, for model and code electrokinetics validation, in the absence of flow effects.

Our electrokinetic validations were successful. We were able to reproduce the experimental observations of sample spreading in the experiments. The effect was due to the non-uniformity of the conductivity, pH, and current, caused by the presence of the protein sample. The generation of large conductivity variations by the presence of the protein is an effect which was first noticed in the numerical results, and which we have since explained theoretically and confirmed experimentally. The phenomenon is analogous to electrodialysis and results in the establishment of a region of low conductivity on the side of the sample toward which the protein ions are migrating, and in a high conductivity region on the other side, as the different concentration distributions evolve in time.

Our simulations of free-flow electrophoresis failed to reproduce the spreading observed in prior laboratory and space experiments. We obtained spreading effects, due both to the electrokinetic effects and to circulating flows driven by variations in the electroosmotic slip velocity. But the effects were much less than in experiments performed by ourselves and others, including experiments in space. In many of these experiments, dramatic spreading is seen as soon as the sample leaves the nozzle, much more rapid than in our simulations.

We have now demonstrated theoretically, experimentally, and numerically that the spreading is caused by electrohydrodynamic effects, as described in Chapter 1. Only the early experimental and analytic work in this area was done under this program, and the results reported below inevitably reflect the later work.

2.3 EXPERIMENTAL VALIDATIONS ON ACETATE FILM

The experiments on acetate film had three objectives. First, we wanted to eliminate free-flow effects by using a porous medium. Secondly, we wished to visualize two-dimensional spreading along diverging field lines. Thirdly, the experiments provided an experimental validation of our electrokinetic model and of its representation in the code.

The experiments were done at Marshall Space Flight Center, by Percy Rhodes and other NASA personnel, with our support.

The acetate film medium consists of flexible sheets of clear plastic with dimensions 7.5cm x 2.5cm, coated on one side with porous cellulose acetate of uniform thickness about 0.2mm. It is sold commercially for quick diagnostic electrophoresis, in which the film is soaked in buffer and set up lengthwise as the connection between baths of buffer containing the platinum electrodes. In those tests, the sample is applied as a straight line across the film, and separates under the action of the field into a series of parallel stripes.

For our tests, we used a barbital buffer (sodium barbiturate and barbituric acid) with a pH of 8.55, at two dilutions, and we used samples consisting of either 8.8% or 1.8% hemoglobin, in the same barbital buffer at different concentrations. The sample was applied to the buffer-moistened film through a syringe, and formed a circle as it spread under the action of surface tension. The field was then turned on, and the spreading of the hemoglobin was observed and photographed. The visual observations and photographs were satisfactory; but for the photographs reproduced below, duplicate experiments were stopped at different times, and the films were removed and the protein fixed and stained by conventional techniques.

The circular initial shape is a natural analog of the circular cross section of the sample filament flowing from an orifice into a continuous-flow electrophoresis chamber. Electrohydrodynamics and normal wall electroosmosis are of course eliminated by the porous medium, and there is no analog of the larger residence time in the chamber experienced by fluid near the walls in CFE. There is electroosmosis in the pores of the porous medium, resulting in what is essentially a plug flow in the field direction. This flow was observed by the motion of the samples with the highest conductivities (which had the least motion of their own), and by the inferred motion of the buffer components in cases where the electrokinetics does not cause motion.

In earlier experiments, visual and photographic observation of the hemoglobin was the only measurement made. Later, we made a grid of 40 fine platinum wire electrodes, projecting about a millimeter from a rigid plastic support, in an 8 x 5 rectangle with a spacing of 2mm (80 mil). This was used to make voltage measurements on the acetate film at successive times during the experiments. The digital voltmeter was switched between the electrodes under computer control. A small bias voltage was used to ensure that every voltage read was more than 2 volts, so that the electrode effect (depending on the current direction) was the same for each electrode. The voltage measurements could then be plotted, and compared with model predictions. These plots were difficult to make and not highly reproducible. There were differences depending on the sign of the bias, and on the quality of the electrical connections between the electrodes and the buffer in the cellulose acetate film.

We did a large number of experiments with this system, since they were easy to perform. In particular, we performed a series of eight definitive runs, with a wide range of relative concentrations of barbital in the buffer and sample, and of hemoglobin in the sample. These eight experiments are summarized in Table 1.

Sample ID	VI	VII	V	III
σ (μmho/cm)	4500	195	206	420
pH	8.4	7.3	7.5	7.6
Hemoglobin %	1.8	8.8	1.8	8.8
Experiment Number				
Buffer σ 160 μmho/cm	1	2	3	4
Buffer σ 454 μmho/cm	5	6	7	8

Table 1. Experimental Parameters for Eight Acetate Film Experiments

The experimental parameters were chosen to illustrate problem conditions, with either large initial conductivity contrasts or relative protein concentrations sufficiently high to cause such contrasts through the electrokinetics. We had previously found that the protein moved uniformly in response to the field when the initial conductivities were matched and the relative protein concentration was low. Sample VI has a very high conductivity, due to large concentrations of the buffer components, and its pH and conductivity are hardly modified at all by the relatively small amount of added hemoglobin. The other samples have lower conductivities, and the hemoglobin plays a significant role.

Figure 1 shows photographs of the hemoglobin distribution for experiment 5, after times of 1, 2, 3 and 4 minutes. For this case, the sample conductivity was relatively high (4500 μmho/cm), with a buffer conductivity of 454 μmho/cm. The hemoglobin concentration was 1.8%, which decreased the pH of the sample only a little, to 8.4. Thus to a first approximation, the electrokinetics was simple, with the hemoglobin passive, and the sodium and barbiturate concentrations changing only through diffusion. The mean field as in all the experiments is 20 V/cm to the left, so the negatively charged hemoglobin moves to the right. The hemoglobin moves slowly in the circle of concentrated sodium and barbiturate which was introduced with the hemoglobin (high conductivity, low field), and moves much faster once it escapes to the lower conductivity and larger field of the buffer. The result is a discontinuity in hemoglobin concentration at the circular edge of the high-conductivity region, visible in the photographs. The hemoglobin "bleeds" out of this circle.

Figure 2 is the corresponding experimental voltage plot, after an experimental time of 4 minutes. The high-conductivity region is visible as the low-field region where the equipotential lines have a wide separation.

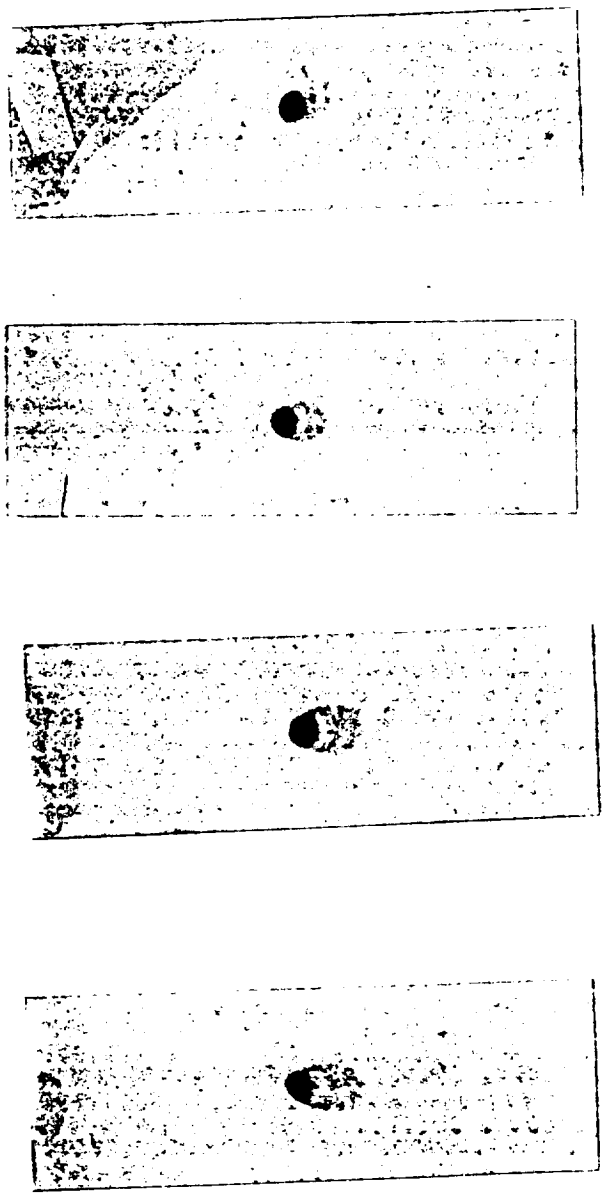

Figure 1. Experimental Hemoglobin Distributions for Case 5. The times are 1, 2, 3 and 4 minutes. The field of 20 V/cm is to the left. The sample-buffer conductivity ratio is 10. The hemoglobin concentration is sufficiently low that it is roughly passive. See the text.

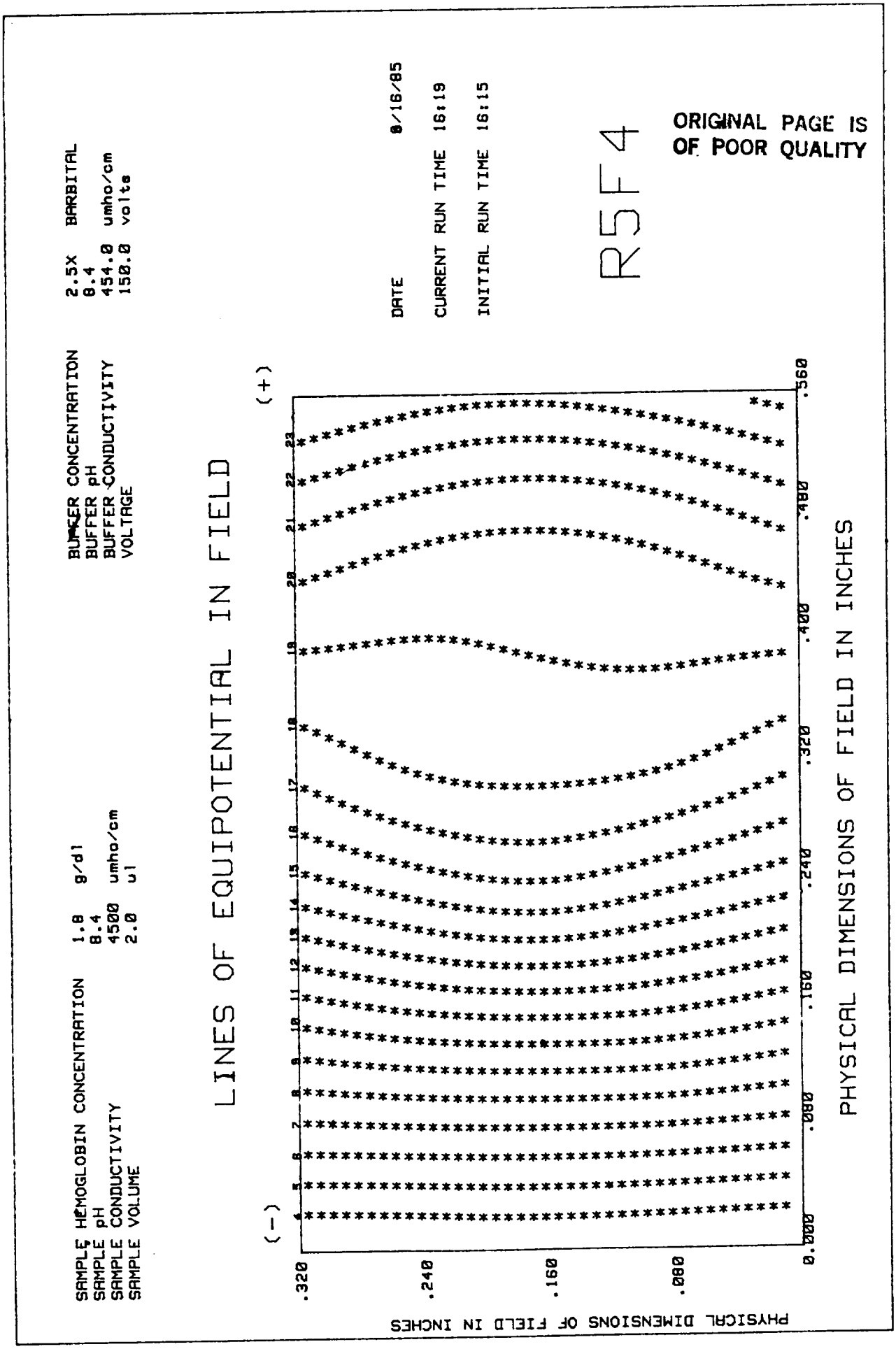

Figure 2. Voltage measurements at 4 Minutes for Case 5

2.4 ELECTROKINETIC AND DIVERGING-FIELD SAMPLE SPREADING

We have used our SAMPLE computer model to perform a very large number of simulations related to the cellulose acetate film experiments. The four objectives of these simulations were to validate the code and its equations and algorithms, to further optimize the algorithms, to improve our understanding of the electrokinetics, and to provide a basis for interpreting the experimental results.

In particular, we performed definitive simulations of the eight experimental cases described above. For Case 1, we performed simulations using meshes of 40x10, 80x20, and 160x40 mesh points, in order to demonstrate convergence of the results with increasing spatial resolution. We performed similar tests of the time resolution.

Figure 3 shows the second of three pages of input data for Case 1. The first page computes 20 seconds of diffusion from the analytic initial condition representing the newly-applied sample. The second page covers 360 seconds of simulation with an applied field, while the third page covers a further 180 seconds (for a total of 9 minutes with the field applied). In the figure, there are three groups of parameters, defining the problem, the method, and the output options. The text on the top line in Figure 3 is copied to the plots and other output, for identification.

The first group of problem parameters define the domain and nonuniform mesh, the sample and field, and the other quantities indicated. The second group are concerned with the three species, giving their concentration in the buffer and sample and their ionization properties.

The method parameters control the numerical method for updating the species concentrations at each time step, together with the Poisson-type iteration for the electric field distribution corresponding to the computed conductivity distribution at each step. TSTEP is the time step in seconds. The other parameters will not be described in detail.

The output parameters in Figure 3 provide many options. ISEGR is 1, indicating a restart from data written to segment 1 of the direct access file by the computation based on the first page of data (20 seconds of diffusion before the field is turned on). ISEGW, IBEGDA, and IINCDA determine that the present state is written to the direct access file, segments 1, 2, 3 and 4, at steps 0, 240, 480, and 720. ZPLL, ZPLR, YPLB and YPLT are the left, right, bottom and top of the plotted region, cf. Figure 6. The plotted region is smaller than the computational domain. Printer plots of the indicated variables in physical coordinates are produced at step 0 and then every 240 steps. The combination 0 -120 in the "PRINT NUMBERS" columns indicates that files are written to produce later superposed plots of the values of the indicated variables on the axis in the field direction, at 120 steps or one minute intervals. The "PLOTTER IDAOUT", "PHYSICAL" columns combination "1 1" indicates that those variable are to be plotted (in a separate run of the separate plot program) at every segment written to the direct access file.

CELLULOSE ACETATE 1/1.8(V1)/0.75X/20 ***PROBLEM PARAMETERS***

Z MESH		Y MESH		SAMPLE ELECTRIC FIELD		WATER MOBILITIES BOUNDARY FLOW		SIDE BOUNDARY CONDITIONS 1/2/3 FOR BUFFER/SAMPLE/NO-FLUX
ZBL =	-1.2000000	YT =	0.6000000	YSAMP =	0.0000000	UH =	0.0036000	ILEFT = 1
ZBR =	1.2000000	YB =	0.0000000	RSAMP =	0.1100000	UOH =	0.0020000	IRIGHT = 1
ZDL =	-0.0000000	DYRAT =	8.0000000	PSAMP =	-6.0000000	UWE =	0.0000000	LCOND = F
ZDR =	0.0000000	IY =	0	CZERO =	-100.0000000	WB =	0.0014000	
DZRAT =	6.0000000	YWALL =	100.0000000	EZERO =	-20.0000000	UB =	1.0000000	
		YMESH =	0.0800000					

SPECIES	BUFFER MOLARITY	SAMPLE MOLARITY	SINGLE ION MOBILITY	IONIZATION DEFINITION CONSTANTS N				N				N				N			
SODIUM	0.00190000	0.07600000	0.00052700	-3.00	1.00	0.00	0.00	0.00	0.00	0.00	0.00	0.00	0.00	0.00	0.00	0.00	0.00	0.00	0.00
BARBITURATE	0.00228000	0.09120000	0.00050000	-1.00	7.85	0.00	0.00	0.00	0.00	0.00	0.00	0.00	0.00	0.00	0.00	0.00	0.00	0.00	0.00
HEMOGLOBIN A	0.00000000	0.00026000	0.00001000	36.09	25.74	3.39	7.86	17.32	6.82	10.45	11.40	6.97	6.99	12.65	4.99	4.79			

METHOD PARAMETERS

SPECIES	TSTEP	UPWNDA	UPWNDC	FIXCZ	FIXCY	THZFX	BETDG	BETAO	BETAD	BETCO	BETCD
SODIUM	0.500	0.150	0.150	T	T	0.167	0.5	0.5	0.5	0.5	0.5
BARBITURATE	0.500	0.150	0.150	T	T	0.167	0.5	0.5	0.5	0.5	0.5
HEMOGLOBIN-A	0.500	0.150	0.150	T	T	0.167	0.5	0.5	0.5	0.5	0.5

NSTEP = 720 NPITER = 12 PEXTRP = 0.500

OUTPUT PARAMETERS

DIRECT ACCESS READ & WRITE SEGMENTS ISEGR = 1 ISEGW = 1
(0: ANALYTIC. -1: AFTER PRIOR CASE)
WRITE STEP BEGINNING & INCREMENT IBEGDA = 0 IINCDA = 240
ZPLL = -0.72 ZPLR = 0.93 YPLB = -0.48 YPLT = 0.48
DIAGNOSTIC FREQUENCY NDIAG = -1 CONTOUR LINES NCLP = 0 NCLI = 0
NCOPIES = 1

VARIABLE	ISTEP BEGIN & INCREMENT FOR PRINTER DIAGNOSTICS PHYSICAL		INTEGER		PRINT NUMBERS		RANGES FOR I AND K IB IE	II	KB	KE	KI	PLOTTER IDAOUT BEGIN & INCREMENT PHYSICAL		INTEGER		INCR
pH	0	240	9903	9904	0	-120	-2 251	1	2	2	-1	1	1	9915	9916	0.0
SIGMA	0	240	9903	9904	0	-120	-2 251	1	2	2	-1	1	1	9915	9916	0.0
PHI	0	240	9903	9904	0	-120	-2 251	1	2	2	-1	1	1	9915	9916	0.0
CURRENT	0	240	9903	9904	9905	9906	-2 251	1	2	2	-1	1	1	9915	9916	0.0
EZ	0	240	9903	9904	8905	8906	-2 251	1	2	2	-1	8913	9914	9915	9916	0.0
EY	0	240	9903	9904	8905	8906	-2 251	1	2	2	-1	8913	9914	9915	9916	0.0
IONDCP	9901	9901	9903	9904	9905	9906	-2 251	1	2	2	-1	9913	9914	9915	9916	0.0
PSI	9901	9901	9903	9904	8905	8906	-2 251	1	2	2	-1	9913	9914	9915	9916	0.0
SODIUM																
CONC	0	240	9903	9904	0	-120	-2 251	1	2	2	-1	1	1	9915	9916	0.0
MEAN ION	9901	9902	9903	9904	9905	9906	-2 251	1	2	2	-1	9913	9914	9915	9916	0.0
MEAN SQU	9901	9902	9903	9904	9905	9906	-2 251	1	2	2	-1	9913	9914	9915	9916	0.0
CHARGE	9901	9902	9903	9904	9905	9906	-2 251	1	2	2	-1	8913	9914	9915	9916	0.0
SIGMA	0	240	9903	9904	8905	8906	-2 251	1	2	2	-1	8913	8914	9915	9916	0.0
DCONC	0	240	9903	9904	8905	8906	-2 251	1	2	2	-1	8913	9914	9915	9916	0.0
VELOCITY	0	240	9903	9904	8905	8906	-2 251	1	2	2	-1	8913	9914	9915	9916	0.0
FLUX	0	240	9903	9904	8905	8906	-2 251	1	2	2	-1	1	1	9915	9916	0.0
BARBITURATE																
CONC	0	240	9903	9904	0	-120	-2 251	1	2	2	-1	1	1	9915	9916	0.0
MEAN ION	0	240	9903	9904	8905	8906	-2 251	1	2	2	-1	8913	9914	9915	9916	0.0
MEAN SQU	9901	9902	9903	9904	9905	9906	-2 251	1	2	2	-1	9913	9914	9915	9916	0.0
CHARGE	0	240	9903	9904	8905	8906	-2 251	1	2	2	-1	8913	9914	9915	9916	0.0
SIGMA	0	240	9903	9904	8905	8906	-2 251	1	2	2	-1	8913	8914	9915	9916	0.0
DCONC	0	240	9903	9904	8905	8906	-2 251	1	2	2	-1	8913	9914	9915	9916	0.0
VELOCITY	0	240	9903	9904	8905	8906	-2 251	1	2	2	-1	8913	9914	9915	9916	0.0
FLUX	0	240	9903	9904	8905	8906	-2 251	1	2	2	-1	1	1	9915	9916	0.0
HEMOGLOBIN A																
CONC	0	240	9903	9904	0	-120	-2 251	1	2	2	-1	1	1	9915	9916	0.0
MEAN ION	0	240	9903	9904	8905	8906	-2 251	1	2	2	-1	8913	9914	9915	9916	0.0
MEAN SQU	9901	9902	9903	9904	9905	9906	-2 251	1	2	2	-1	9913	9914	9915	9916	0.0
CHARGE	0	240	9903	9904	8905	8906	-2 251	1	2	2	-1	8913	9914	9915	9916	0.0
SIGMA	0	240	9903	9904	8905	8906	-2 251	1	2	2	-1	8913	8914	9915	9916	0.0
DCONC	0	240	9903	9904	8905	8906	-2 251	1	2	2	-1	8913	9914	9915	9916	0.0
VELOCITY	0	240	9903	9904	8905	8906	-2 251	1	2	2	-1	8913	9914	9915	9916	0.0
FLUX	0	240	9903	9904	8905	8906	-2 251	1	2	2	-1	8913	9914	9915	9916	0.0

Figure 3. Input Data for Case 1

Figure 4 shows these one-dimensional plots for the hemoglobin concentration, for Case 1, at one minute intervals. The check marks on the horizontal (z) axis are at interval of 0.4 cm. The pattern is shifted left by an imposed electroosmosis flow of 0.0007 cm/sec, or 0.042 cm/min. The initial hemoglobin distribution has a radius of 0.11 cm, and has smoothed edges to represent the effects of mixing during sample application. The 20 seconds of diffusion has negligible effect on the hemoglobin.

Figure 5 shows the corresponding plots for sodium, and the barbiturate concentration plots are very similar, with molar concentration 20% more than the sodium, at each point and time. The hemoglobin is approximately passive, its molarity is too low to change the sample pH. The electrokinetics does not modify the concentration in a two-component buffer with monovalent species, to a first approximation. Therefore these sodium plots represent pure diffusion, together with the effects of electroosmosis carrying the profiles to the left. The sodium molarity tends to its buffer value of 0.0019 at large distances (cf. Figure 3), and is slightly less to the right of its peaks.

Comparison of Figures 4 and 5 shows that the hemoglobin leaks ("bleeds") out to the right of the region of elevated sodium concentration, with a more or less fixed molarity of 10^{-5}, while the hemoglobin left within the elevated sodium region is progressively shifted to the extreme right of that region.

Figure 6 is a contour plot of the initial hemoglobin distribution (unchanged by 20 seconds of diffusion because of its low diffusivity. The initial distributions of sodium and barbiturate, prior to diffusion, look similar, but of course the value at infinity is not zero.

Figures 7 and 8 are contour plots of the hemoglobin and sodium molarities after 9 minutes. The sodium distribution is only minutely distorted from the circular diffusion solution. The far-field value is 0.0019, the maximum of 0.0259 is the lowest maximum in Figure 5. The hemoglobin contour plot in Figure 7 can be compared with the lowest curve in Figure 4. The large region on the right, with molarity about 10^{-5} is apparent. Comparison of Figure 7 and 8 (which have the same domain as Figure 6) shows that the hemoglobin peak has moved to the far right of the region of elevated sodium concentration and conductivity.

In Figure 7, the hemoglobin on the right has spread laterally from its initial distribution region. The cause of this phenomenon is seen in Figure 9, which is a plot of the current lines at time 2 minutes. The plots at other times are similar. The current lines diverge away from the high-conductivity sample region, and the hemoglobin ions move along the current lines in response to the electric field.

The physics of Case 1 is the same as that of Case 5, as shown in Figures 1 and 2. The hemoglobin in Figure 1 shows a sharp discontinuity between the value in the circular high-conductivity region and the value to the right. The hemoglobin is displaced to the right of the circular region, and the discontinuity is seen as a circle, especially at times 3 and 4 minutes. For Case 1, the concentration of the escaped hemoglobin is so low that it is hard to see in the photographs which correspond to Figure 1.

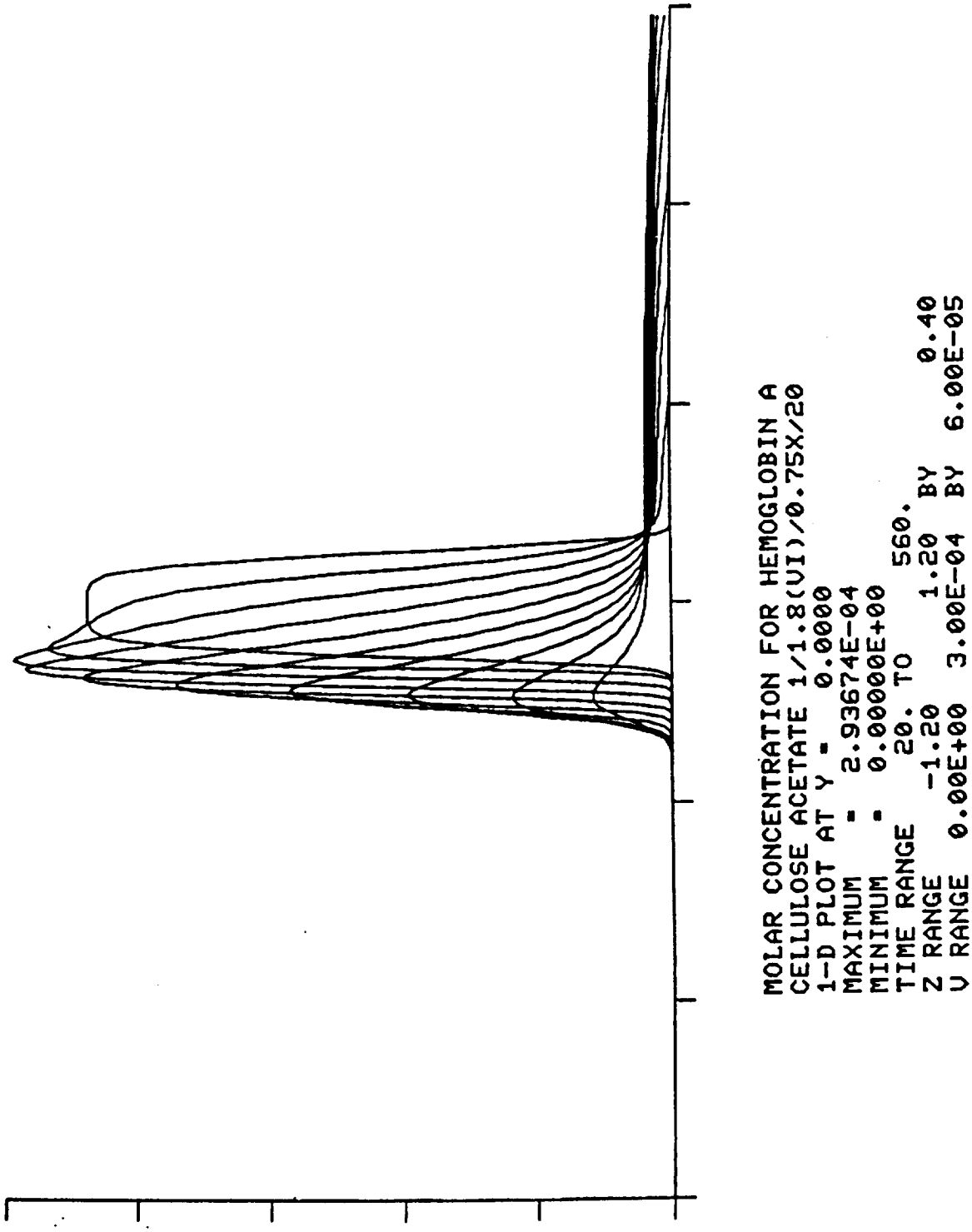

Figure 4. Axis Hemoglobin Molarity Plots every Minute for Case 1

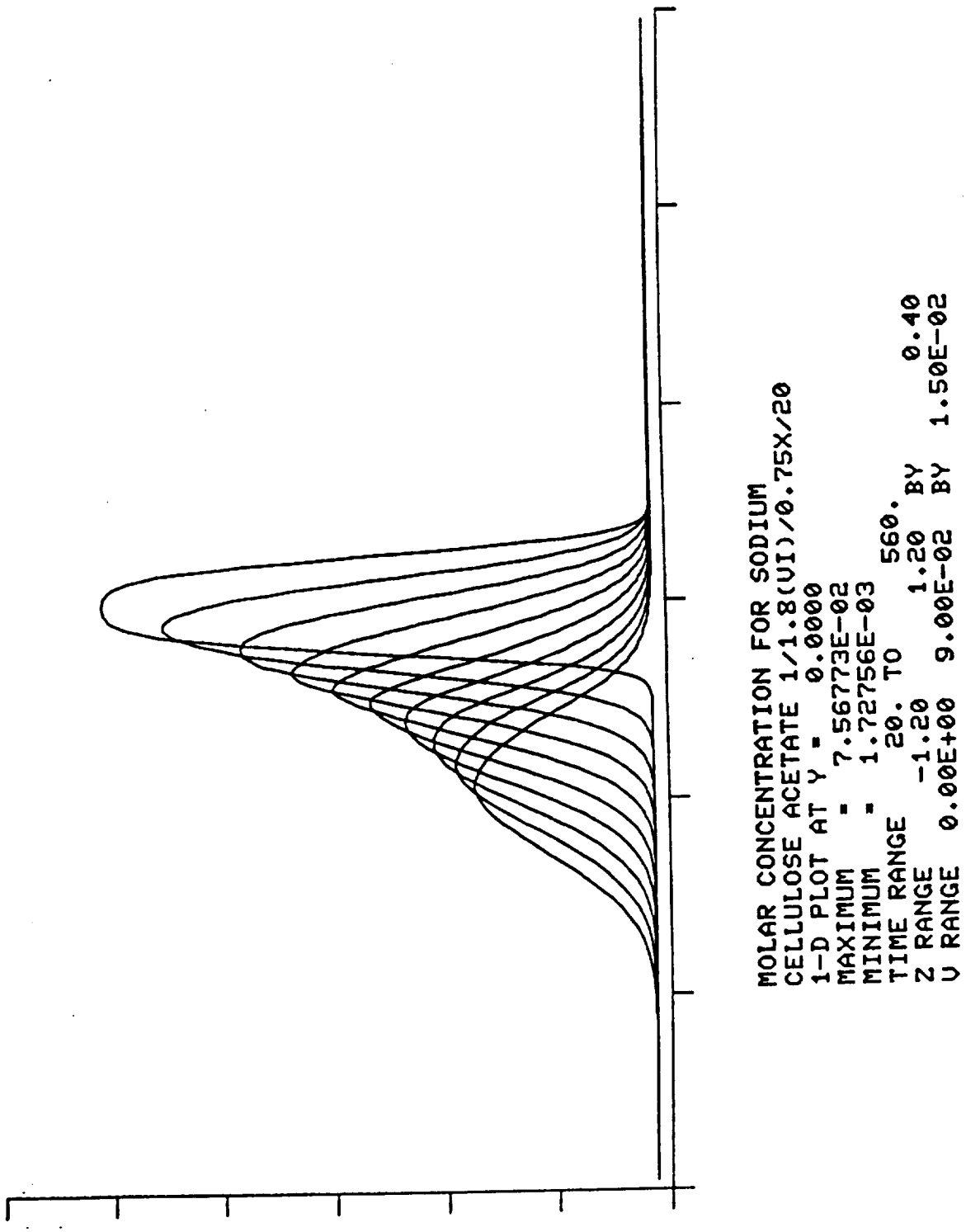

Figure 5. Axis Sodium Molarity Plots every Minute for Case 1

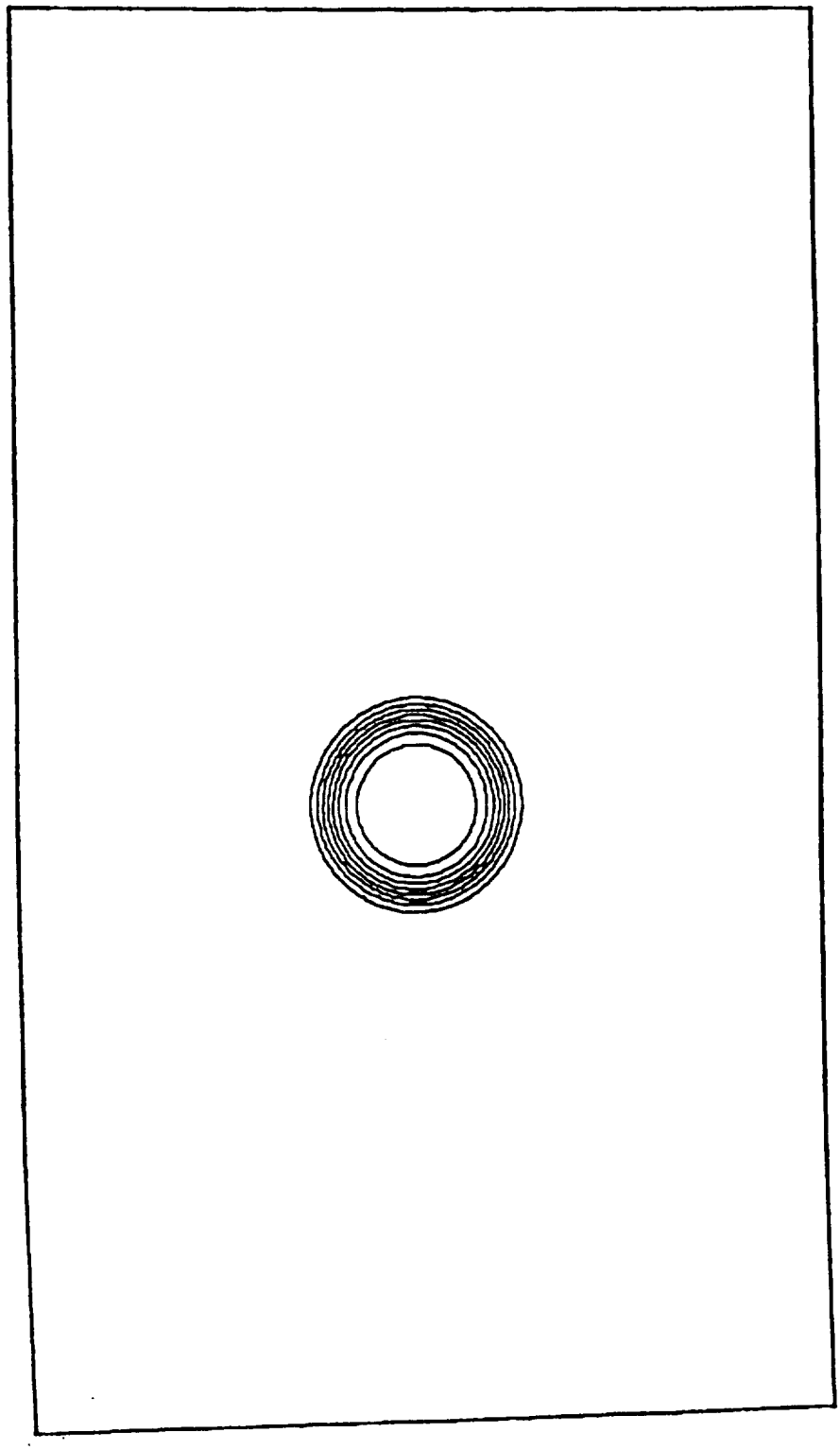

Figure 6. Contour Plot of Initial Hemoglobin Molarity for Case 1

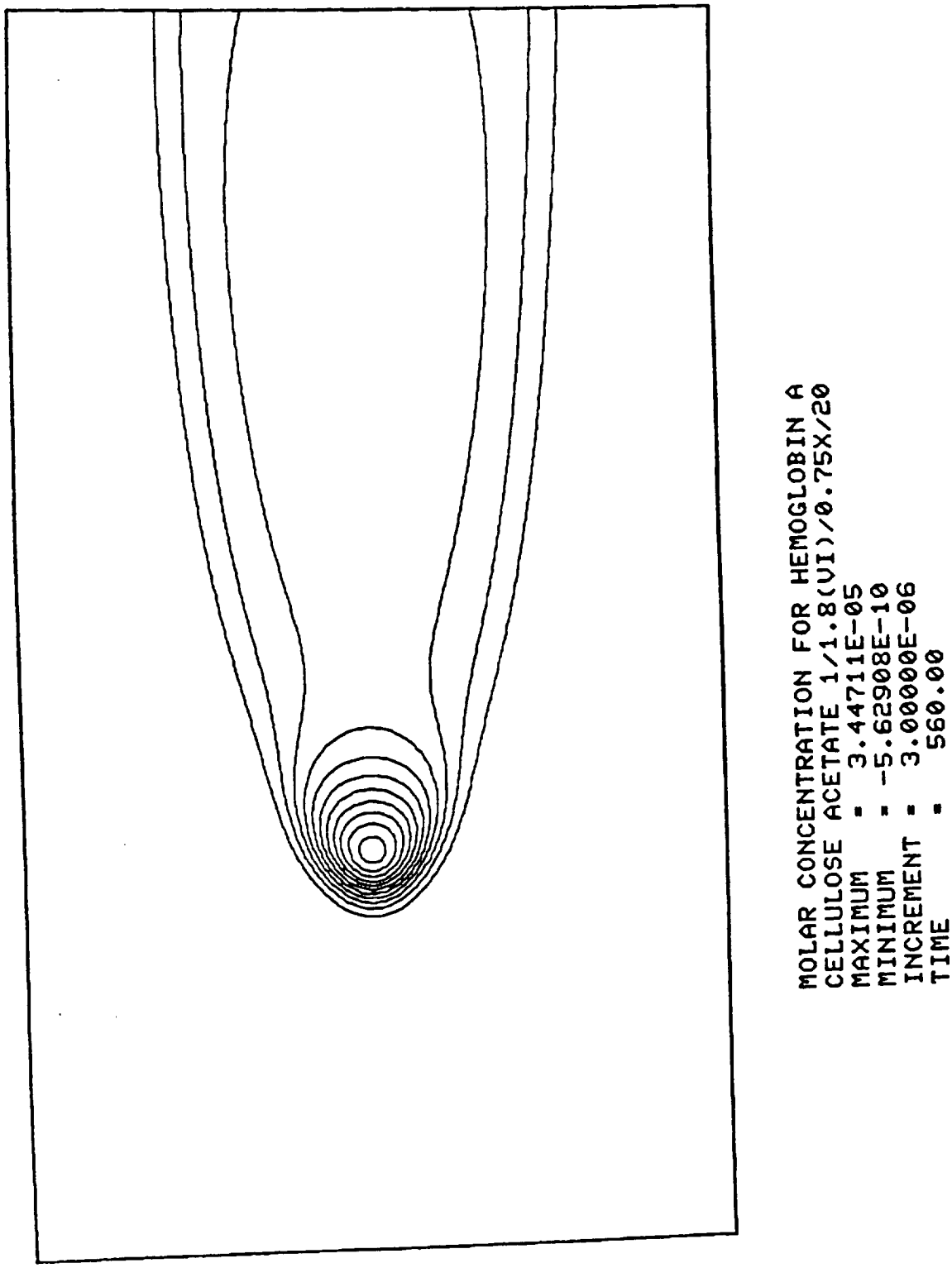

Figure 7. Contour Plot of Hemoglobin Molarity at 9 Minutes for Case 1

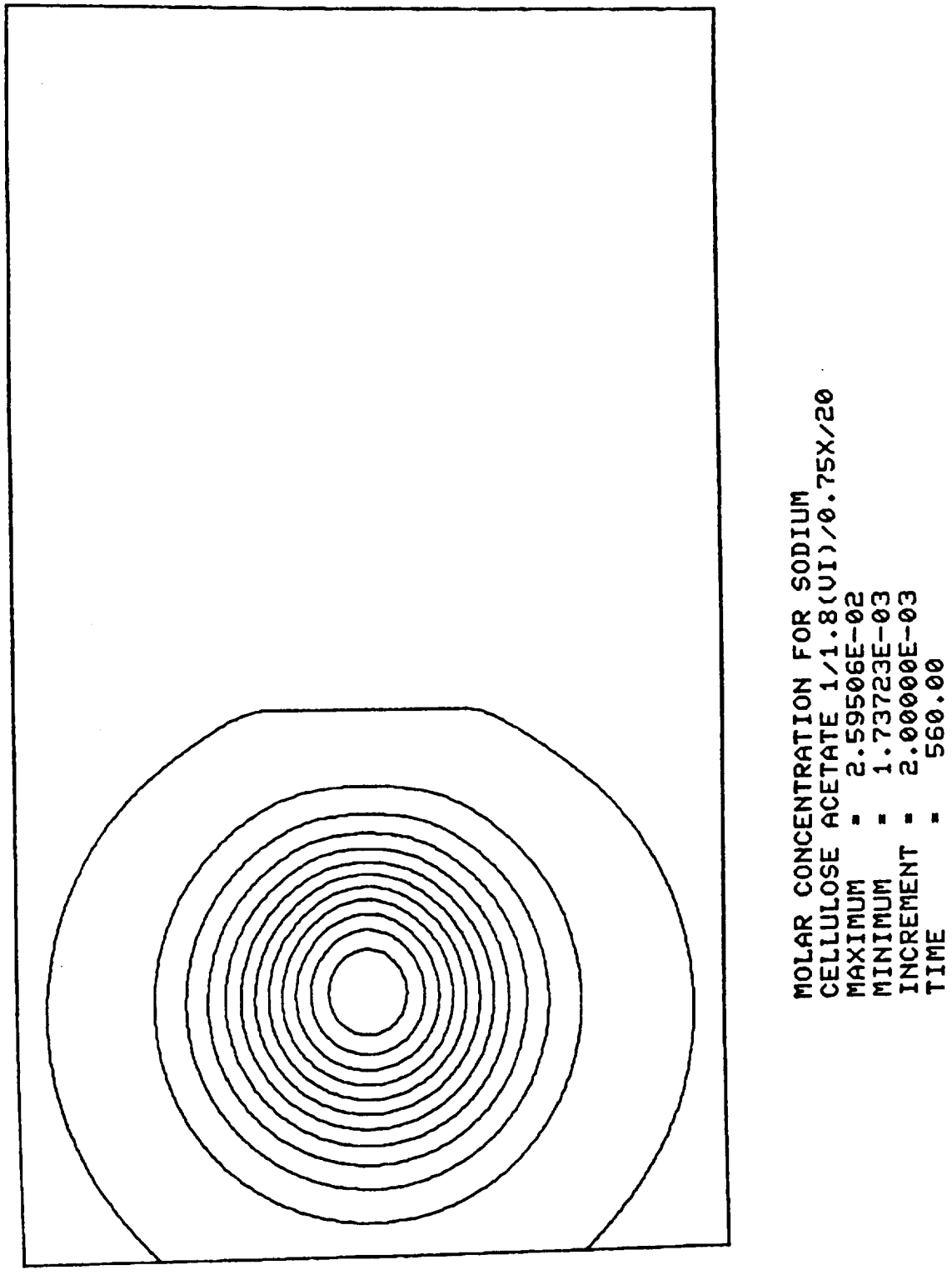

Figure 8. Contour Plot of Sodium Molarity at 9 Minutes for Case 1

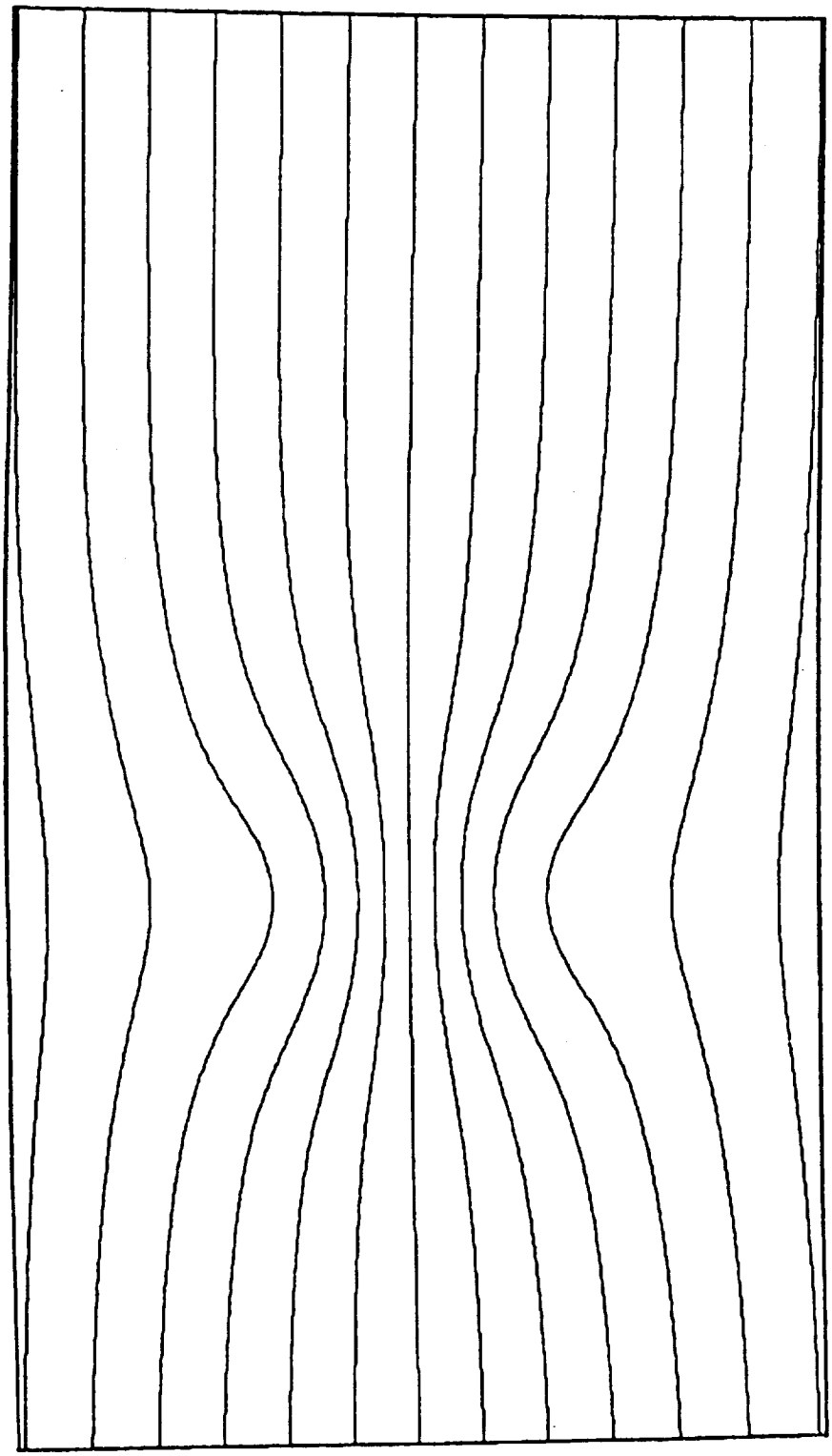

Figure 9. Current Lines at 2 Minutes for Case 1

Figure 10 is the model voltage plot corresponding to the Case 5 experimental measurements displayed in Figure 2. The scale is the same in each case, and the voltage increment is 1 Volt. The agreement is good. For this case, with a smaller conductivity contrast than in Case 1, all the hemoglobin leaks out of the high-conductivity sample in less than five minutes.

Case 2 is more complicated, because the hemoglobin concentration is high in the sample, relative to the buffer components, cf. Table 1. Thus the hemoglobin decreases the pH considerably to 7.3, compared with the value 8.55 for our barbital buffer. As a result, the barbituric acid, with a pK of 7.85, is only ionized in the sample to a low degree, and can only carry a very small portion of the current. The hemoglobin is not highly ionized, and therefore carries little current. Therefore the sodium ions carry the bulk of the current in the sample region. But outside the sample, the barbiturate and sodium ions are carrying roughly equal parts of the current. As a result, both sodium and barbiturate tend to increase on the left of the sample, and to be depleted on the right. The sodium ions are moving to the left, and the flux is doubled in the sample. The barbiturate radicals are moving to the right, except in the sample where they are unionized and stationary. This qualitative discussion is confirmed by a detailed analysis. Note that as in Case 1, the molarities of sodium and barbiturate preserve a roughly fixed ratio. However, the reason for this is very different.

Figures 11, 12 and 13 are plots of the molarities of hemoglobin, sodium, and barbiturate on the symmetry axis for Case 2, at times of 0, 1, 2, 3, 4, 5 and 6 minutes. Note that this is a low-resolution run; the resolution problems are apparent. The hemoglobin in Figure 11 shows "bleeding", similar to that in Figure 4, but the underlying cause is different. The initial sodium and barbiturate concentrations are almost constant (the small wiggles arise from the ion diffusion current during the initial 20-second diffusion period). But as soon as the current is turned on, a rapid segregation occurs for both species. For sodium, the molarity range (disregarding the under-resolved portion) is from 0.0183 to 0.0002. The corresponding figures for barbiturate are 0.0226 and 0.0003.

Figures 14 and 15 are contour plots of the hemoglobin molarity and of the conductivity, after six minutes, for the same Case 2. The bulk of the hemoglobin straddles the interface between high and low conductivities. The hemoglobin "tail" in Figure 11, with a molarity of 6×10^{-5}, is not apparent in Figure 14, because of the contour increment of 15×10^{-5}. The maxima and minima for the conductivity, again disregarding the under-resolved portion, are 1620 and 10 μmho/cm, an incredible range. The voltage and current distributions after six minutes, corresponding to this conductivity, are shown in Figures 16 and 17.

In general, a significant local concentration of a large protein molecule in a buffer will migrate in response to a field. The pH alteration it produces will lead to a depletion in the concentrations of the buffer components on the side to which it migrates, and an increase in the concentrations on the other side. The phenomenon is analogous to electrodialysis, in which a membrane changes the pH of the fluid within it, because of radical chemically bonded to the membrane material.

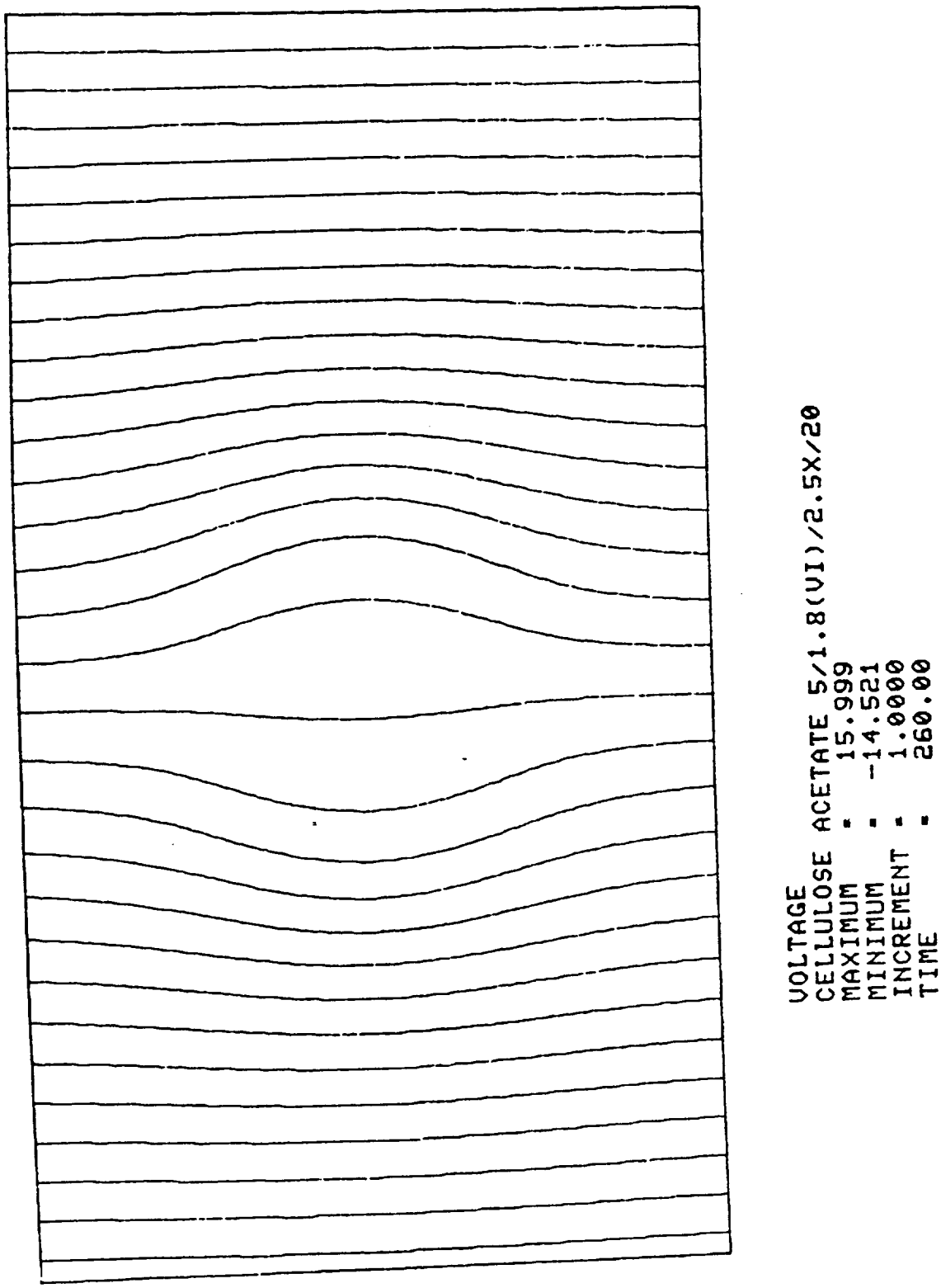

Figure 10. Voltage Plot at 4 Minutes for Case 5, cf. Figure 2.

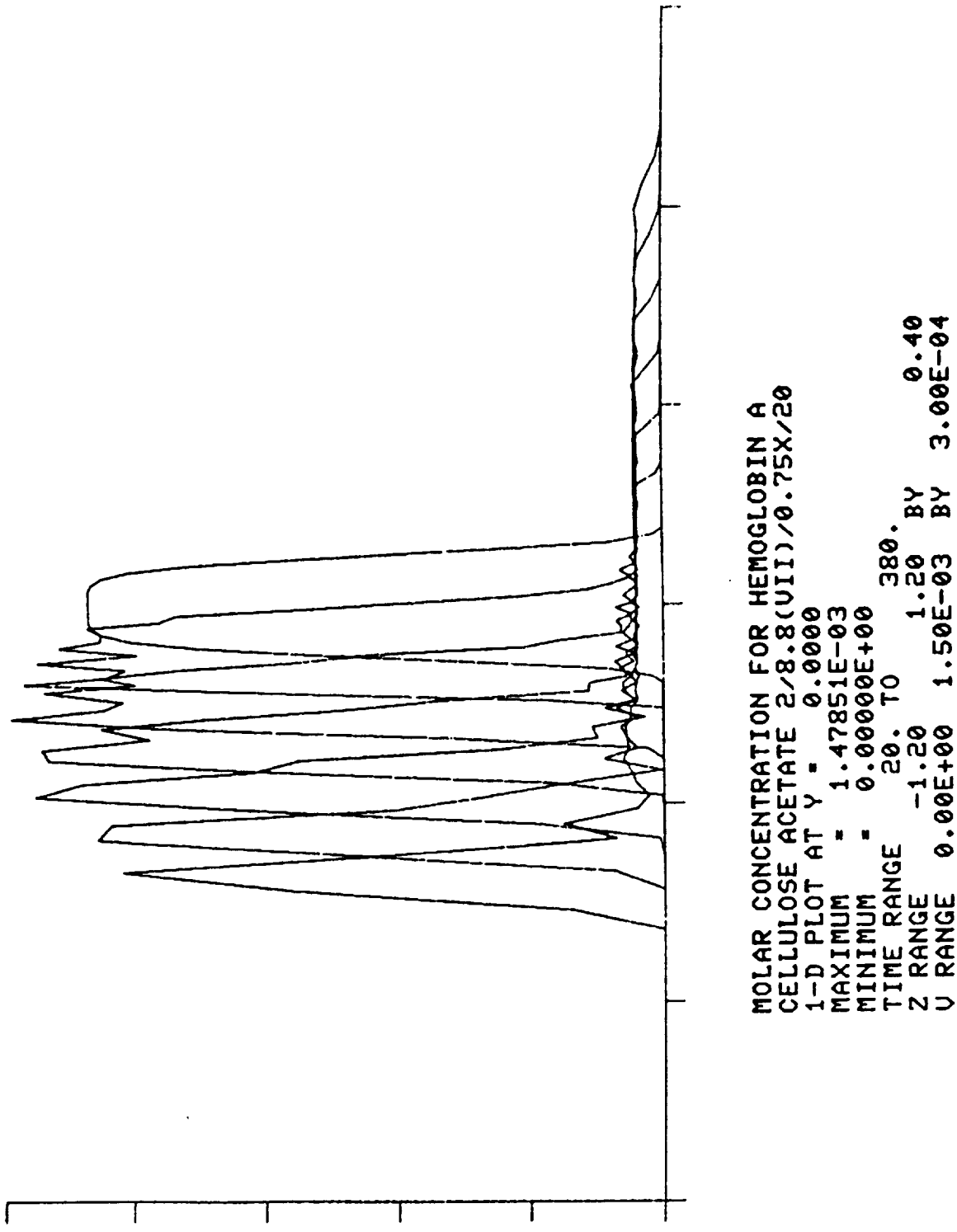

Figure 11. Axis Hemoglobin Molarity Plots every Minute for Case 2

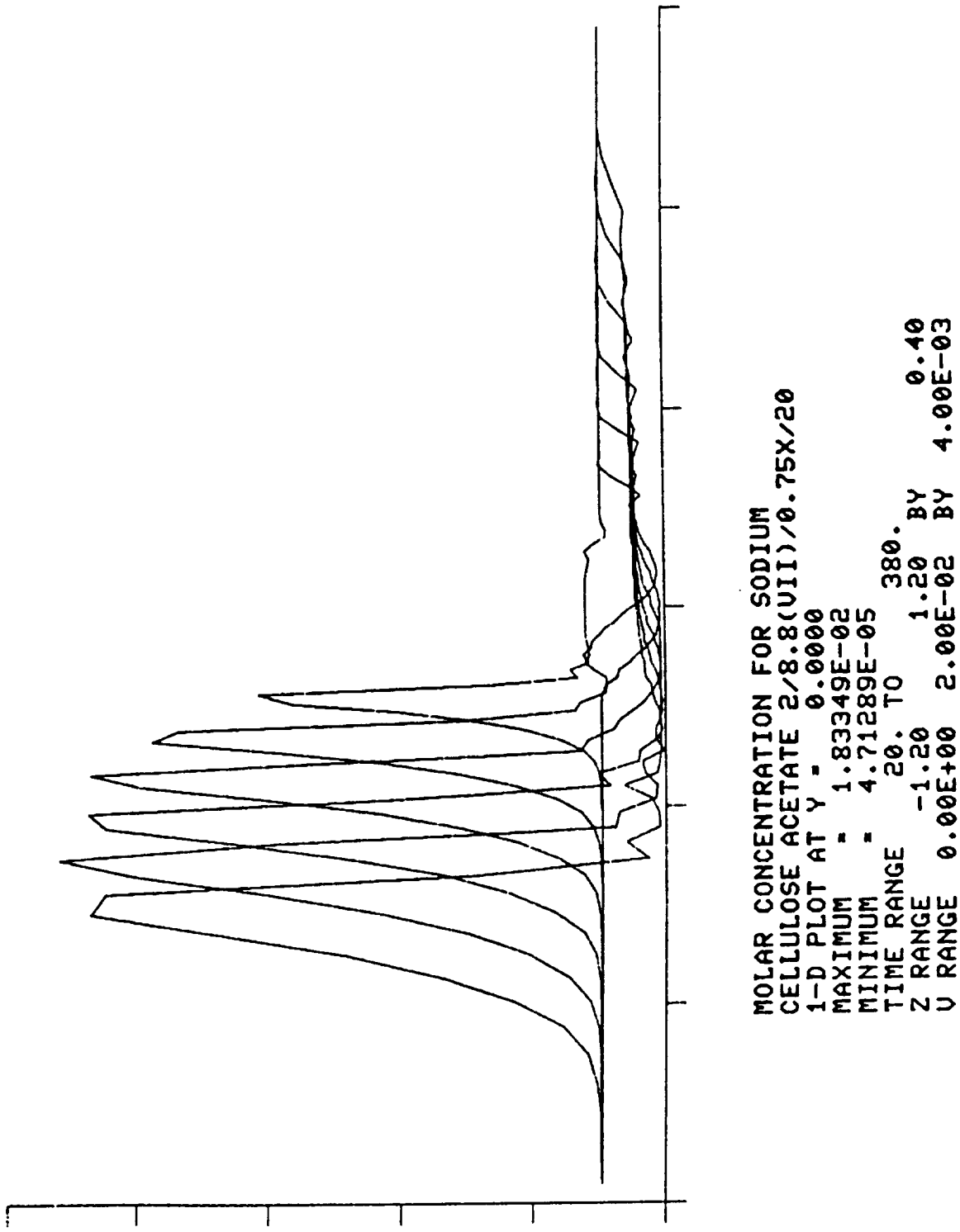

Figure 12. Axis Sodium Molarity Plots every Minute for Case 2

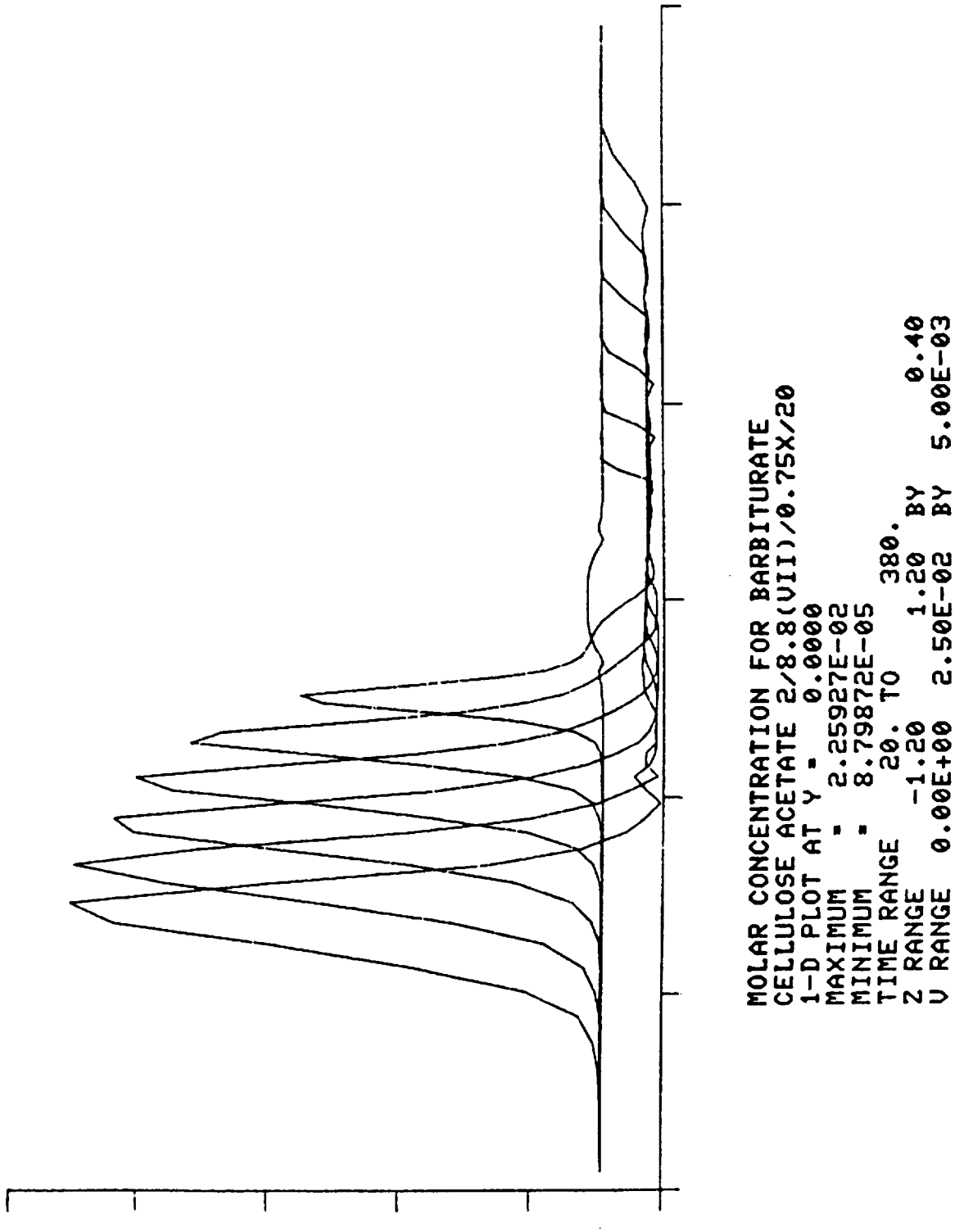

Figure 13. Axis Barbiturate Molarity Plots every Minute for Case 2

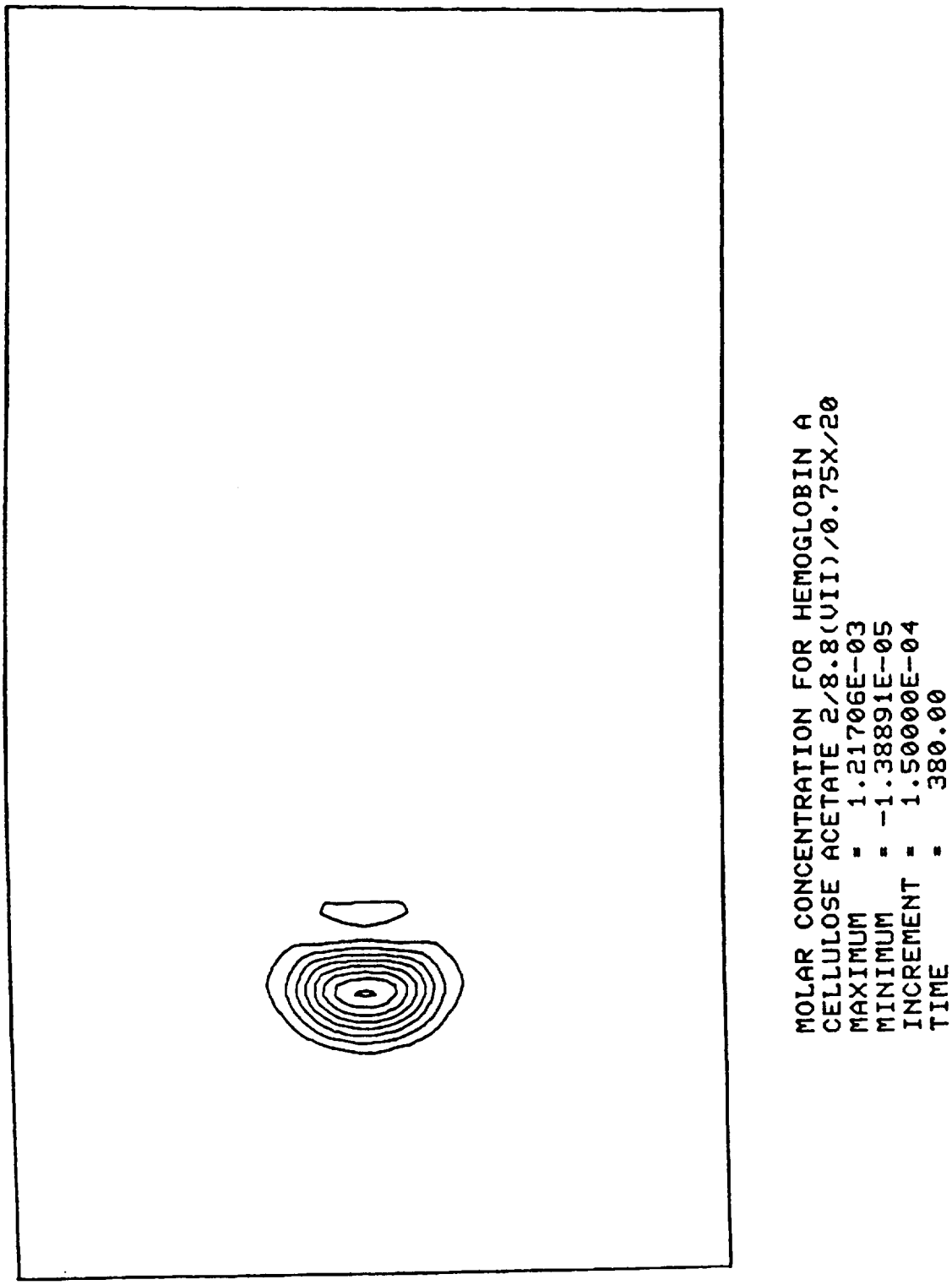

Figure 14. Contour Plot of Hemoglobin Molarity at 6 Minutes for Case 2

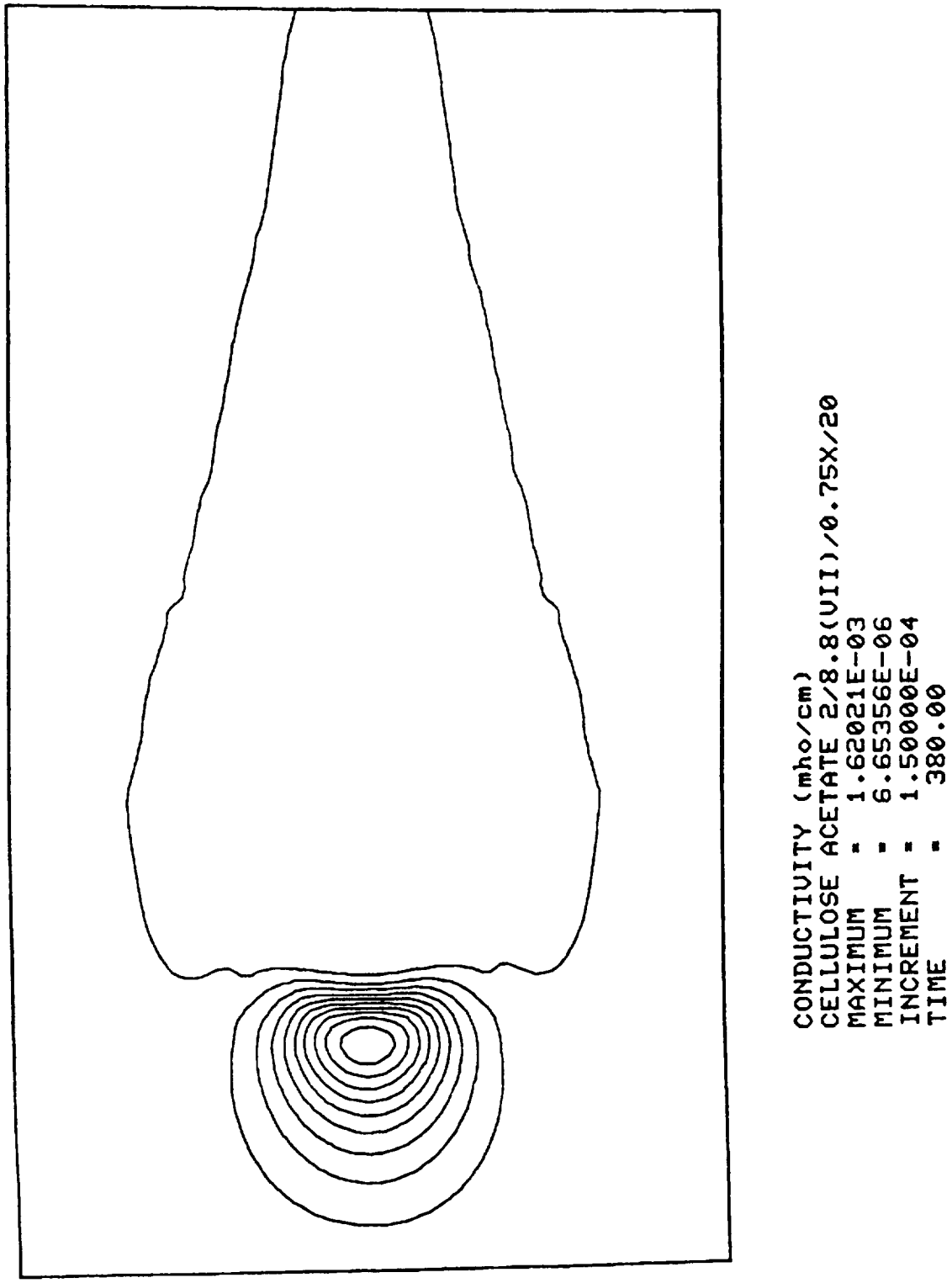

Figure 15. Contour Plot of Conductivity at 6 Minutes for Case 2

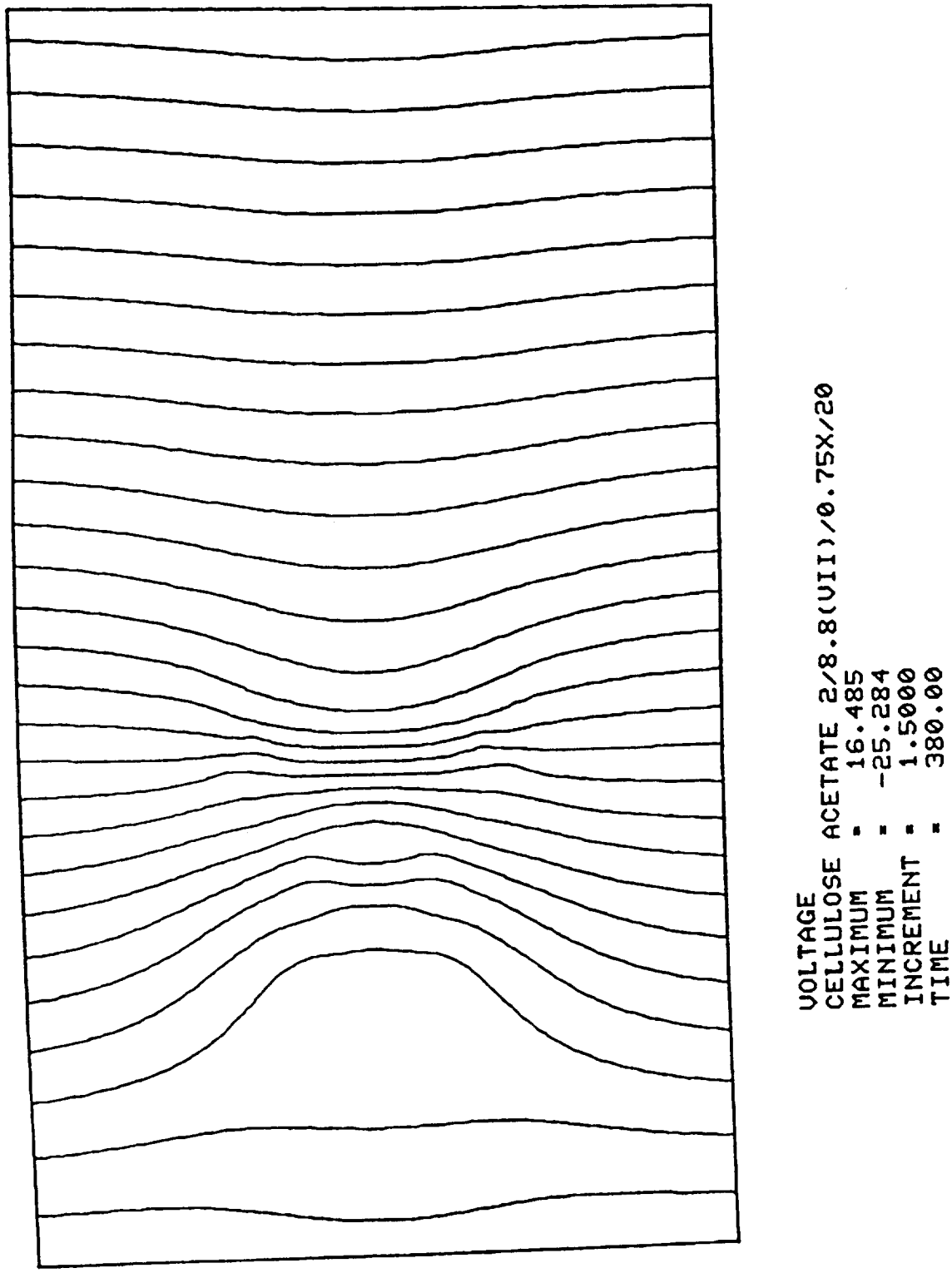

Figure 16. Contour Plot of Voltage at 6 Minutes for Case 2

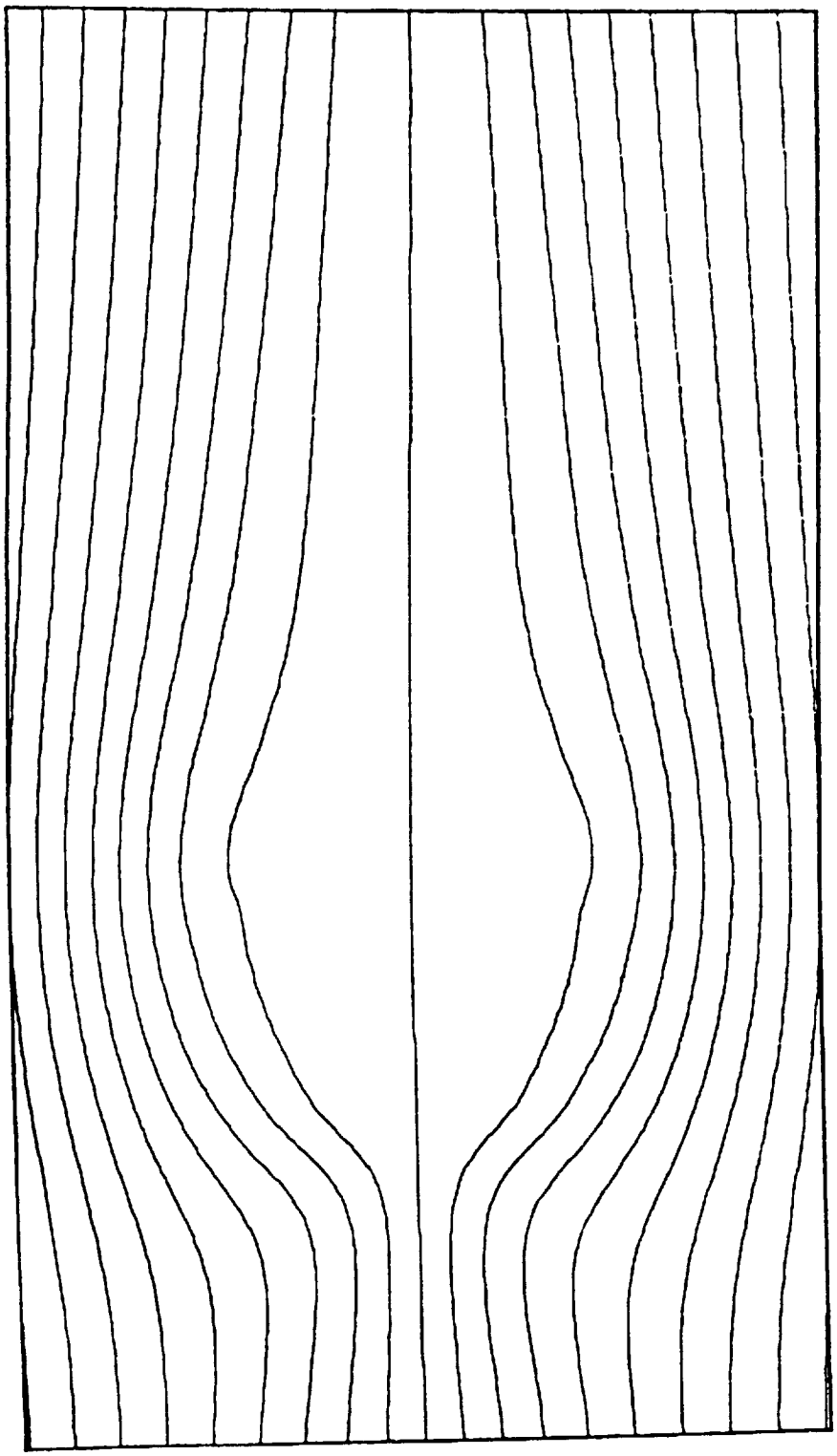

Figure 17. Current Lines at 6 Minutes for Case 2

Case 3 is intermediate between Case 1 and 2, with a new feature added. Figures 18, 19 and 20 are plots of the molarities of hemoglobin, sodium and barbiturate on the symmetry axis, at 1 minute intervals from time zero (following 20 seconds of diffusion) to 9 minutes. Initially the sodium concentration is almost constant. However, the hemoglobin in the sample is not passive, and it produces an increase in the sodium and barbiturate on the left, and a depletion on the right, during the first 2 minutes. After this, all the hemoglobin has leaked away, and the sodium and barbiturate excesses on the left spread through diffusion in a passive manner. The hemoglobin on the right propagates to the right as a sort of wave packet, with a sharp leading edge and a log tail, with little or no change of shape. The propagating wave carries with it proportional decreases in the sodium and barbiturate concentrations, to 40% and 20%, respectively, of their buffer values. Other plots (not shown here) indicate that the conductivity minimum in the packet is 30% of the buffer value, while the pH is 7.5, compared with the buffer value of 8.55. Figure 21 shows the hemoglobin concentration in the propagating packet, after 4 minutes.

Case 4 differs from Case 2 only by having about twice as much sodium and barbiturate in the sample, cf. Table 1. The results are qualitatively similar, with similar large contrasts between the maximum and minimum of the buffer component concentrations and of the conductivity. The hemoglobin takes about 11 minutes to "bleed" away from the initial single peak. The axis plots for hemoglobin concentration and for conductivity, at 1 minute intervals from zero to 9 minutes, are shown in Figures 22 and 23.

Cases 5 through 8 are the same as Cases 1 through 4, except for the use of a stronger buffer. Buffer strength is given in the plot captions as 0.75X or 2.5X; these are multiples of a nominally standard "X" buffer. Case 5 was discussed above. Axis plots for the hemoglobin and sodium molarities for Case 6 and 8, at times 0 through 9 minutes, are shown in Figures 24 through 27. These results are similar to Case 4. Case 7 is similar to Case 3, and shows the smallest amount of hemoglobin spreading among the eight cases. Figures 28 and 29 are plots of the axis hemoglobin and barbiturate concentrations, while Figure 30 shows the propagating hemoglobin packet after 2 minutes.

Some sample spreading in the field direction was observed in all these cases. In a few cases, there was a great deal of spreading. It is clear that electrokinetic processes can play a considerable role in electrophoresis performance degradation.

Nevertheless, the nature of the sample spreading in these simulations and in the corresponding acetate film experiments was qualitatively different from the explosive spreading straight out of the nozzle, observed in many experiments in the laboratory and in space. It became clear that we should look at free-flow electrophoresis effects.

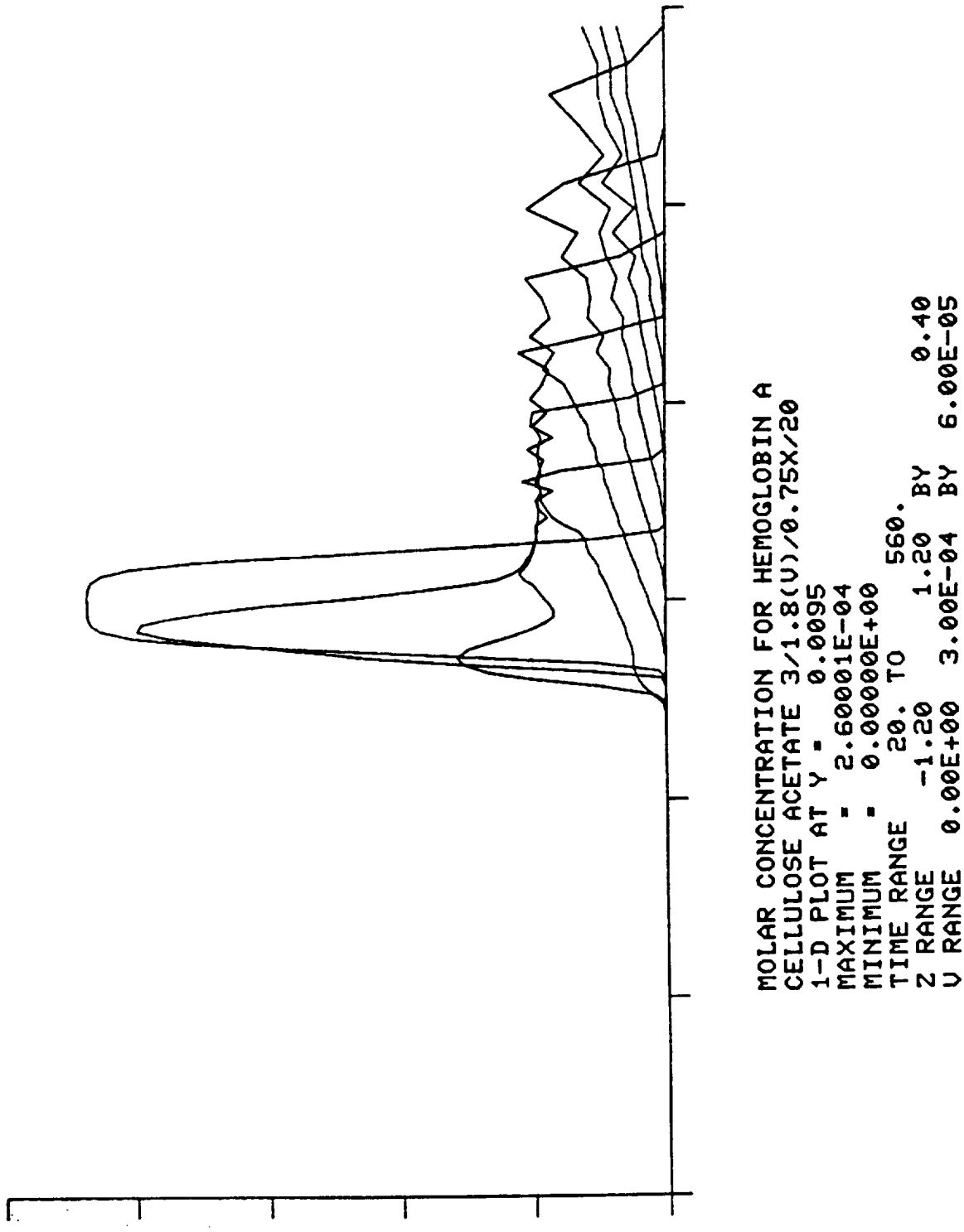

Figure 18. Axis Hemoglobin Molarity Plots every Minute for Case 3

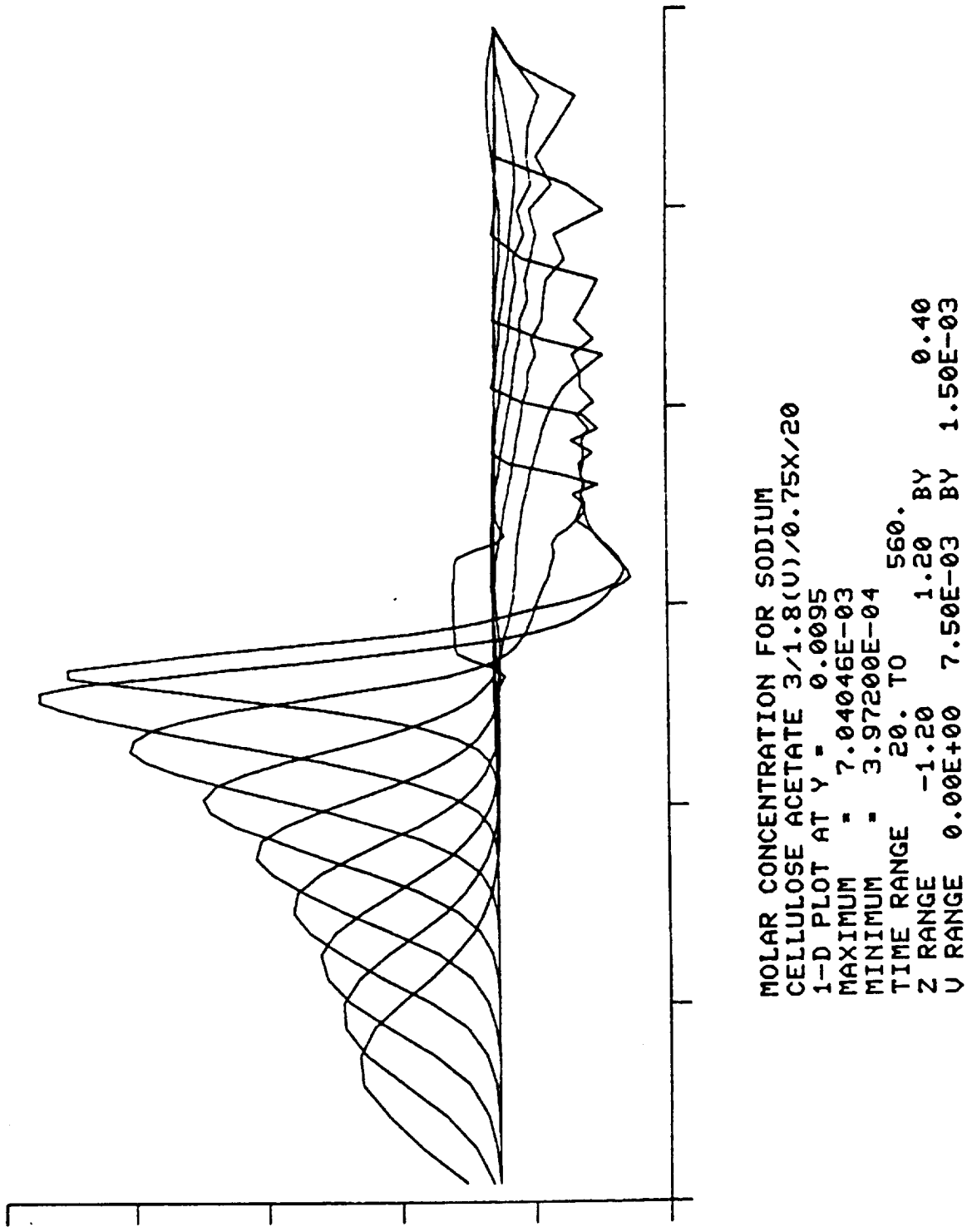

Figure 19. Axis Sodium Molarity Plots every Minute for Case 3

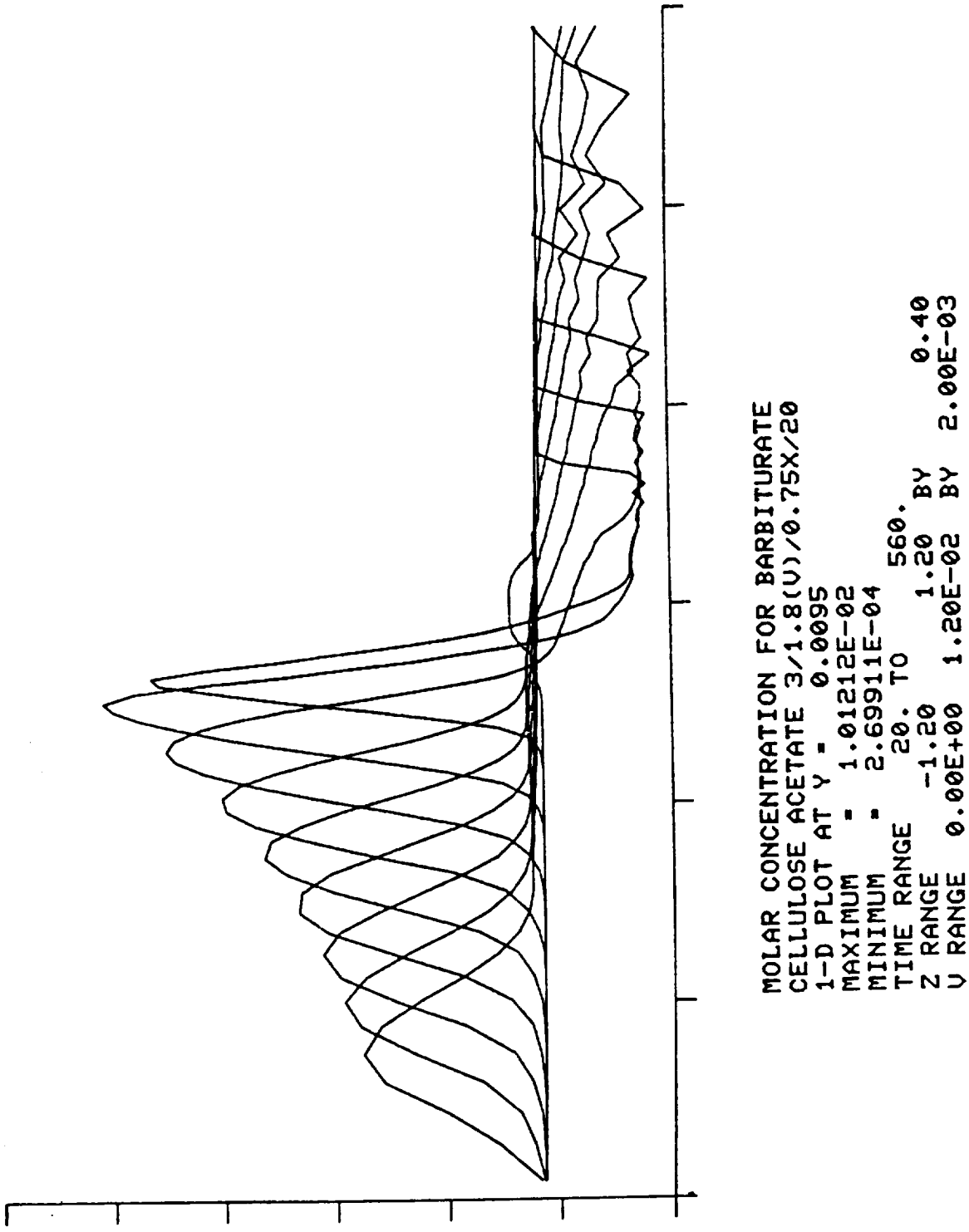

Figure 20. Axis Barbiturate Molarity Plots every Minute for Case 3

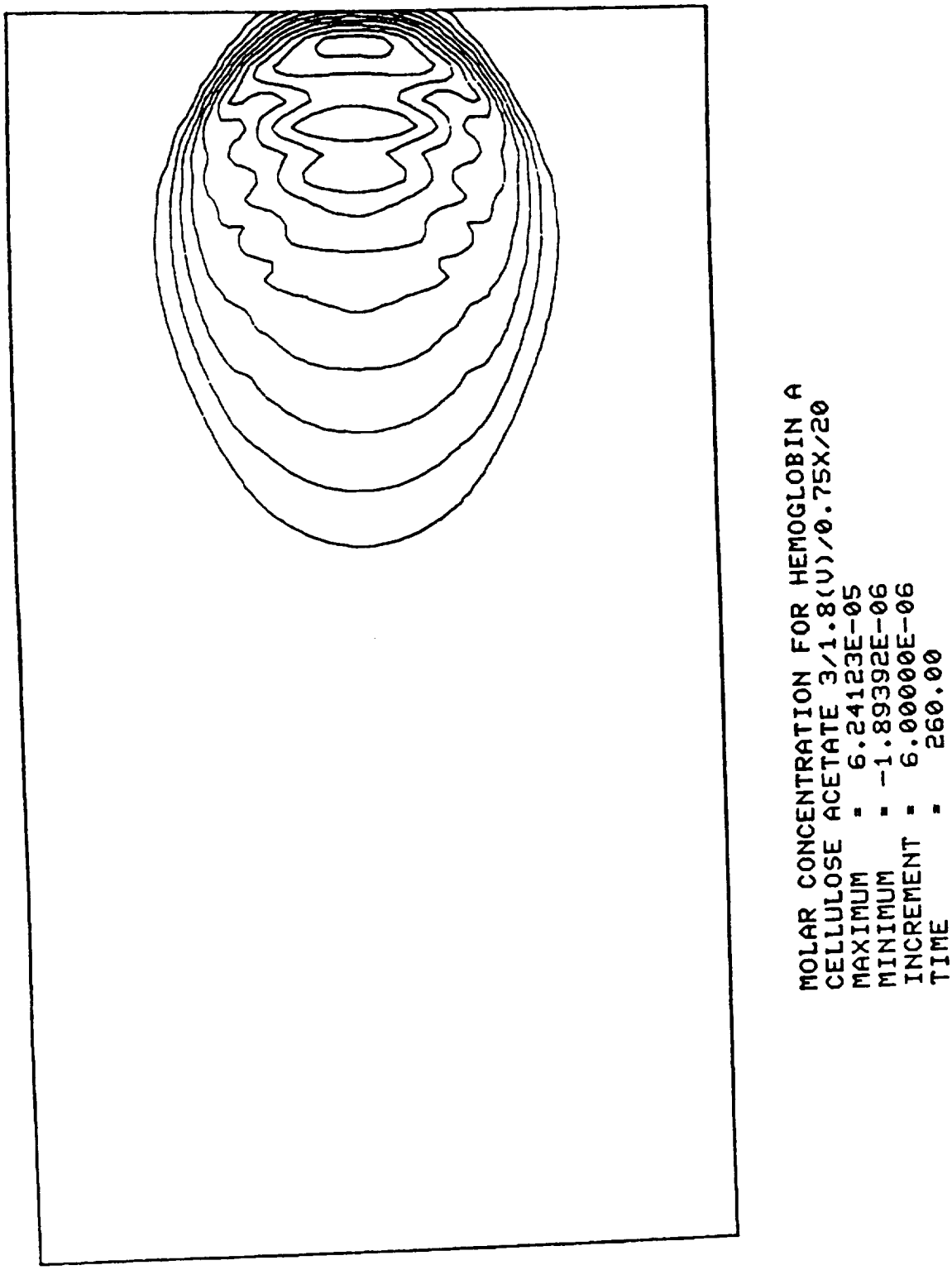

Figure 21. Contour Plot of Hemoglobin Packet at 4 Minutes for Case 3

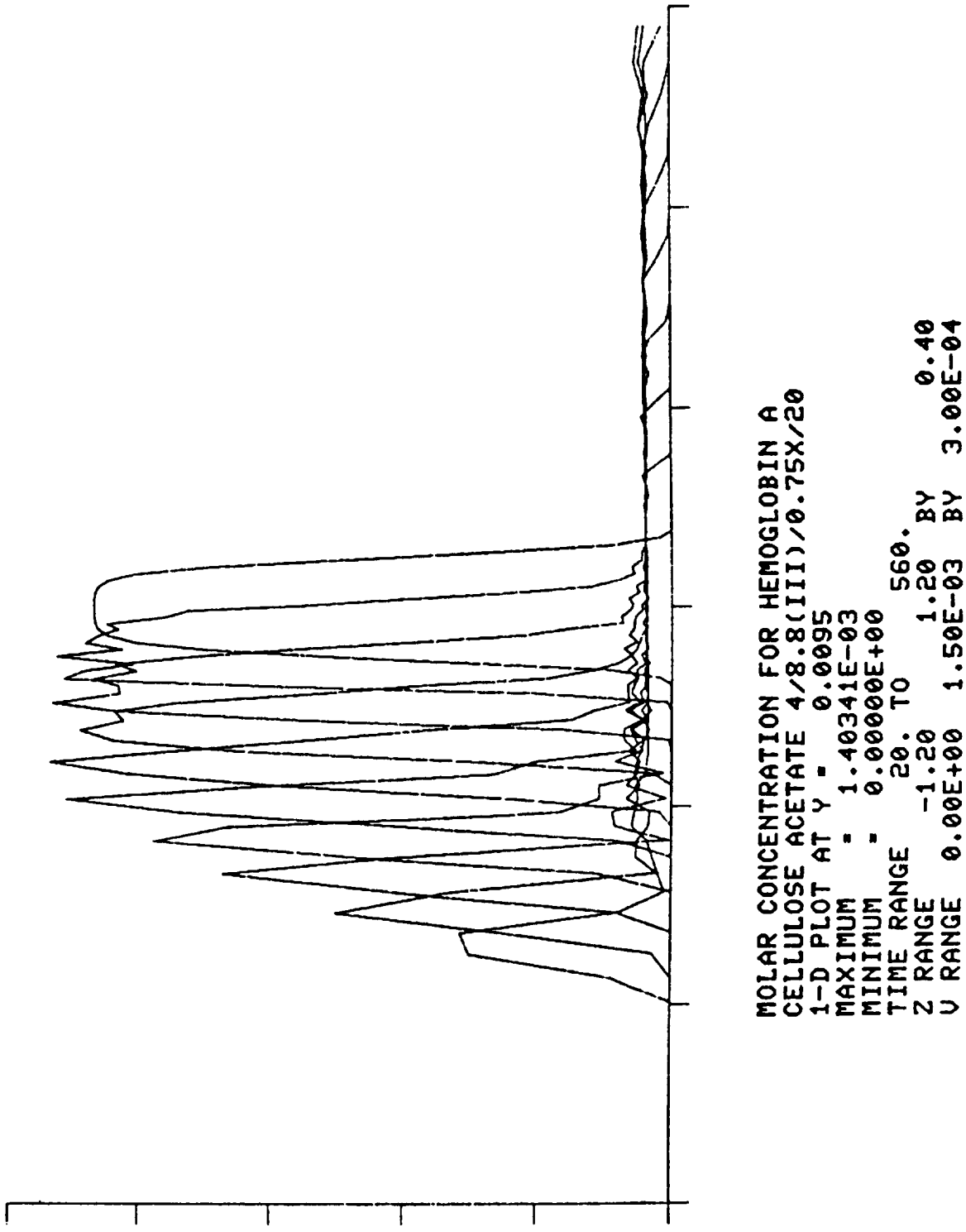

Figure 22. Axis Hemoglobin Molarity Plots every Minute for Case 4

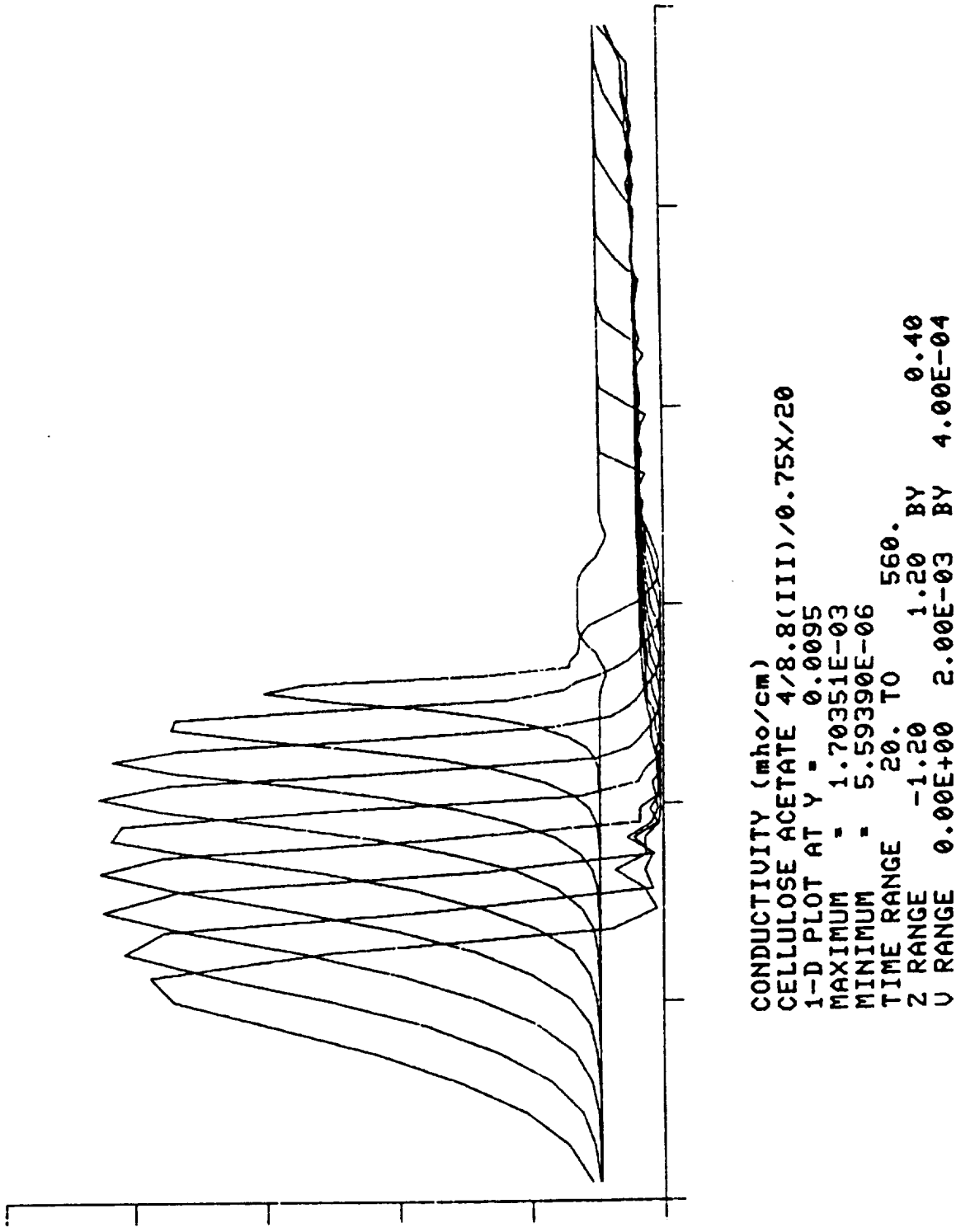

Figure 23. Axis Conductivity Plots every Minute for Case 4

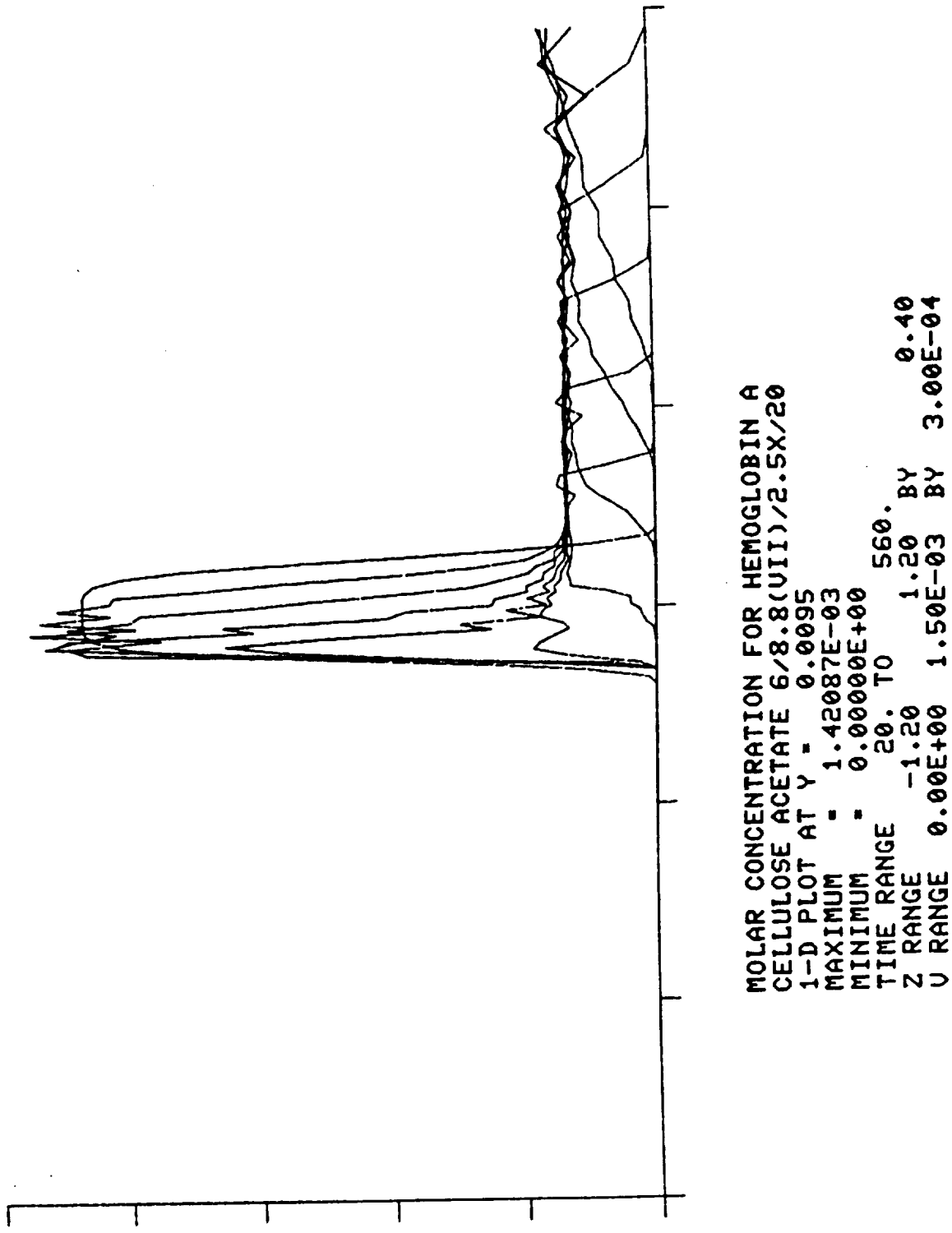

Figure 24. Axis Hemoglobin Molarity Plots every Minute for Case 6

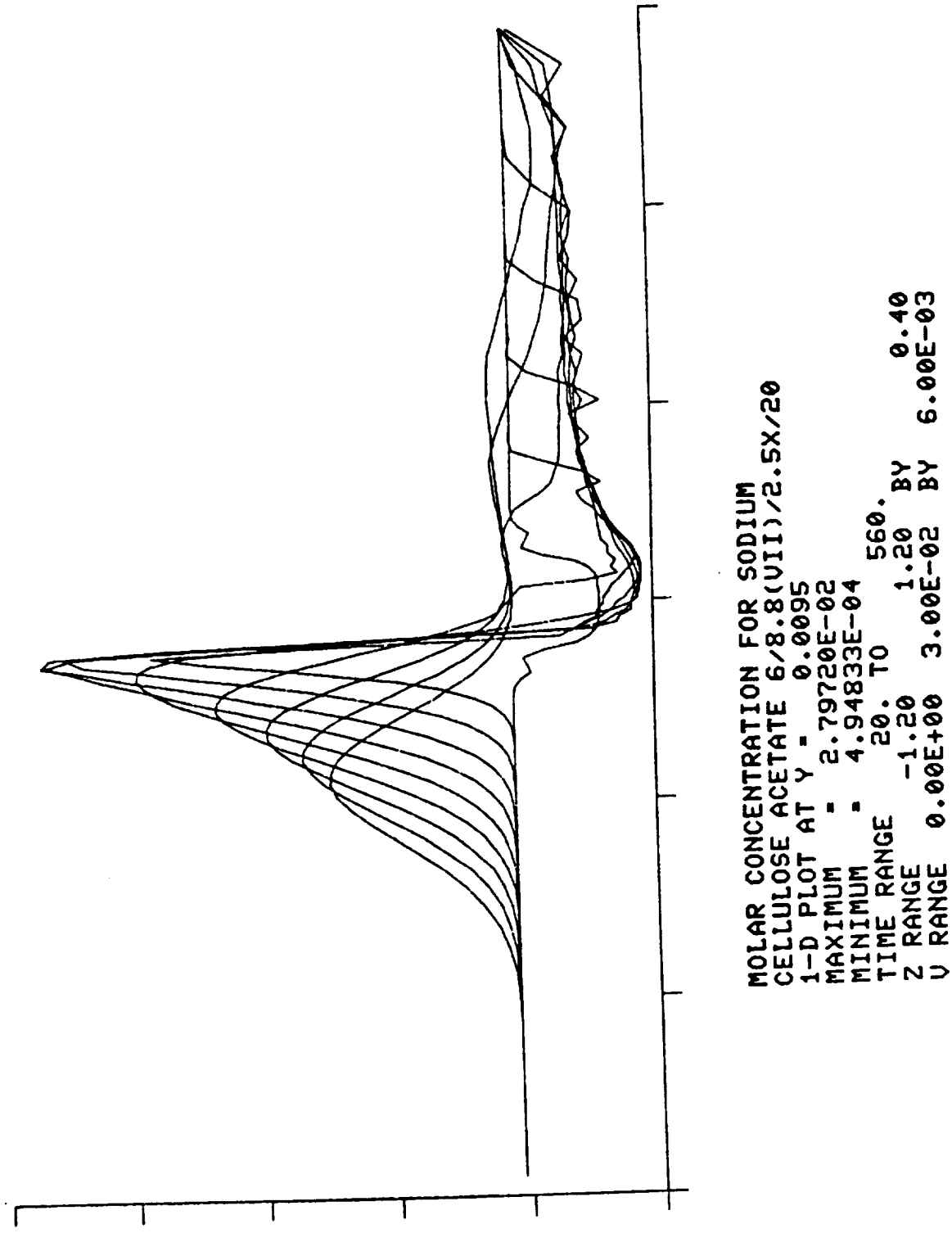

Figure 25. Axis Sodium Molarity Plots every Minute for Case 6

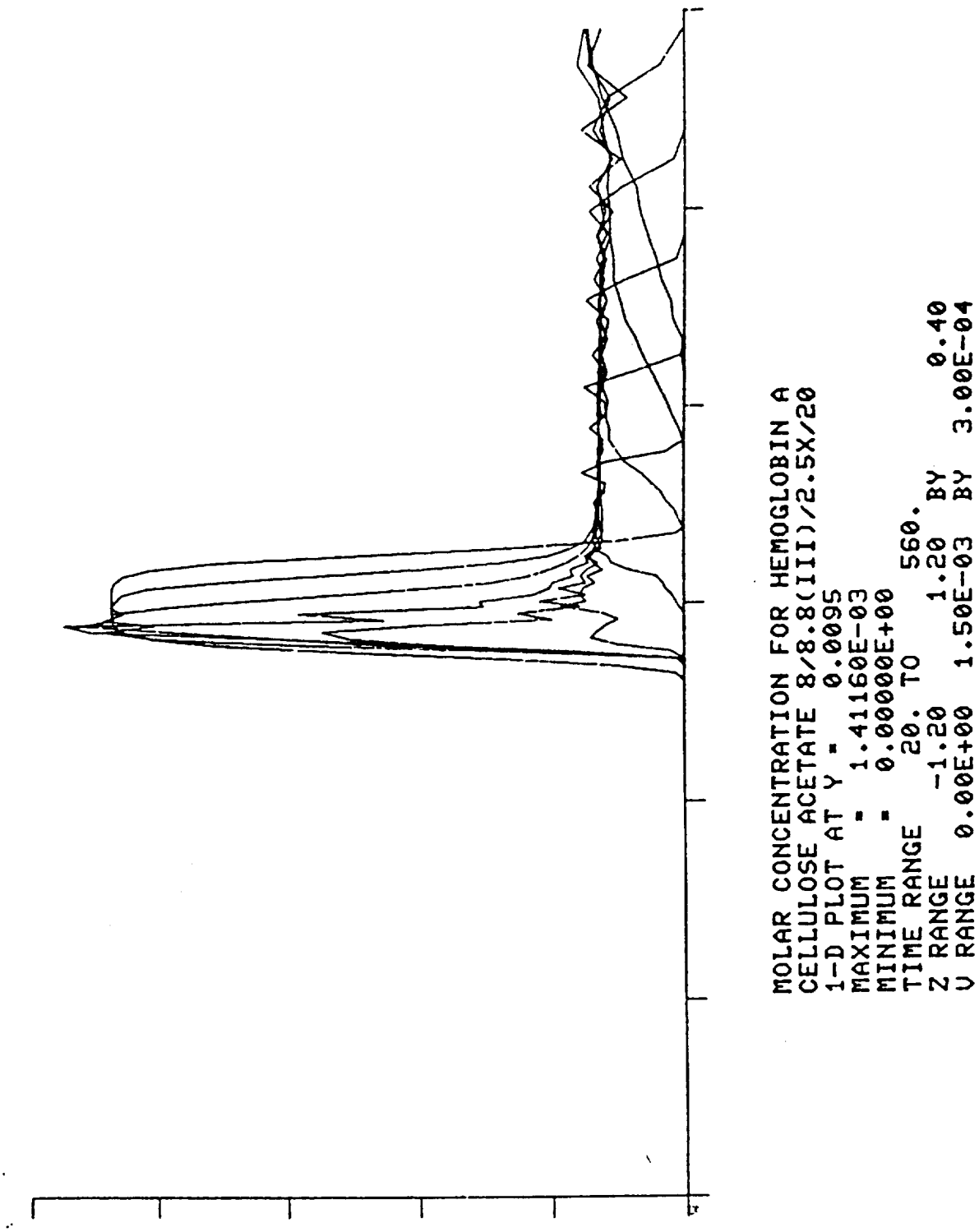

Figure 26. Axis Hemoglobin Molarity Plots every Minute for Case 8

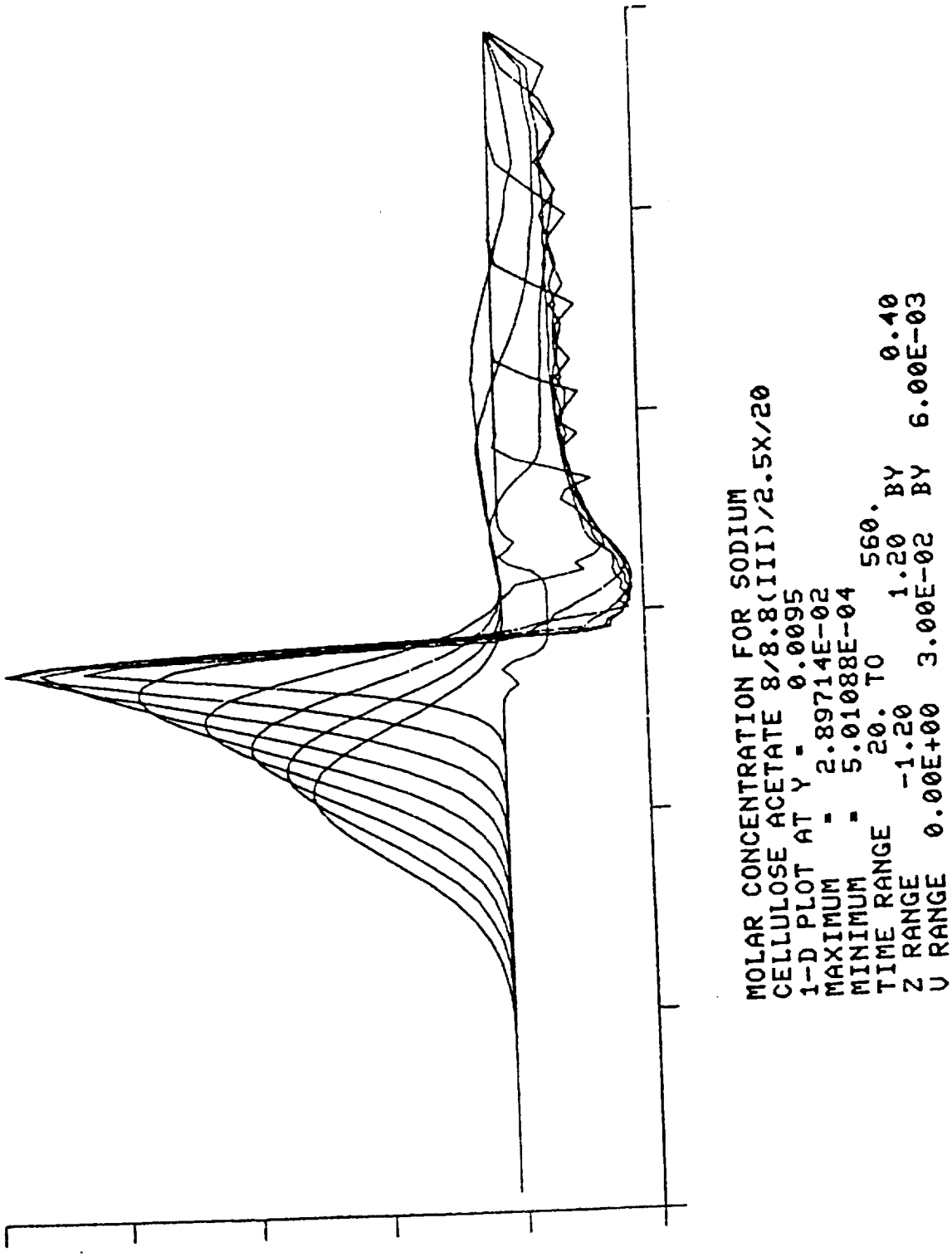

Figure 27. Axis Sodium Molarity Plots every Minute for Case 6

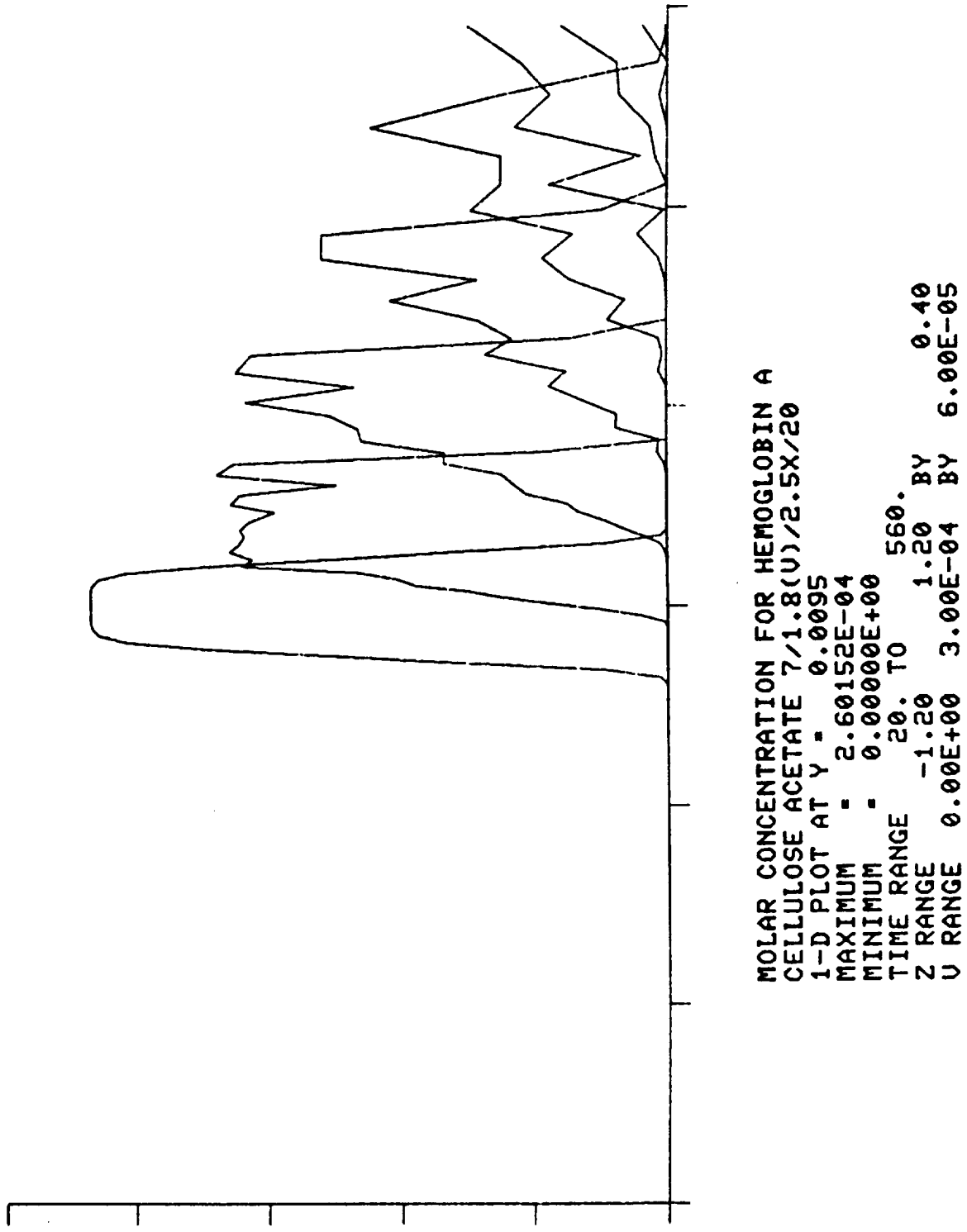

Figure 28. Axis Hemoglobin Molarity Plots every Minute for Case 7

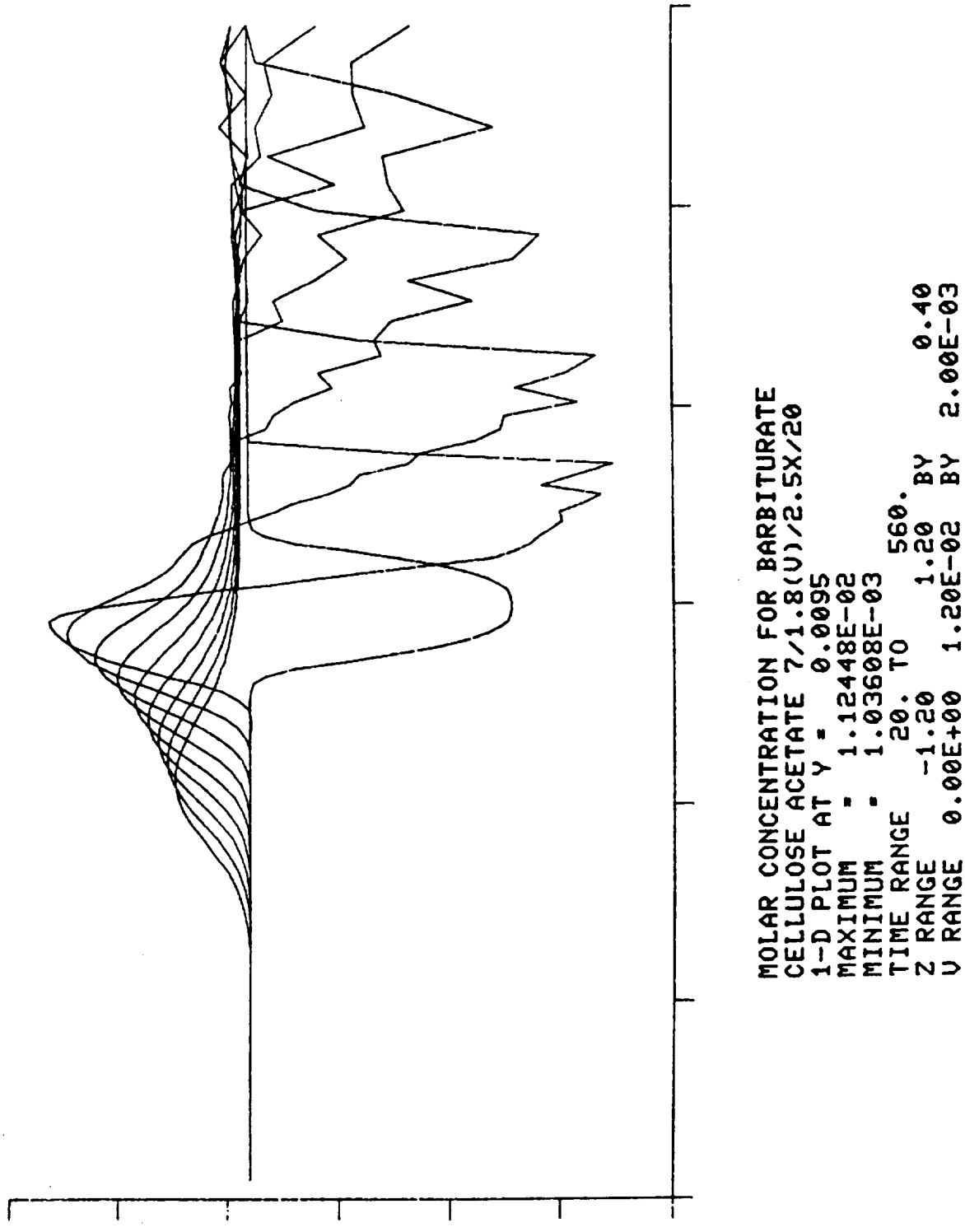

Figure 29. Axis Barbiturate Molarity Plots every Minute for Case 7

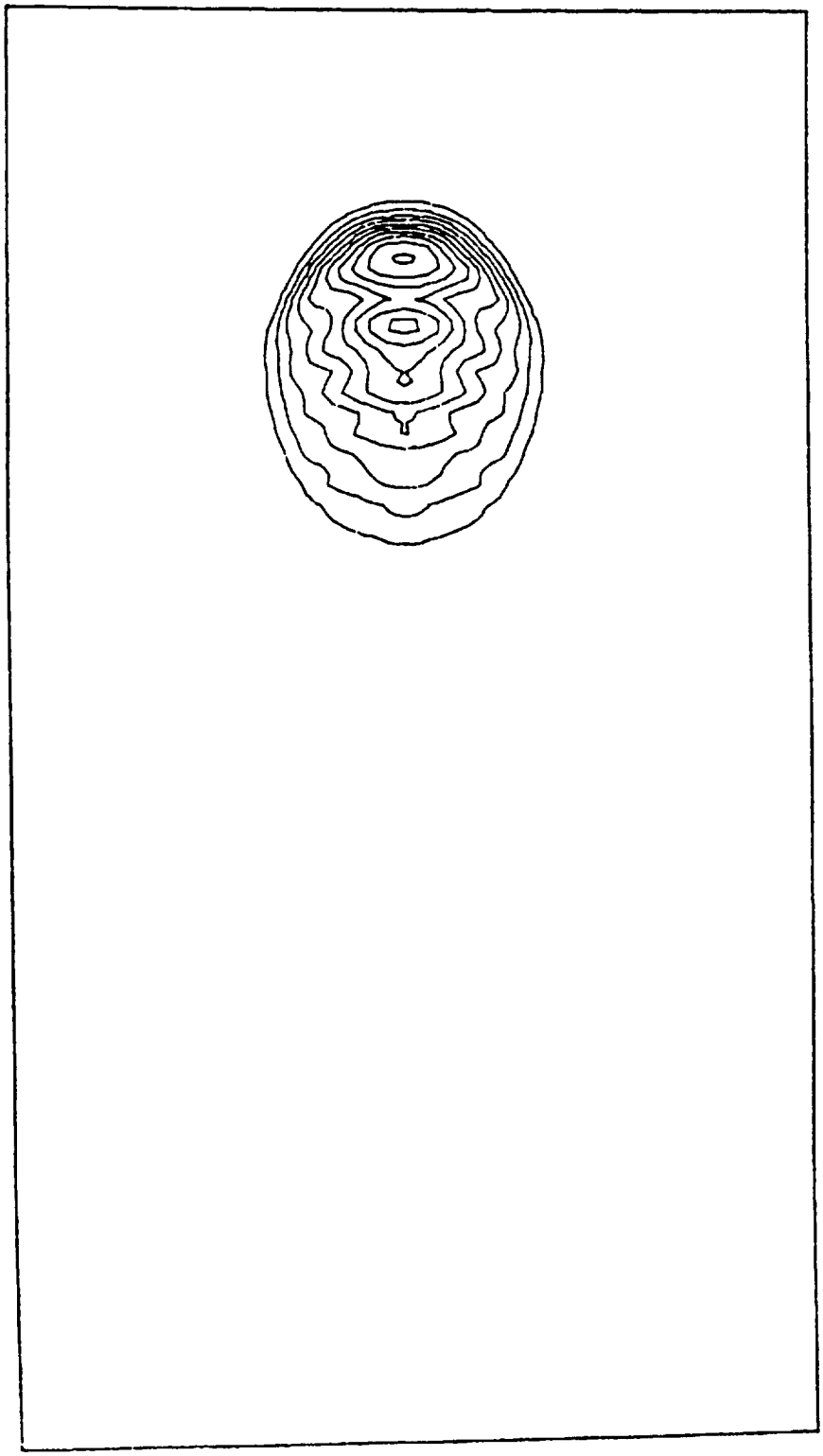

Figure 30. Contour Plot of Hemoglobin Packet at 2 Minutes for Case 7

2.5 FREE-FLOW SAMPLE SPREADING

We have performed extensive simulations using the code's two-dimensional rectangular option, with the upgraded formulations for varying wall electroosmosis. The objective of these computations was to understand and reproduce some of the observations of very rapid sample spreading as the sample left the nozzle and entered the electric field region. These observations were made both in space (particularly on STS6) and in the laboratory at MSFC.

We believed at the beginning of this program that the spreading was basically associated with the wall electroosmosis, and that all that was required was a mechanism for spreading the sample to the walls from its initial position near the center plane of the CFE chamber. We considered two mechanisms, as follows.

> The non-uniform conductivity distribution results in field and current lines which are not parallel to the walls. In particular, the electrodialysis effect associated with high concentrations of a large protein molecule like hemoglobin leads to a high conductivity on one side of the hemoglobin and a reduced conductivity on the other side, the side towards which the large protein is moving. Inevitably the field and current lines diverge, and the sample is dispersed towards the wall.
>
> The non-uniform conductivity distribution also leads to variations in the electric field along the wall. This in turn produces variations in the electroosmotic slip velocity. From continuity, the varying electroosmosis implies a flow field in the transverse direction, which can act to advect the sample into the region close to the wall where the electroosmosis flow is strongest (or to elongate it in the field direction).

We performed several series of computations in order to test these two hypotheses. We used samples and buffers with a wide range of different pH and conductivity values, and we tested a number of different choices for the electroosmosis slip parameters.

Our conclusions from these tests were as follows.

> Both phenomena occur, and either one can be dominant depending on the conditions.
>
> The model was successful in simulating the phenomena.
>
> The effects are not large enough to explain the observations.

The results of two of these series of tests are summarized below.

2.5.1 Polystyrene Latex Simulations

We use suspensions of polystyrene latex microspheres in some of our experiments. Their advantage is that they make the flow and electrophoresis visible, while they make no contribution to the charge neutrality balance (which determines the pH), nor to the conductivity.

For this first simulation, we wanted a simple case. So we chose a passive sample simulation. No corresponding experimental measurements were attempted.

We used a barbital buffer. Since the latex was passive, there are really just two components. Our results on the evolution of the latex concentration are significant only in that they show the integrated effect of the flow and electrokinetics alone. The buffer component distributions are modified by diffusion, but diffusion is negligible for the latex.

As previously stated, electrokinetics has no effect on the concentrations for a two-component monovalent buffer (with the excellent approximation of neglecting the hydrogen and hydroxyl ions). Thus the sodium and barbiturate concentrations vary only because of advection and diffusion. The only complicating factor is the effect of the conductivity distribution on the electric field at the wall, and thus on the electroosmotic slip velocity. When this velocity varies, transverse flows result, and the buffer component distributions, together with any sample, are moved either towards or away from the walls.

We computed two cases, with sample strengths 7.5X and .075X, where the buffer is the 0.75X buffer used in Cases 1 through 4 of the cellulose acetate experiments. In each case, the sample diameter is a millimeter, the gap thickness is 3 mm, the wall mobility is 4×10^{-4} cm/sec/(V/cm), while the passive polystyrene mobility is fixed at -2×10^{-4} cm/sec/(V/cm). The mean field is 30 V/cm to the left. Typical input data for the weak sample case is shown in Figure 31; the parameters in the input data page were discussed in the description of Figure 3.

Figure 32 is a contour plot of the initial PSL concentration, for both the strong and weak sample cases. The maximum (for comparison with later plots) is 0.05. The plots of the initial sodium and barbiturate concentrations are similar, with a ratio of ten between the sample and buffer concentrations.

Figure 33 shows the conductivity at the cross section corresponding to a mean residence time of 60 seconds. This means that the mean flow down the chamber will cover the distance in 60 seconds. The center plane flow speed covers the distance in 40 seconds, while the fluid at the no-slip wall naturally takes an infinite amount of time. Note in the figure that through the effects of diffusion and of the effectively large step near the wall, the 200 μmho/cm contour has reached the wall. The maximum conductivity is now only 6.6 times the buffer value.

The current lines solution corresponding to this conductivity is shown in Figure 34. The bulk of the current bends along the crescent of maximum conductivity. The electric field component is plotted in Figure 35, with numerical values drawn in. The electric field component on the wall drives the flow shown in Figure 36; note that the wall slip velocity is low in the middle and high at the ends. This results in a flow away from the wall on the right, and towards the wall on the left, in addition to the flow component parallel to the wall.

(continued on page 54)

POLYSTYRENE/.075,.75/2.,-2./.05,.15/-30 ***PROBLEM PARAMETERS***

Z MESH		Y MESH		SAMPLE ELECTRIC FIELD		WATER MOBILITIES BOUNDARY FLOW		SIDE BOUNDARY CONDITIONS 1/2/3 FOR BUFFER/SAMPLE/NO-FLUX	
ZBL =	-0.2000000	YT =	0.1500000	YSAMP =	0.0000000	UH =	0.0036000	ILEFT =	1
ZBR =	0.2000000	YB =	0.0000000	RSAMP =	0.0500000	UOH =	0.0020000	IRIGHT =	1
ZDL =	0.0020000	DYRAT =	1.7000000	PSAMP =	2.0000000	UWE =	0.0002000	LCOND =	F
ZDR =	0.0060000	IY =	0	CZERO =	-100.0000000	WB =	0.0000000		
DZRAT =	1.5000000	YWALL =	0.0000000	EZERO =	-30.0000000	UB =	0.0000000		
		YMESH =	0.6000000						

SPECIES		BUFFER MOLARITY	SAMPLE MOLARITY	SINGLE ION MOBILITY	IONIZATION DEFINITION CONSTANTS N		N		N		N		N		N			
SODIUM		0.00190000	0.00019000	0.00052700	-3.00	1.00	0.00	0.00	0.00	0.00	0.00	0.00	0.00	0.00	0.00	0.00	0.00	0.00
BARBITURATE		0.00228000	0.00022800	0.00050000	-1.00	7.85	0.00	0.00	0.00	0.00	0.00	0.00	0.00	0.00	0.00	0.00	0.00	0.00
PSL	P	0.00000000	0.05000000	0.00000200	-3.00	-99.99	0.00	0.00	0.00	0.00	0.00	0.00	0.00	0.00	0.00	0.00	0.00	0.00

METHOD PARAMETERS

SPECIES	TSTEP	UPWNDA	UPWNDC	FIXCZ	FIXCY	THZFX	BETDG	BETAO	BETAD	BETCO	BETCD
SODIUM	0.500	0.200	0.000	T	T	0.167	0.5	0.5	0.5	0.0	0.0
BARBITURATE	0.500	0.200	0.000	T	T	0.167	0.5	0.5	0.5	0.0	0.0
PSL	0.500	0.300	0.300	T	T	0.167	0.5	0.5	0.5	0.5	0.5

NSTEP = 400 NPITER = 10 PEXTRP = 0.500

OUTPUT PARAMETERS

DIRECT ACCESS READ & WRITE SEGMENTS ISEGR = 0 ISEGW = 1 (0: ANALYTIC, -1: AFTER PRIOR CASE)

WRITE STEP BEGINNING & INCREMENT IBEGDA = 100 IINCDA = 100 ZPLL = 0.00 ZPLR = 0.00

DIAGNOSTIC FREQUENCY NDIAG = 0 YPLB = 0.00 YPLT = 0.00

CONTOUR LINES NCLP = 28 NCLI = 0 NCOPIES = 1

VARIABLE	ISTEP BEGIN & INCREMENT FOR PRINTER DIAGNOSTICS PHYSICAL CONTOUR		INTEGER CONTOUR		PRINT NUMBERS		RANGES FOR I AND K IB	IE	II	KB	KE	KI	PLOTTER IDAOUT BEGIN & INCREMENT PHYSICAL		INTEGER		INCR
pH	100	100	9903	9904	9905	9906	1	42	1	17	1	-1	1	1	9915	9916	0.0
SIGMA	100	100	9903	9904	9905	9906	1	42	1	17	1	-1	1	1	9915	9916	0.0
PHI	9901	9902	9903	9904	9905	9906	1	42	1	17	1	-1	9913	9914	9915	9916	0.0
CURRENT	100	100	9903	9904	9905	9906	1	41	1	16	1	-1	1	1	9915	9916	0.0
EZ	100	100	9903	9904	9905	9906	1	41	1	16	1	-1	1	1	9915	9916	0.0
EY	9901	9902	9903	9904	9905	9906	1	41	1	16	1	-1	9913	9914	9915	9916	0.0
IONDCP	9901	9902	9903	9904	9905	9906	1	41	1	16	1	-1	9913	9914	9915	9916	0.0
PSI	100	100	9903	9904	9905	9906	1	41	1	16	1	-1	1	1	9915	9916	0.0
SODIUM																	
CONC	100	100	9903	9904	9905	9906	1	42	1	17	1	-1	1	1	9915	9916	0.0
MEAN ION	9901	9902	9903	9904	9905	9906	1	42	1	17	1	-1	9913	9914	9915	9916	0.0
MEAN SQU	9901	9902	9903	9904	9905	9906	1	42	1	17	1	-1	9913	9914	9915	9916	0.0
CHARGE	9901	9902	9903	9904	9905	9906	1	42	1	17	1	-1	9913	9914	9915	9916	0.0
SIGMA	9901	9902	9903	9904	9905	9906	1	42	1	17	1	-1	9913	9914	9915	9916	0.0
DCONC	9901	9902	9903	9904	9905	9906	1	42	1	17	1	-1	9913	9914	9915	9916	0.0
VELOCITY	9901	9902	9903	9904	9905	9906	1	42	1	17	1	-1	9913	9914	9915	9916	0.0
FLUX	9901	9902	9903	9904	9905	9906	1	42	1	17	1	-1	9913	9914	9915	9916	0.0
BARBITURATE																	
CONC	100	100	9903	9904	9905	9906	1	42	1	17	1	-1	1	1	9915	9916	0.0
MEAN ION	9901	9902	9903	9904	9905	9906	1	42	1	17	1	-1	9913	9914	9915	9916	0.0
MEAN SQU	9901	9902	9903	9904	9905	9906	1	42	1	17	1	-1	9913	9914	9915	9916	0.0
CHARGE	9901	9902	9903	9904	9905	9906	1	42	1	17	1	-1	9913	9914	9915	9916	0.0
SIGMA	9901	9902	9903	9904	9905	9906	1	42	1	17	1	-1	9913	9914	9915	9916	0.0
DCONC	9901	9902	9903	9904	9905	9906	1	42	1	17	1	-1	9913	9914	9915	9916	0.0
VELOCITY	9901	9902	9903	9904	9905	9906	1	42	1	17	1	-1	9913	9914	9915	9916	0.0
FLUX	9901	9902	9903	9904	9905	9906	1	42	1	17	1	-1	9913	9914	9915	9916	0.0
PSL																	
CONC	0	100	9903	9904	9905	9906	1	42	1	17	1	-1	1	1	9915	9916	-1.
MEAN ION	9901	9902	9903	9904	9905	9906	1	42	1	17	1	-1	9913	9914	9915	9916	0.0
MEAN SQU	9901	9902	9903	9904	9905	9906	1	42	1	17	1	-1	9913	9914	9915	9916	0.0
CHARGE	9901	9902	9903	9904	9905	9906	1	42	1	17	1	-1	9913	9914	9915	9916	0.0
SIGMA	9901	9902	9903	9904	9905	9906	1	42	1	17	1	-1	9913	9914	9915	9916	0.0
DCONC	9901	9902	9903	9904	9905	9906	1	42	1	17	1	-1	9913	9914	9915	9916	0.0
VELOCITY	9901	9902	9903	9904	9905	9906	1	42	1	17	1	-1	9913	9914	9915	9916	0.0
FLUX	9901	9902	9903	9904	9905	9906	1	42	1	17	1	-1	9913	9914	9915	9916	0.0

Figure 31. Input Data for Weak PSL Case

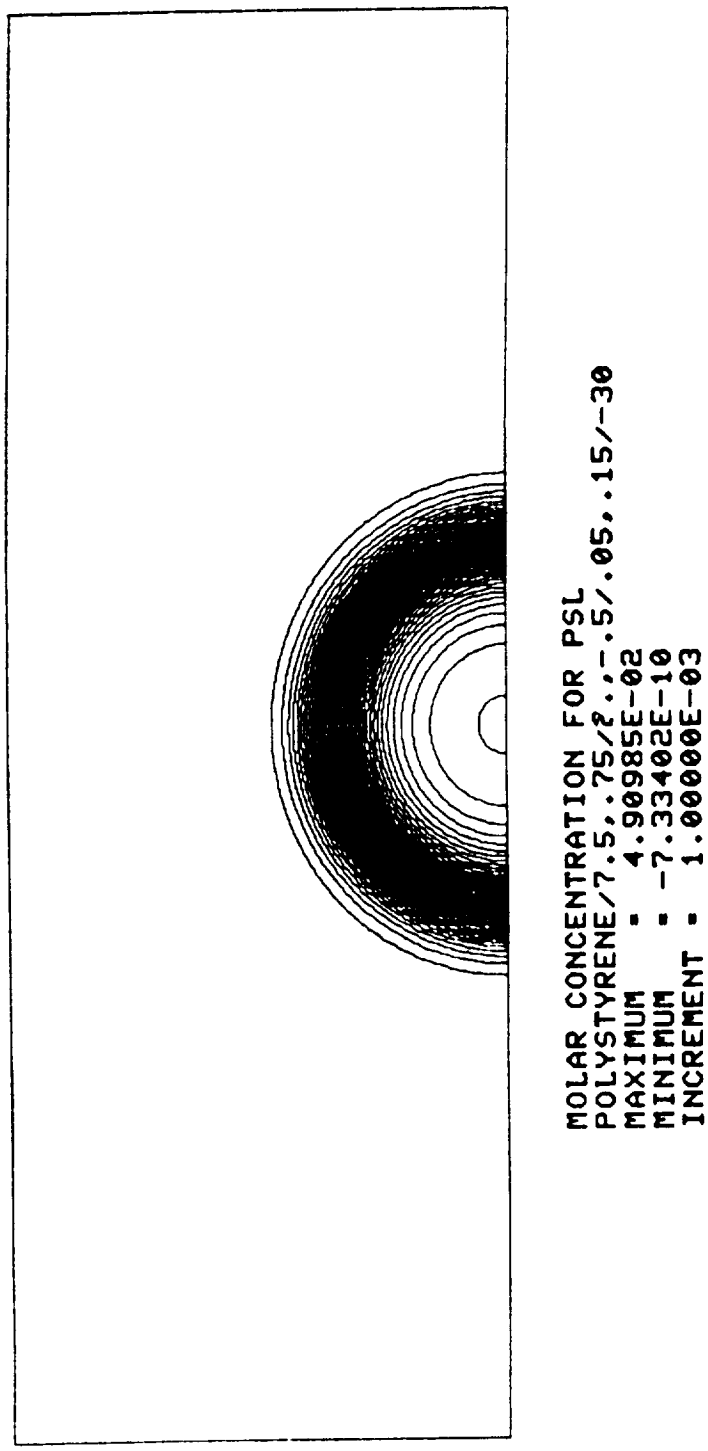

Figure 32. Initial PSL Distribution for both PSL Cases

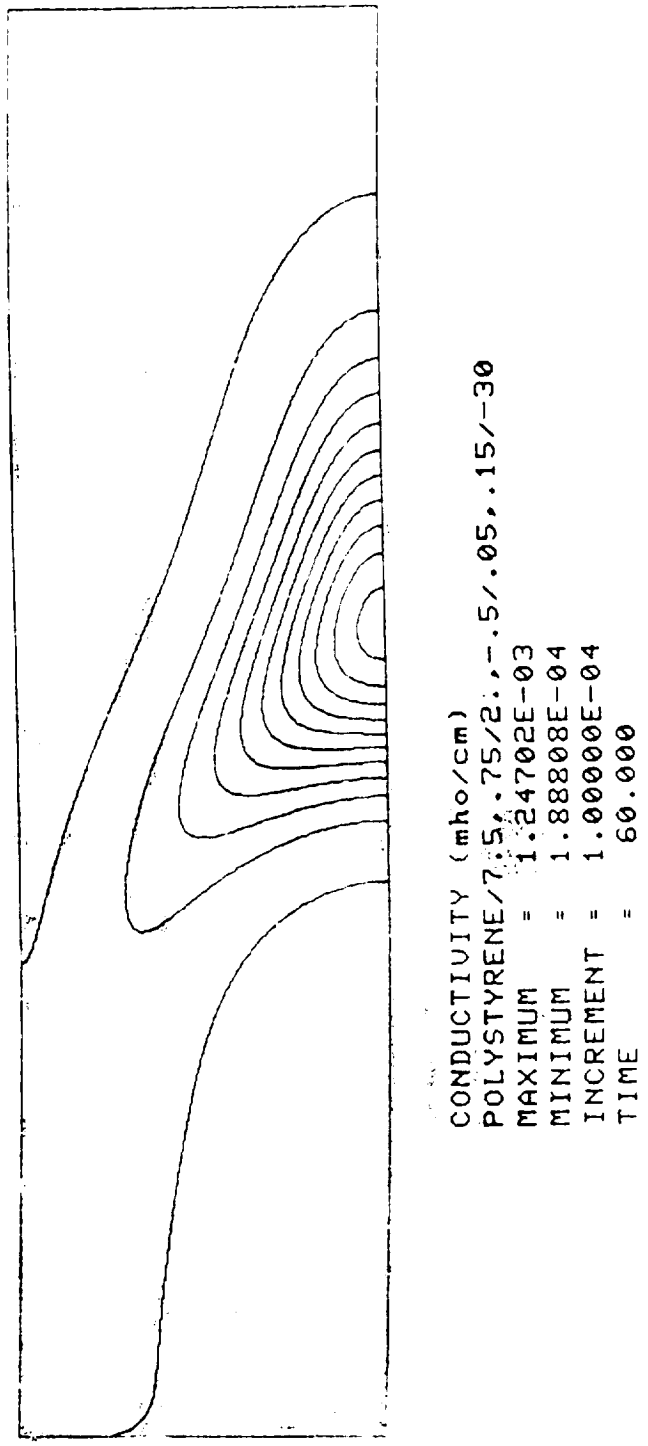

Figure 33. Conductivity for Strong PSL Case at 60 Seconds

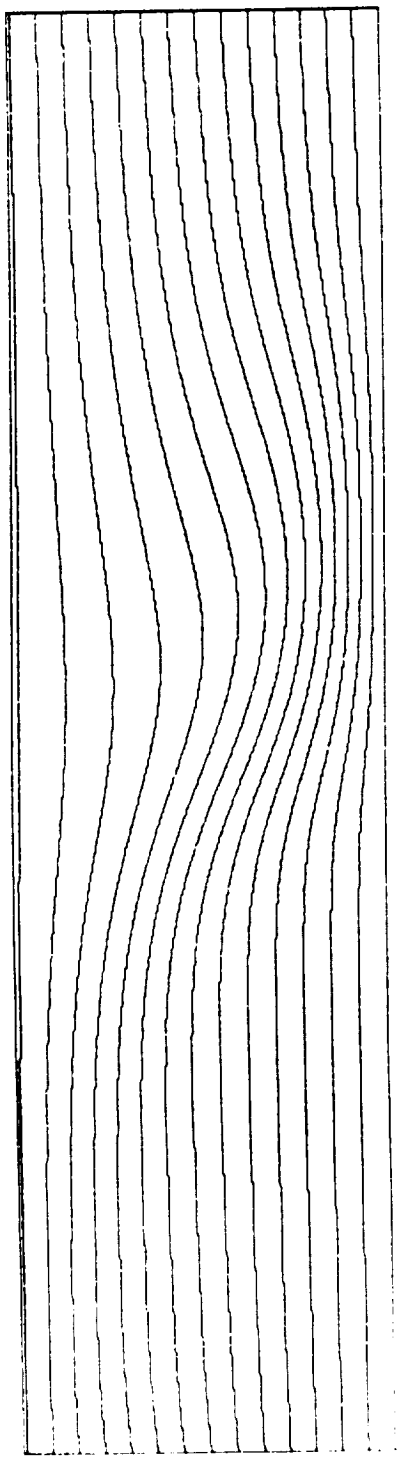

Figure 34. Current Lines for Strong PSL Case at 60 Seconds

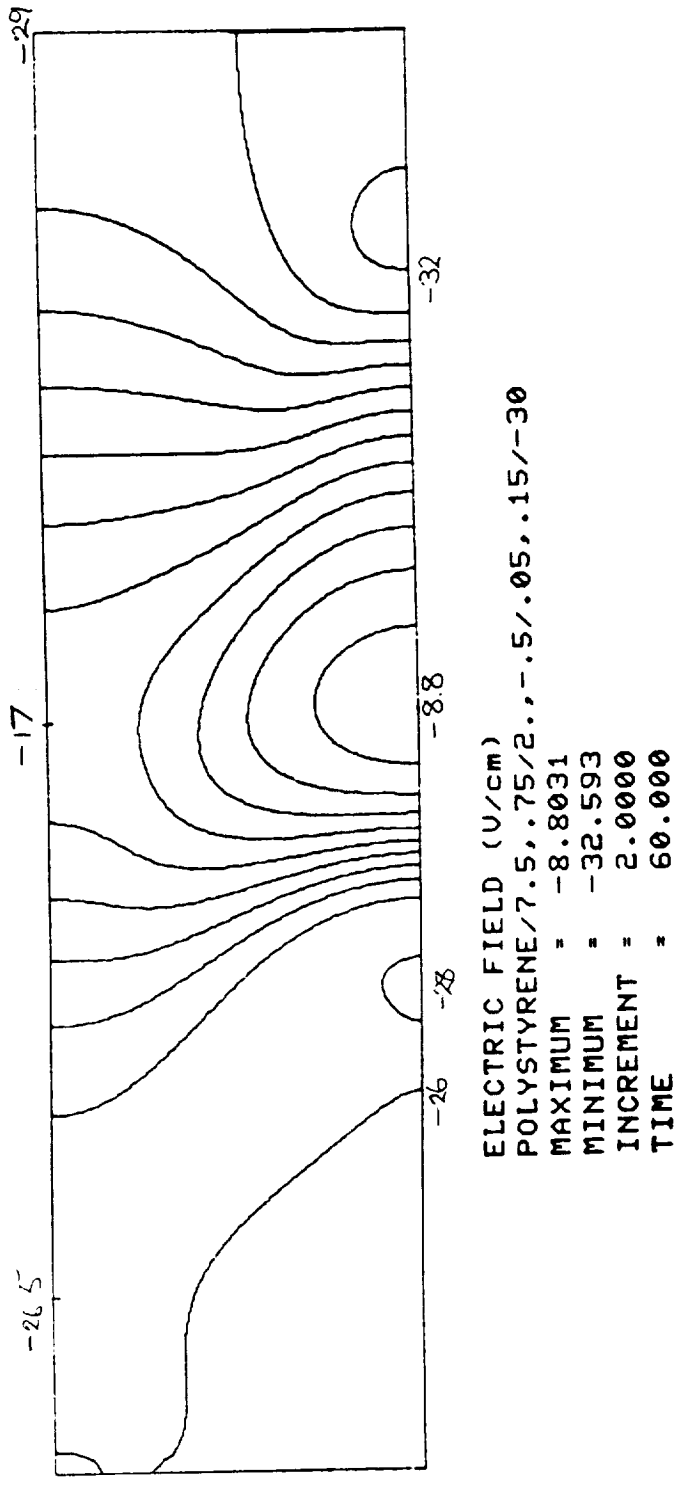

Figure 35. Electric Field for Strong PSL Case at 60 Seconds

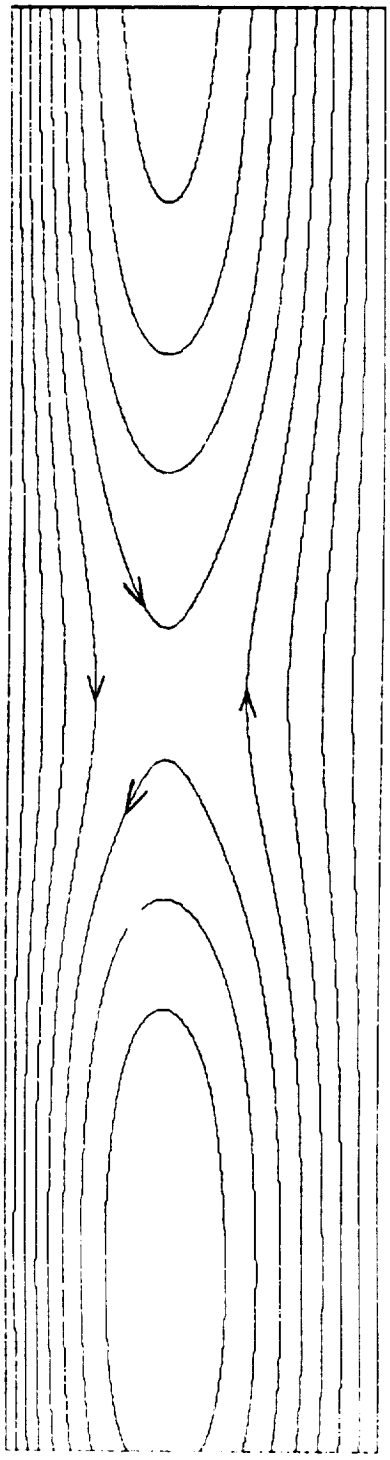

Figure 36. Stream Function for Strong PSL Case at 60 Seconds

The PSL concentration at 60 seconds is shown in Figure 37. While the stream function is pulling the tip towards the wall, the negative mobility implies that the PSL near the tip is moving to the right along the current lines, and therefore away from the wall. If the mobility was positive (the same sign as the wall mobility), then the two effects would reinforce each other at the tip.

The PSL concentrations at 120 seconds and at 180 seconds are shown in Figures 38 and 39. While the tip has hardly moved under the counteracting influences, the rest of the distribution has been moved by the transverse flow towards the axis, and stretched along the axis by the combined effects of the flow and the electrokinetics.

The conductivity at 60 seconds for the case with a low concentration sample is shown in Figure 40; the minimum is already 41% of the buffer value. The current lines are therefore almost straight, and the electric field variation on the wall is limited, as shown in Figures 41 and 42. The stream function is shown in Figure 43; the circulation is weak. The 120-second PSL concentration is shown in Figure 44. The main effects are the crescent formation and the electrokinetic focusing (due to the large field in the sample and the low field outside). The contrast between Figures 38 and 44 is remarkable.

2.5.2 Hemoglobin in Sodium Acetate Buffer

Figure 45 shows input data for another free-flow case. The buffer and sample contain sodium and acetate in the ratio 2 to 3, with the same concentration in each. The sample is 8.8% hemoglobin. The pK of acetic acid is 4.7; the pH of the buffer is 5.0. The pH of the sample is 6.1, reflecting the dominant influence of the large concentration of hemoglobin. The parameters are somewhat analogous to Case 2, cf. Table 1.

The hemoglobin is positively charged in this pH range, and "bleeds" out to the left. The acetic acid is pretty much fully ionized in the sample, and carries more than half the current; outside the sample it carries less than half. Hence the sodium and acetate concentrations increase on the right and decrease on the left.

The hemoglobin bleeds slowly to the left, since in the sample it so dominates the pH that it is practically unionized.

Superposed on the effects which would be seen in a porous medium like the acetate film are the electroosmosis, the larger steps near the wall, the nonuniform electroosmosis resulting in flows towards and away from the wall, and the nonuniform conductivity, resulting in ion movement along field lines which are not parallel to the axis.

Figure 46 shows the initial hemoglobin concentration, with a peak of 0.00127. The initial sodium and acetate concentrations are of course uniform.

Figure 47 contours the hemoglobin molarity at the cross-section corresponding to a mean residence time of 90 seconds. The peak is down only 12% from its initial value, and the bleeding to the left is not visible, because of the contour increment. The conductivity range in Figure 48 is a

(continued on page 67)

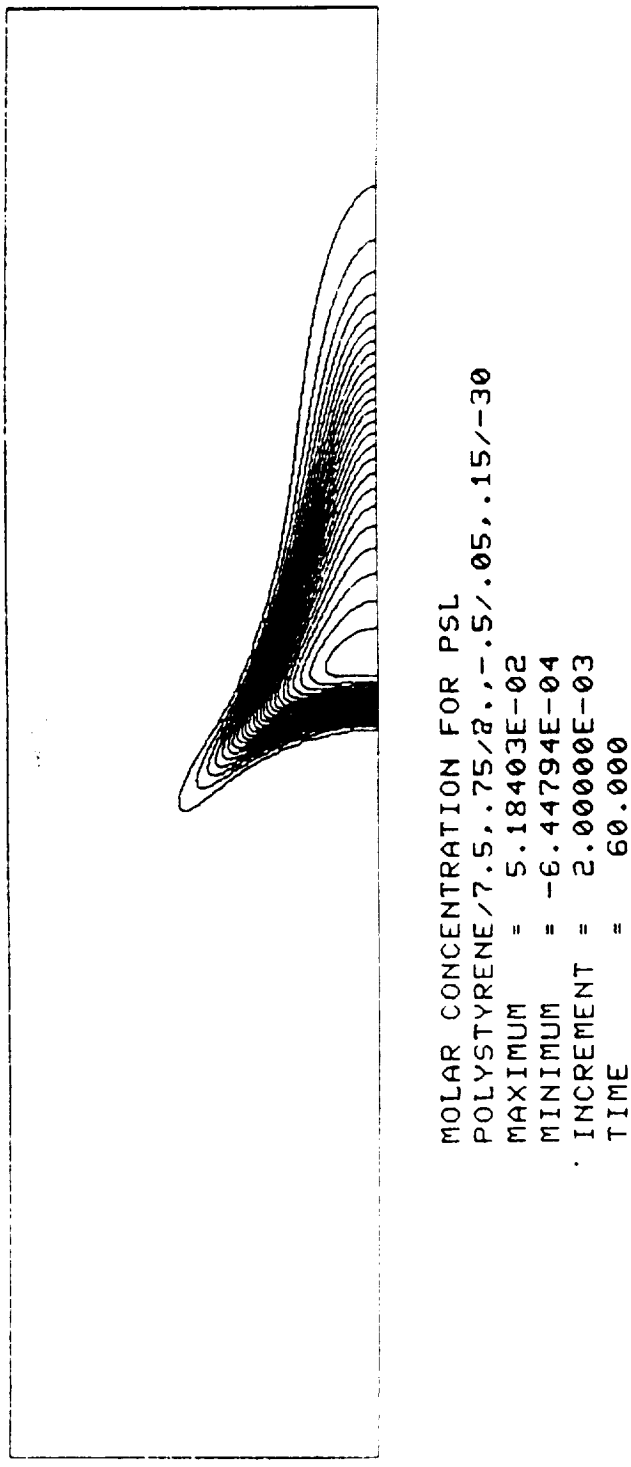

Figure 37. Latex Concentration for Strong PSL Case at 60 Seconds

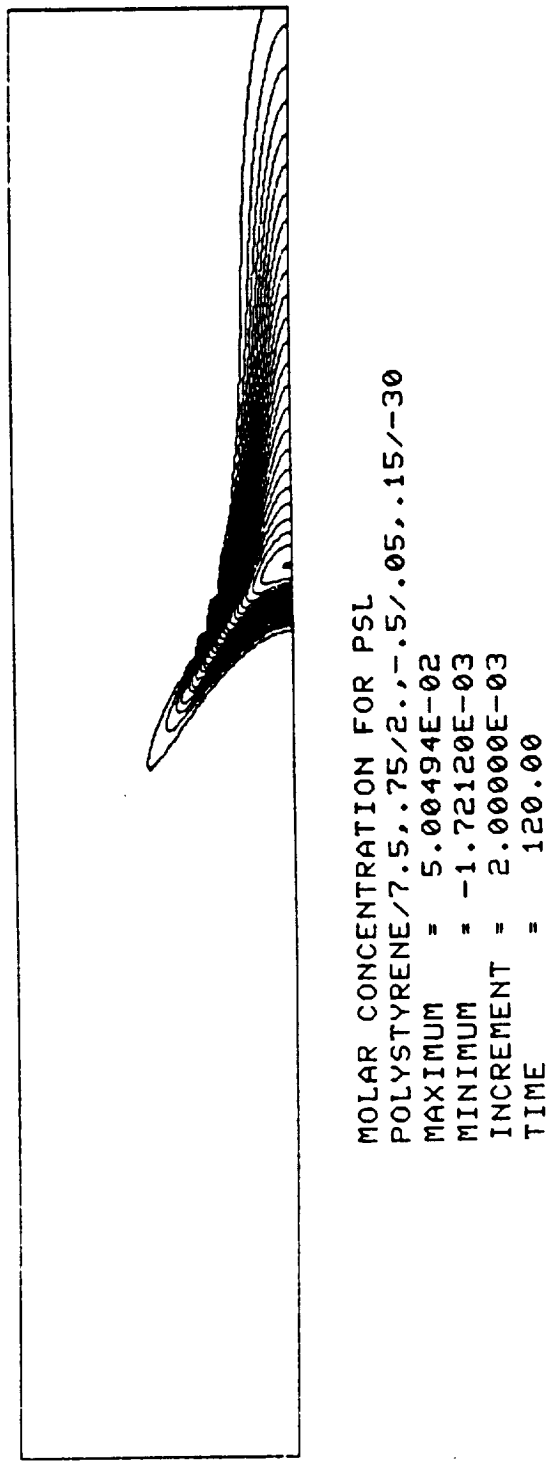

Figure 38. Latex Concentration for Strong PSL Case at 120 Seconds

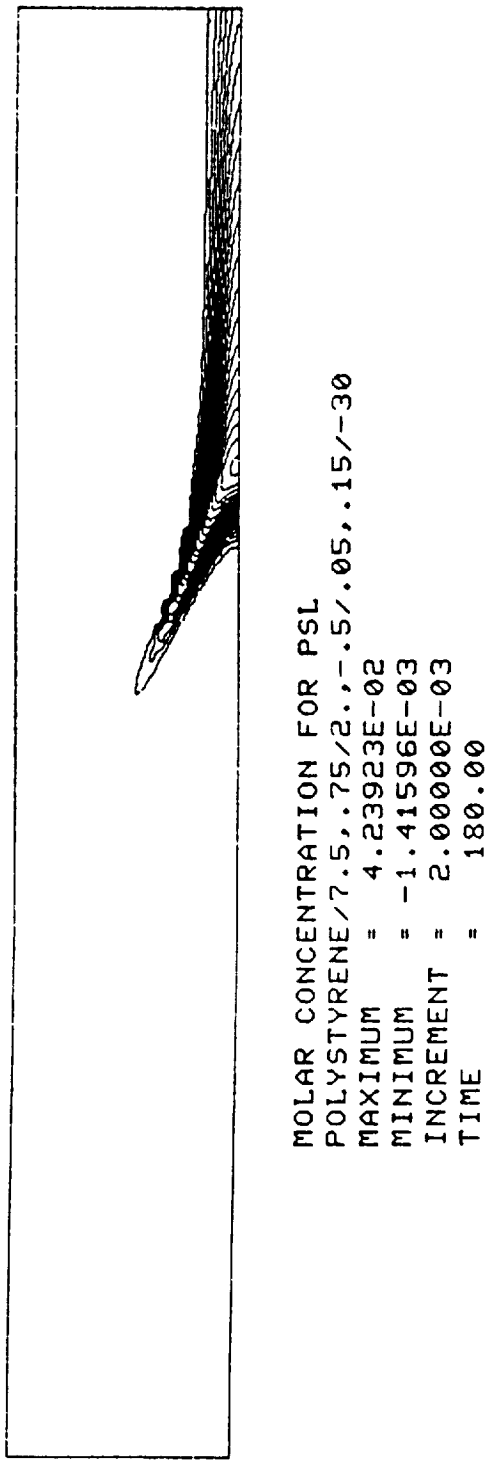

Figure 39. Latex Concentration for Strong PSL Case at 180 Seconds

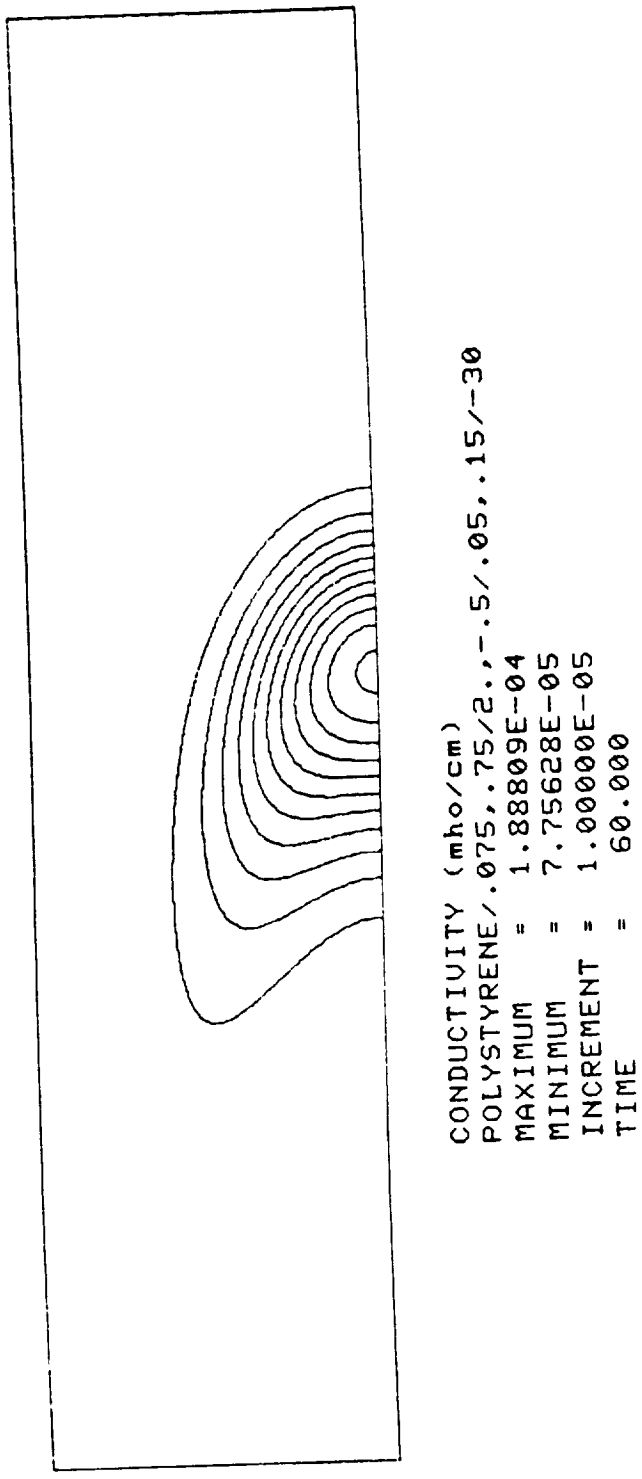

Figure 40. Conductivity for Weak PSL Case at 60 Seconds

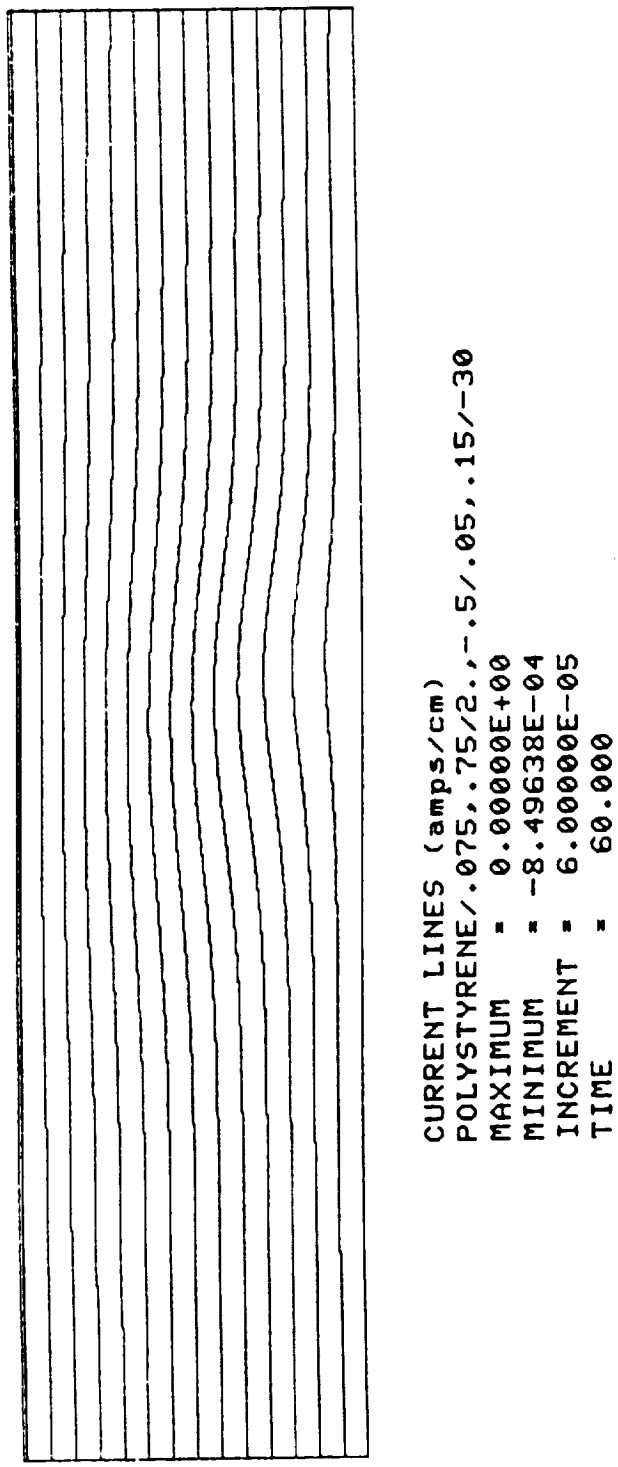

Figure 41. Current Lines for Weak PSL Case at 60 Seconds

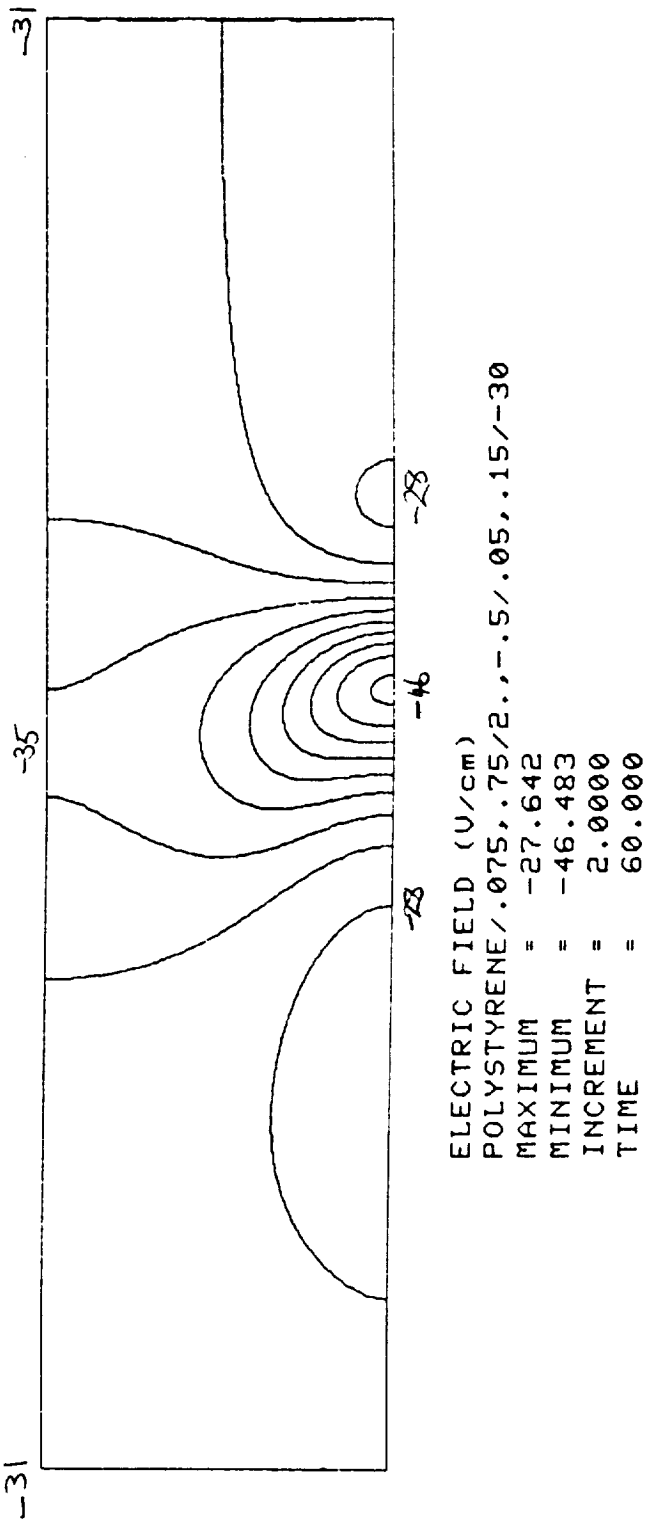

Figure 42. Electric Field for Weak PSL Case at 60 Seconds

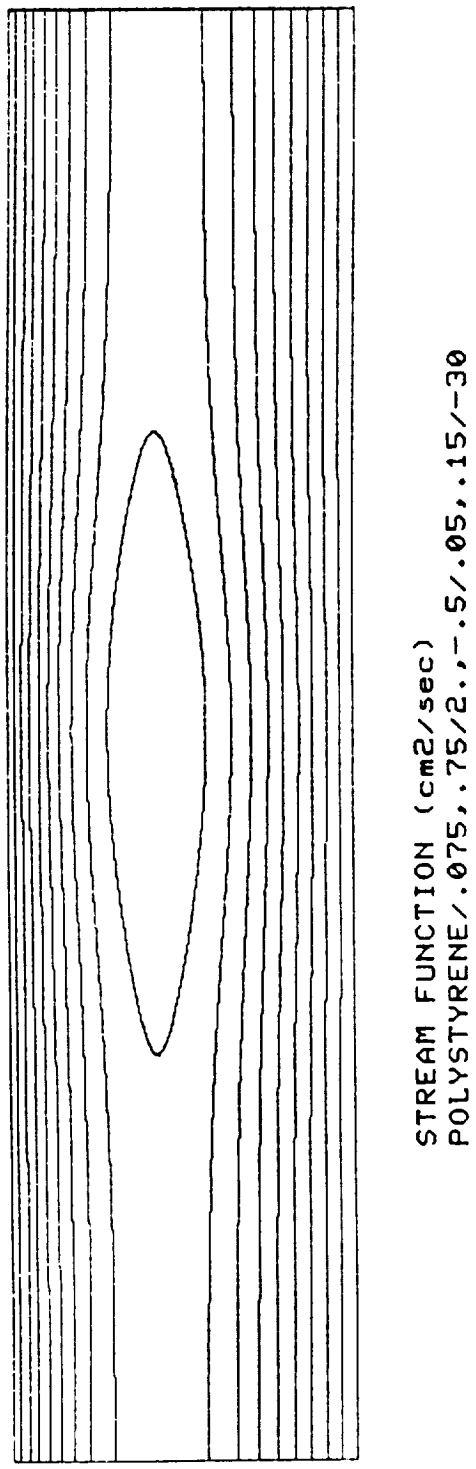

Figure 43. Stream Function for Weak PSL Case at 60 Seconds

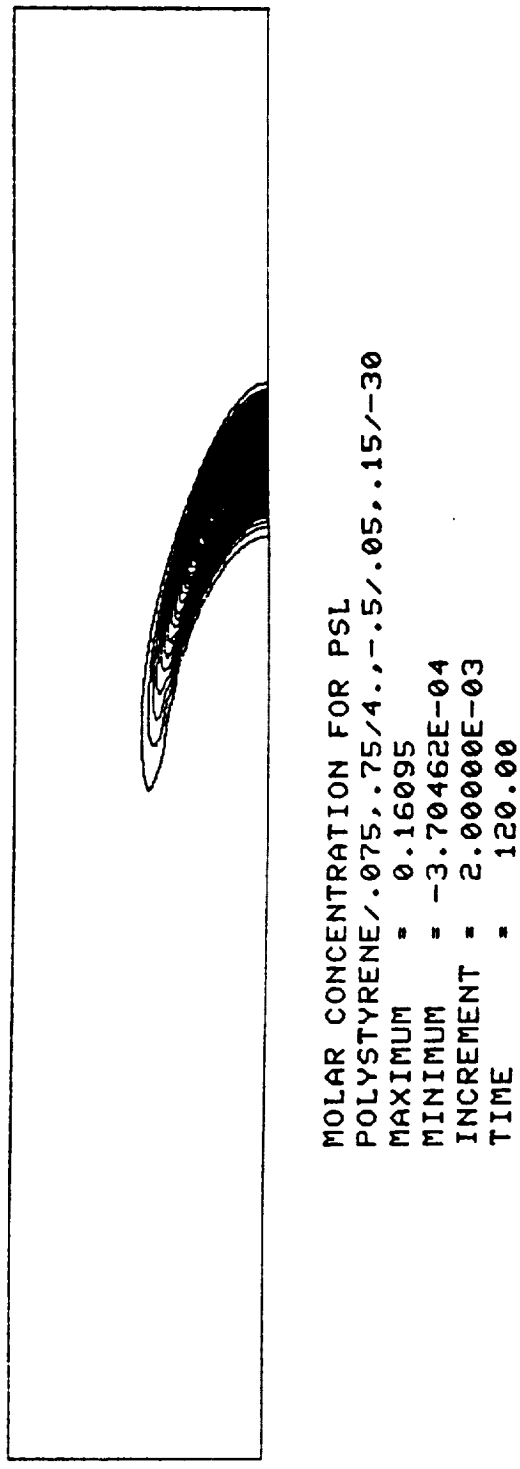

Figure 44. Latex Concentration for Weak PSL Case at 120 Seconds

HEM-ACETATE-CFE/.75X,8.8%/4E-4/.05,.15/-30 ***PROBLEM PARAMETERS***

Z MESH		Y MESH		SAMPLE ELECTRIC FIELD		WATER MOBILITIES BOUNDARY FLOW		SIDE BOUNDARY CONDITIONS 1/2/3 FOR BUFFER/SAMPLE/NO-FLUX	
ZBL =	-0.2000000	YT =	0.1500000	YSAMP =	0.0000000	UH =	0.0036000	ILEFT =	1
ZBR =	0.2000000	YB =	0.0000000	RSAMP =	0.0500000	UOH =	0.0020000	IRIGHT =	1
ZDL =	0.0000000	DYRAT =	1.4000000	PSAMP =	2.0000000	UWE =	0.0004000	LCOND =	F
ZDR =	0.0030000	IY =	0	CZERO =	-100.0000000	WB =	0.0000000		
DZRAT =	2.0000000	YWALL =	0.0000000	EZERO =	-30.0000000	UB =	0.0000000		
		YMESH =	0.0300000						

SPECIES	BUFFER MOLARITY	SAMPLE MOLARITY	SINGLE ION MOBILITY	IONIZATION DEFINITION CONSTANTS N				N			N			N		
SODIUM	0.00200000	0.00200000	0.00052700	-3.00	1.00	0.00	0.00	0.00	0.00	0.00	0.00	0.00	0.00	0.00	0.00	0.00
ACETATE	0.00300000	0.00300000	0.00050000	-1.00	4.70	0.00	0.00	0.00	0.00	0.00	0.00	0.00	0.00	0.00	0.00	0.00
HEMOGLOBIN A	0.00000000	0.00130000	0.00001000	36.09	25.74	3.39	7.86	17.32	6.82	10.45	11.40	6.97	6.99	12.65	4.99	4.79

METHOD PARAMETERS

SPECIES	TSTEP	UPWNDA	UPWNDC	FIXCZ	FIXCY	THZFX	BETDG	BETAO	BETAD	BETCO	BETCD
SODIUM	0.200	0.950	0.950	T	T	0.167	0.6	0.6	0.6	0.6	0.6
ACETATE	0.200	0.950	0.950	T	T	0.167	0.6	0.6	0.6	0.6	0.6
HEMOGLOBIN-A	0.200	0.950	0.950	T	T	0.167	0.6	0.6	0.6	0.6	0.6

NSTEP = 450 NPITER = 7 PEXTRP = 0.500

OUTPUT PARAMETERS

DIRECT ACCESS READ & WRITE SEGMENTS ISEGR = 2 ISEGW = 1
(0: ANALYTIC, -1: AFTER PRIOR CASE)
WRITE STEP BEGINNING & INCREMENT IBEGDA = 150 IINCDA = 150
ZPLL = 0.00 ZPLR = 0.00 YPLB = 0.00
DIAGNOSTIC FREQUENCY NDIAG = 0
CONTOUR LINES NCLP = 28 NCLI = 0 YPLT = 0.00 NCOPIES = 1

VARIABLE	ISTEP BEGIN & INCREMENT FOR PRINTER DIAGNOSTICS PHYSICAL	CONTOUR	INTEGER	CONTOUR	PRINT NUMBERS		RANGES FOR I AND K IB	IE	II	KB	KE	KI	PLOTTER IDAOUT BEGIN & INCREMENT PHYSICAL		INTEGER		INCR
pH	150	150	9903	9904	9905	9906	1	42	1	17	1	-1	1	1	9915	9916	0.0
SIGMA	150	150	9903	9904	9905	9906	1	42	1	17	1	-1	1	1	9915	9916	0.0
PHI	9901	9902	9903	9904	9905	9906	1	42	1	17	1	-1	9913	9914	9915	9916	0.0
CURRENT	150	150	9903	9904	9905	9906	1	41	1	16	1	-1	1	1	9915	9916	0.0
EZ	150	150	9903	9904	9905	9906	1	41	1	16	1	-1	1	1	9915	9916	0.0
EY	9901	9902	9903	9904	9905	9906	1	41	1	16	1	-1	9913	9914	9915	9916	0.0
IONDCP	9901	9902	9903	9904	9905	9906	1	41	1	16	1	-1	9913	9914	9915	9916	0.0
PSI	150	150	9903	9904	9905	9906	1	41	1	16	1	-1	1	1	9915	9916	0.0
SODIUM																	
CONC	150	150	9903	9904	9905	9906	1	42	1	17	1	-1	1	1	9915	9916	0.0
MEAN ION	9901	9902	9903	9904	9905	9906	1	42	1	17	1	-1	9913	9914	9915	9916	0.0
MEAN SQU	9901	9902	9903	9904	9905	9906	1	42	1	17	1	-1	9913	9914	9915	9916	0.0
CHARGE	9901	9902	9903	9904	9905	9906	1	42	1	17	1	-1	9913	9914	9915	9916	0.0
SIGMA	9901	9902	9903	9904	9905	9906	1	42	1	17	1	-1	9913	9914	9915	9916	0.0
DCONC	9901	9902	9903	9904	9905	9906	1	42	1	17	1	-1	9913	9914	9915	9916	0.0
VELOCITY	9901	9902	9903	9904	9905	9906	1	42	1	17	1	-1	9913	9914	9915	9916	0.0
FLUX	9901	9902	9903	9904	9905	9906	1	42	1	17	1	-1	9913	9914	9915	9916	0.0
ACETATE																	
CONC	150	150	9903	9904	9905	9906	1	42	1	17	1	-1	1	1	9915	9916	0.0
MEAN ION	9901	9902	9903	9904	9905	9906	1	42	1	17	1	-1	9913	9914	9915	9916	0.0
MEAN SQU	9901	9902	9903	9904	9905	9906	1	42	1	17	1	-1	9913	9914	9915	9916	0.0
CHARGE	9901	9902	9903	9904	9905	9906	1	42	1	17	1	-1	9913	9914	9915	9916	0.0
SIGMA	9901	9902	9903	9904	9905	9906	1	42	1	17	1	-1	9913	9914	9915	9916	0.0
DCONC	9901	9902	9903	9904	9905	9906	1	42	1	17	1	-1	9913	9914	9915	9916	0.0
VELOCITY	9901	9902	9903	9904	9905	9906	1	42	1	17	1	-1	9913	9914	9915	9916	0.0
FLUX	9901	9902	9903	9904	9905	9906	1	42	1	17	1	-1	9913	9914	9915	9916	0.0
HEMOGLOBIN A																	
CONC	150	150	9903	9904	9905	9906	1	42	1	17	1	-1	1	1	9915	9916-5.E-5	
MEAN ION	9901	9902	9903	9904	9905	9906	1	42	1	17	1	-1	9913	9914	9915	9916	0.0
MEAN SQU	9901	9902	9903	9904	9905	9906	1	42	1	17	1	-1	9913	9914	9915	9916	0.0
CHARGE	9901	9902	9903	9904	9905	9906	1	42	1	17	1	-1	9913	9914	9915	9916	0.0
SIGMA	9901	9902	9903	9904	9905	9906	1	42	1	17	1	-1	9913	9914	9915	9916	0.0
DCONC	9901	9902	9903	9904	9905	9906	1	42	1	17	1	-1	9913	9914	9915	9916	0.0
VELOCITY	9901	9902	9903	9904	9905	9906	1	42	1	17	1	-1	9913	9914	9915	9916	0.0
FLUX	9901	9902	9903	9904	9905	9906	1	42	1	17	1	-1	9913	9914	9915	9916	0.0

Figure 45. Input Data for Hemoglobin Acetate Case

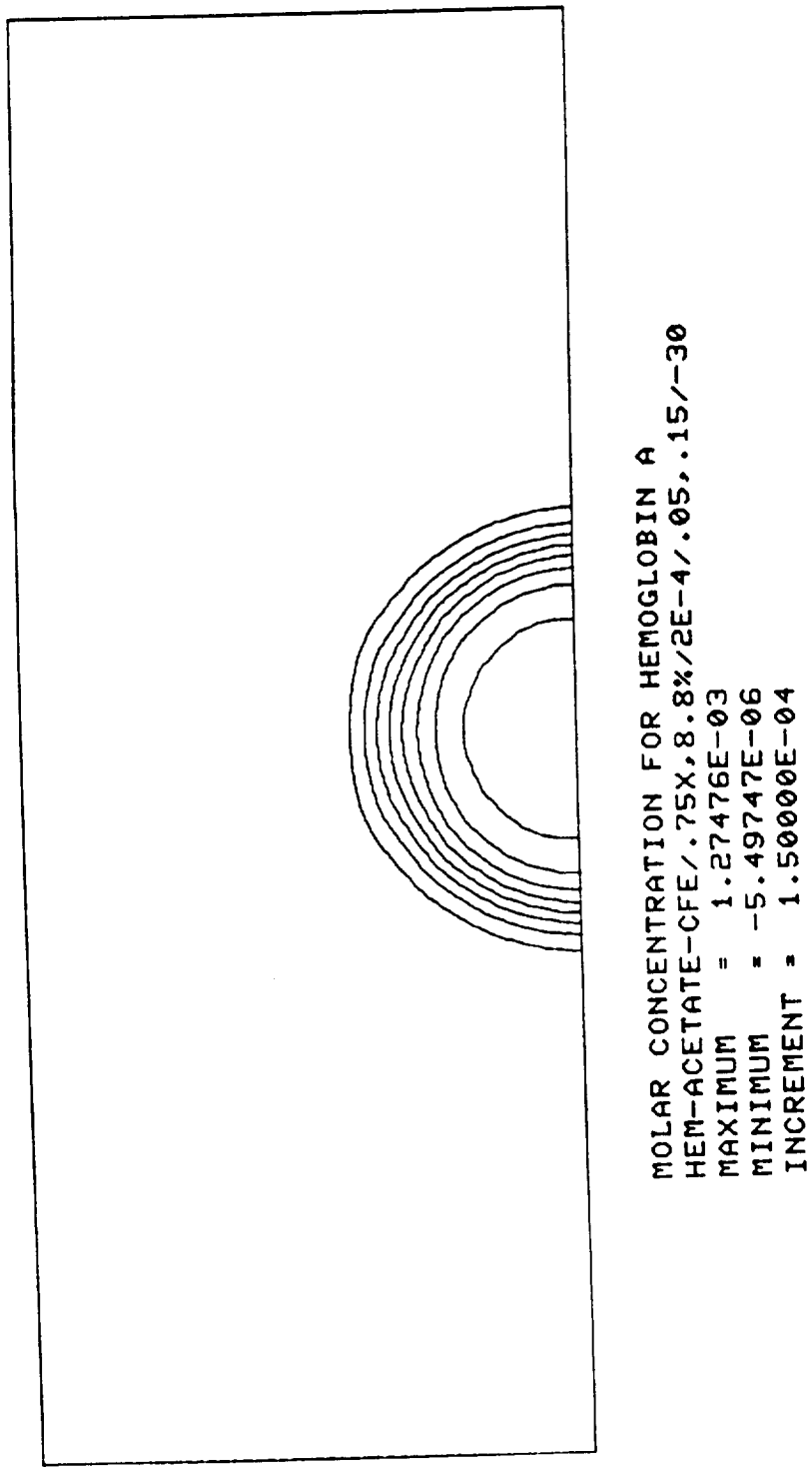

Figure 46. Initial Hemoglobin Concentration for Hemoglobin Acetate Case

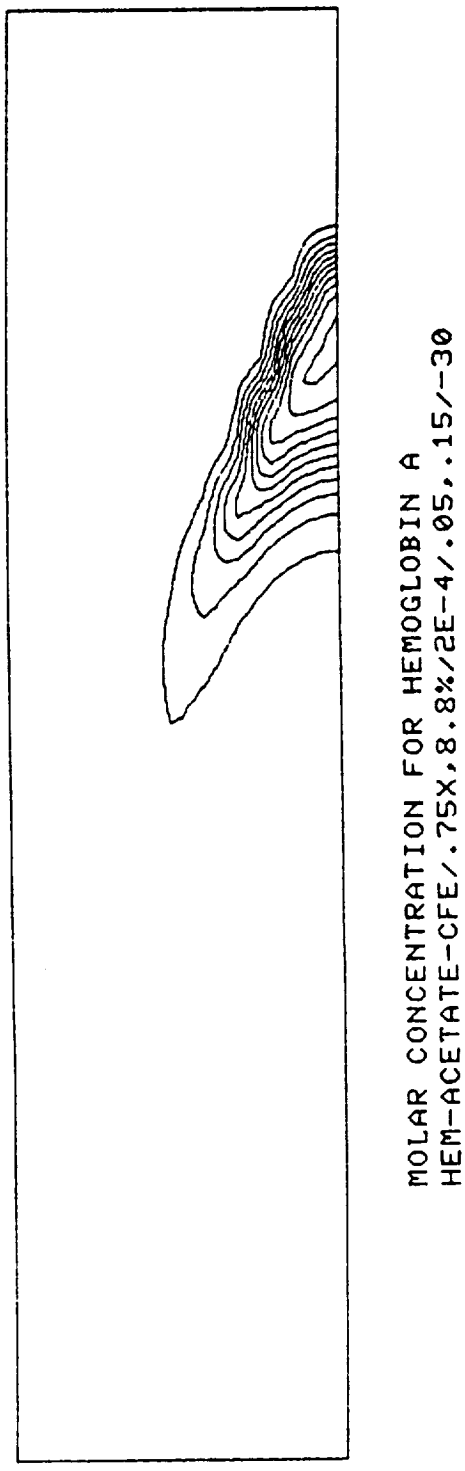

Figure 47. Hemoglobin Concentration for Hemoglobin Acetate Case at 90 Sec

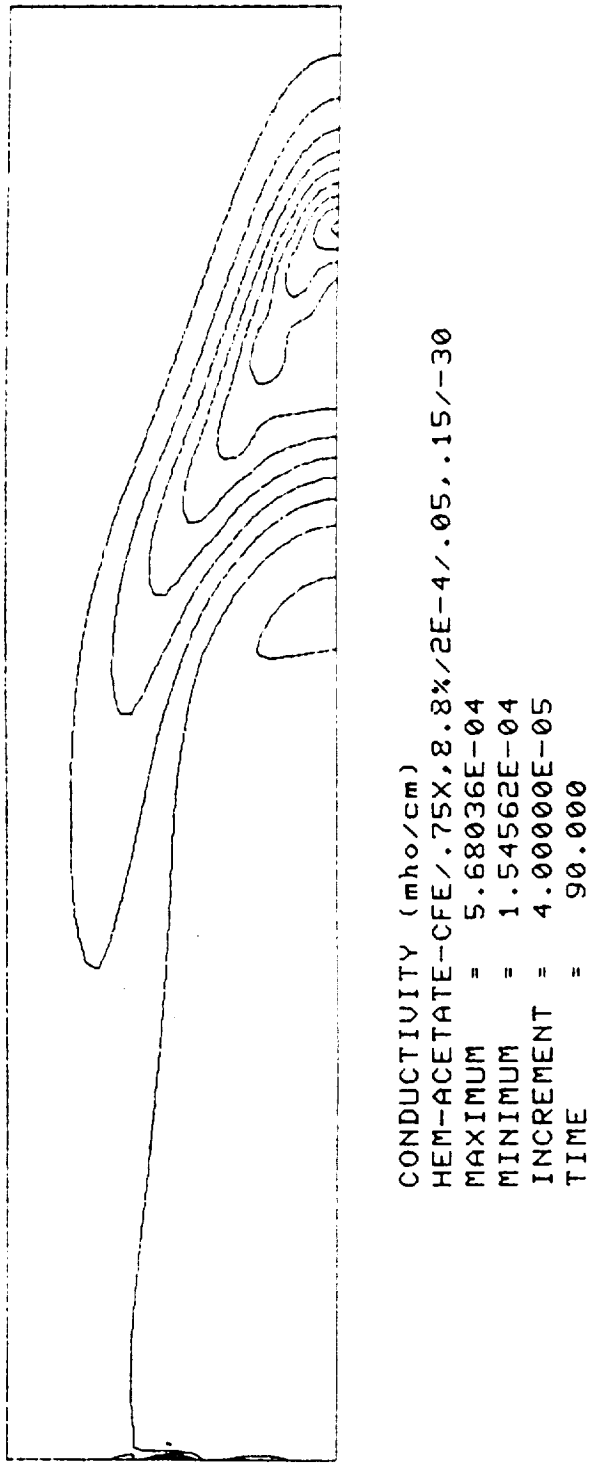

Figure 48. Conductivity for Hemoglobin Acetate Case at 90 Sec

(continued from page 54)

factor of almost 4; much less than the huge factors which developed in Case 2. The current lines are shown in Figure 49; and the electroosmosis flow driven by the nonuniform field at the wall is shown in Figure 50.

Figure 51 contours the hemoglobin molarity at the cross-section corresponding to a mean residence time of 240 seconds. The peak is now down only 27% from its initial value, and the bleeding to the left is still not visible, because of the contour increment. The current lines are shown in Figure 52; and the electroosmosis flow driven by the nonuniform field at the wall is shown in Figure 53. A lot of spreading has occurred, though less than in corresponding cases on the cellulose acetate film. We believe that the bending of the high conductivity region on the right into a crescent around the hemoglobin and the depleted region on the left provides a path for the current, and decreases the effectiveness of the process which maintains and amplifies the conductivity contrast.

However, the mean residence time to achieve this spreading is 4 minutes. Experimentally, the same spreading is achieved in 20 seconds or so. It is apparent that these mechanisms are not adequate to explain the observations.

2.6 ANALYTIC STUDIES OF THE ELECTRIC AND DIELECTRIC BODY FORCE

We have concluded that the electric and dielectric body forces play a significant role in sample spreading.

Taylor (1966) analyzed the electrohydrodynamic flow near a fluid sphere with conductivity and dielectric constant different from those of the surrounding fluid. We have extended his analysis to the cylindrical case, and to the time-dependent case where the circular cross section becomes an ellipse, and we can follow the early stages of its evolution (Snyder, et al., 1988). Only a small part of this analysis was done under this contract.

2.7 EXPERIMENTAL VALIDATIONS OF THE BODY FORCE

The conclusive experimental validations were done with an AC applied voltage, and resulted in the flattening of a circular sample stream to a ribbon, either aligned with the field (for a high-conductivity sample) or normal to the field (for a low conductivity sample). We provided extensive support in the preliminary experiments to analyze the electric and dielectric body forces. These experiments used a suspension of polystyrene latex microspheres in a barbital buffer, injected as sample into a barbital buffer with a differing conductivity, and used an AC electric field. The use of AC eliminates net ion migration and electroosmosis, and by using relatively low buffer conductivities, convection can be kept at negligible levels. Depending on the relative size of the conductivities (and on the magnitude of the field), the initially circular sample was either compressed or stretched by the electric field into a flat ribbon. This was in agreement with analytic predictions based on the force on the charge density. This work is reported in Snyder, et al., (1988).

We have also worked with MSFC personnel in the development of a moving-wall electrophoresis device.

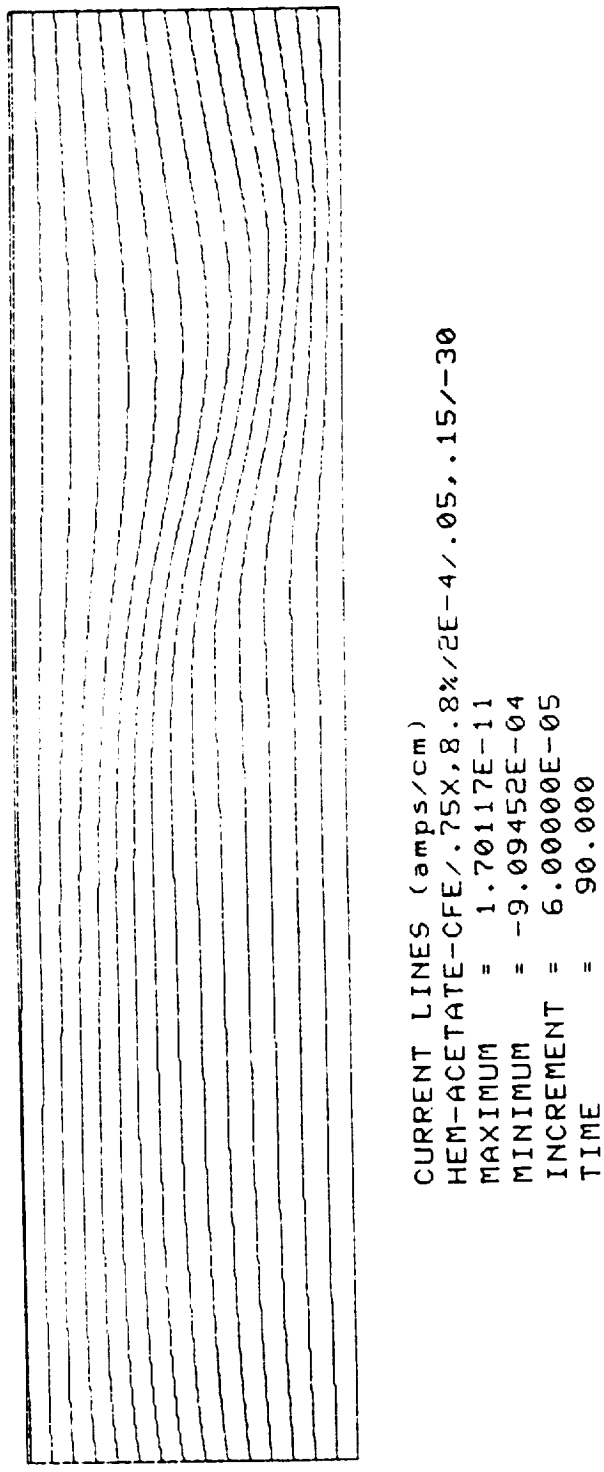

Figure 49. Current Lines for Hemoglobin Acetate Case at 90 Sec

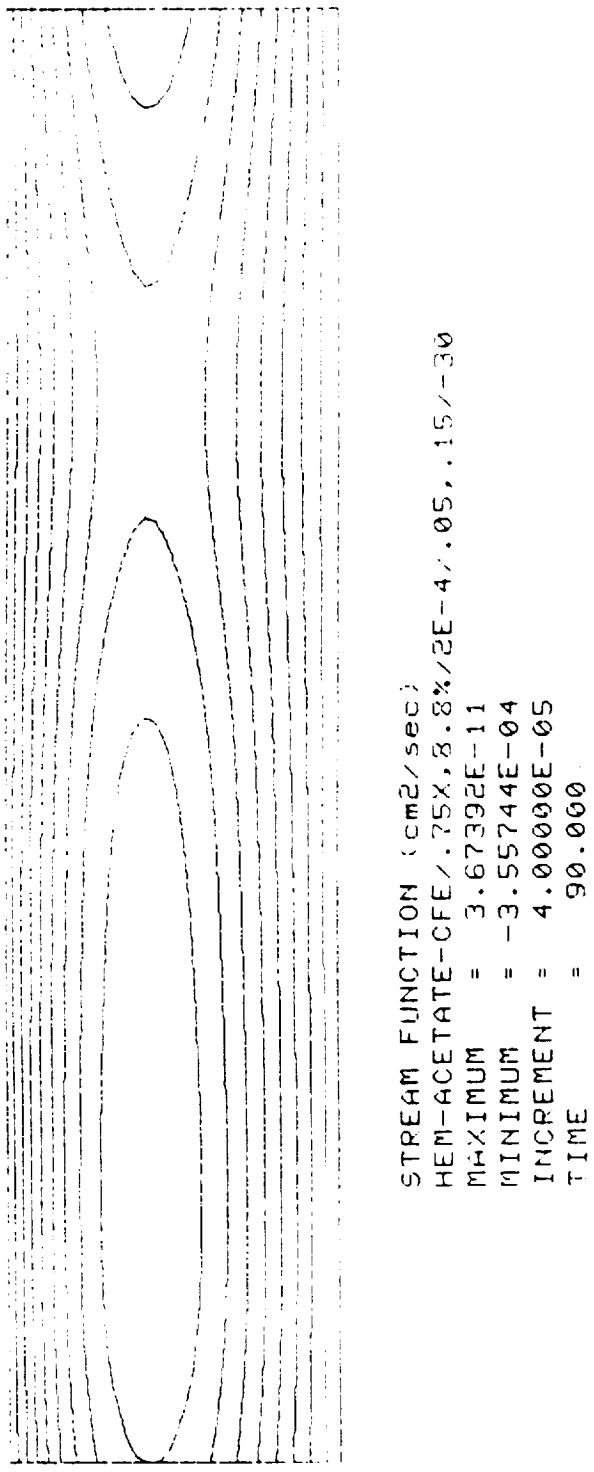

Figure 50. Stream Function for Hemoglobin Acetate Case at 90 Sec

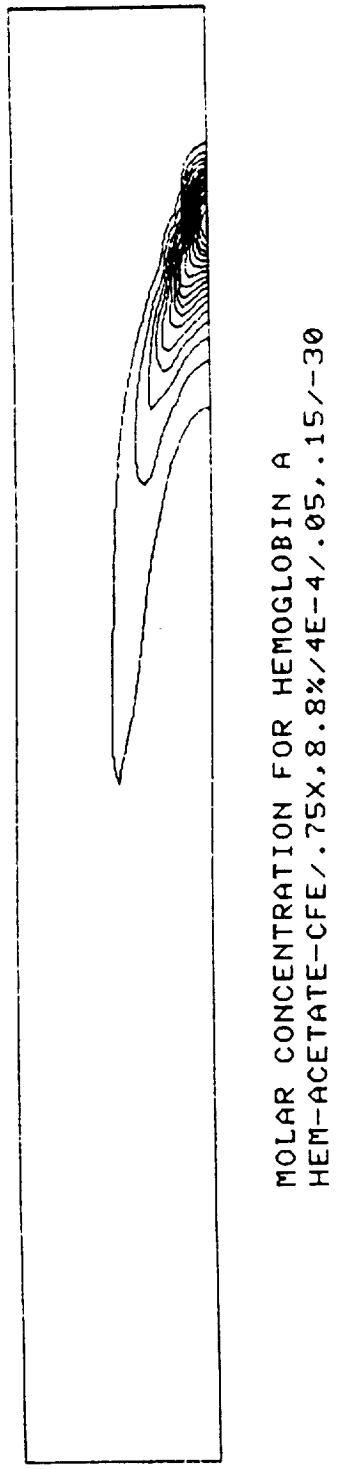

Figure 51. Hemoglobin Concentration for Hemoglobin Acetate Case at 240 Sec

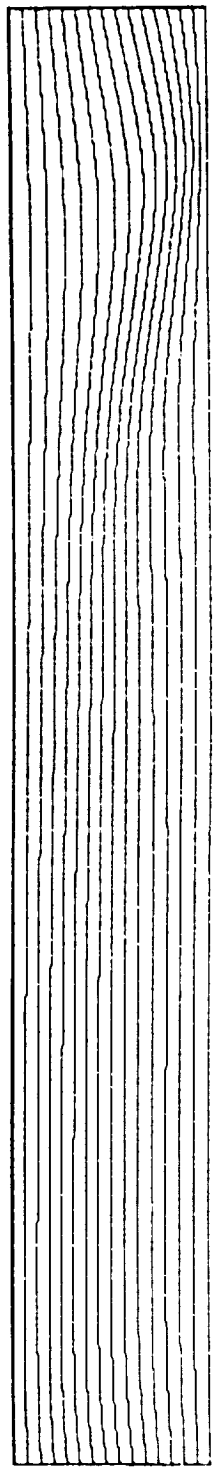

Figure 52. Current Lines for Hemoglobin Acetate Case at 240 Sec

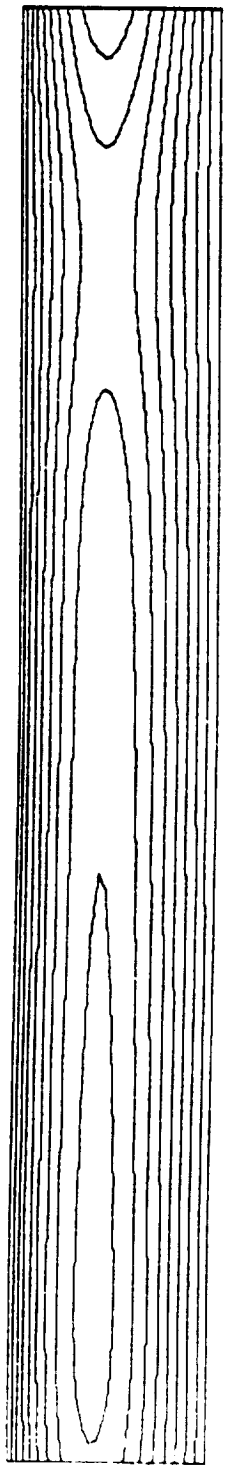

Figure 53. Stream Function for Hemoglobin Acetate Case at 240 Sec

Chapter 3
SUMMARY OF FINDINGS

Our key finding in the program was this discovery of the importance of the electric and dielectric body forces. Together with this was the finding that electroosmosis and electrokinetics alone are inadequate to explain the observed spreading phenomena near the injection port.

In addition, our understanding of the electrokinetics has been much extended.

We discovered that even when the protein concentration are low, and the protein is essentially passive, protein can be trapped in a sample column of high conductivity (and therefore low field). It leaks out slowly, and as a consequence is stretched in the field direction.

We discovered the phenomenon of electrodialysis, which occurs when the sample includes large concentrations of big protein molecules like hemoglobin. The protein suppresses or increases the ionization of one of the buffer components, by moving the pH towards its own pI value. This changes the proportions of the current carried by the two buffer components, travelling in opposite directions with opposite charges. As a result, both components are depleted on the side of the sample towards which the big protein molecules are moving, and accumulate on the other.

We discovered that the electrokinetic equation can allow the propagation with minimal change in shape of strongly nonlinear wave packets.

We have analyzed free-flow electrophoresis effects in the distortion of a single-protein sample. These studies were undertaken prior to our discovery of the importance of electrohydrodynamic body forces, and therefore did not include them. The hydrodynamics was limited to the streamwise Poiseuille flow and to electroosmosis. We made the following discoveries.

The field at the wall is nonuniform, due to conductivity variations either between the sample and buffer or caused by the presence of significant amounts of large protein molecules in the sample. This leads to a nonuniform slip velocity. The divergence of the corresponding electroosmosis flux near the wall leads to transverse flows, which can distort the sample towards or away from the symmetry axis.

The electroosmotic distortion of a high-conductivity region into a crescent provides a path for the electric current around the crescent, and thus reduces the field in its interior. This can slow the processes which amplify the high-conductivity region.

Electroosmosis is probably not a major contributing factor in electrophoresis performance degradation, except when there is some other effect forcing the sample very rapidly away from the center of the chamber.

Chapter 4
REFERENCES

M. Bier, O.A. Palusinski, R.A. Mosher, and D.A. Saville, 1983, "Electrophoresis. Mathematical Modeling and Computer Simulation", Science 219, pp. 1281-1287.

D. Dewey and A. Graham, 1983, "Models and Simulations of Electroosmosis in Segmented Channels", Manuscript.

B. Ellerbroek and A. Kolin, 1979, "Thermal Convection in a Uniformly Heated Fluid Between Vertical Parallel Plates", J. Appl. Phys. 50, pp. 5544-6.

E.D. Lynch and D.A. Saville, 1981, "Heat Transfer in the Thermal Entrance Region of an Internally Heated Flow", Chem. Eng. Comm. 9, pp. 201-211.

T.Y. Miller, G.O. Williams and R.S. Snyder, 1985, "Effect of Conductivity and Concentration on the Sample Stream in the Transverse Axis of a Continuous Flow Electrophoresis Chamber", Electrophoresis 1985, 6, 377-381.

P.H. Rhodes, 1979, "Sample Stream Distortion Modeled in Continuous-Flow Electrophoresis", NASA TM-78178, MSFC, Alabama.

P.H. Rhodes and R.S. Snyder, 1981, "Numerical Analysis of Continuous Flow Electrophoresis", pp. 899-917, Electrophoresis '81, ed. Allen and Arnaud, Walter de Gruyter & Co., Berlin.

P.H. Rhodes and R.S. Snyder, 1982, "The Effect of Small Temperature Gradients on Flow in a Continuous Flow Electrophoresis Chamber", pp. 225-232, Materials Processing in the Reduced Gravity Environment of Space, ed. G. Rindone, Elsevier.

P.H. Rhodes and R.S. Snyder, 1986, "Sample Band Spreading Phenomena in Ground and Space-Based Electrophoretic Separators", Electrophoresis 1986, 7, 113-120.

P.H. Rhodes, G.O. Roberts and R.S. Snyder, 1988, "Electrokinetics of Sample Spreading in Continuous Flow Electrophoresis", To appear.

D. Richman, 1984, Private communication.

G.O. Roberts, 1984a, "Models of Electroosmosis in Segmented Cylinders and the effects of Rotation", Report RAI-84-A-1, 29pp.

G.O. Roberts, 1984b, "Analysis of Electrophoresis Performance", Report RAI-84-E-3, 58pp.

G.O. Roberts, 1984c, "Simulations of Uniform Electroosmosis Effects on Isoelectric Focusing", Report RAI-84-A-2, 78pp.

G.O. Roberts, 1984d, "Further Simulations of Uniform Electroosmosis Effects on Isoelectric Focusing", Report RAI-84-A-3, 128pp.

G.O. Roberts, 1985, "Analysis of Electrophoresis Performance", Report RAI-85-E-4, 3pp.

G.O. Roberts, 1986, "Three-Dimensional Electrophoresis Code" Report RAI-86-E3-1, 152pp.

D.A. Saville, 1978, "Fluid Mechanics of Continuous Flow Electrophoresis", Princeton University, Final report on Contract NAS8-31349.

R.S. Snyder, P.H. Rhodes and G.O. Roberts, 1988, "Electrohydrodynamic Distortion of Sample Streams in Continuous Flow Electrophoresis", Accepted for J. of Colloid and Interface Science.

G.I. Taylor, 1966, "Studies in Electrohydrodynamics. I. The Circulation Produced in a Drop by an Electric Field", Proc. Roy. Soc. Lond., Ser. A, 291, pp. 159ff.

ACKNOWLEDGEMENTS

It is a pleasure to acknowledge the significant contributions of David Donovan of RAI to this work. We also benefited from many discussions with Percy Rhodes of MSFC, and enjoyed his leadership in the experimental work. Invaluable support was provided by Dr. Robert S. Snyder, the COTR.

APPENDIX

MODEL EQUATIONS

On the following pages we present copies of viewgraphs which provide a summary of the model equation and numerical methods used in the SAMPLE code.

ORGANIZATION: RAI	MARSHALL SPACE FLIGHT CENTER	NAME: GLYN ROBERTS
CHART NO.: 1	ELECTROPHORESIS PERFORMANCE THE SAMPLE CODE	DATE: JUNE 30, 1988

CONTENTS

ORGANIZATION: RAI	MARSHALL SPACE FLIGHT CENTER ELECTROPHORESIS PERFORMANCE THE SAMPLE CODE	NAME: GLYN ROBERTS
CHART NO.: 2		DATE: JUNE 30, 1988

PROTEIN SEPARATION BY ELECTROPHORETIC MOBILITY AT VARYING pH

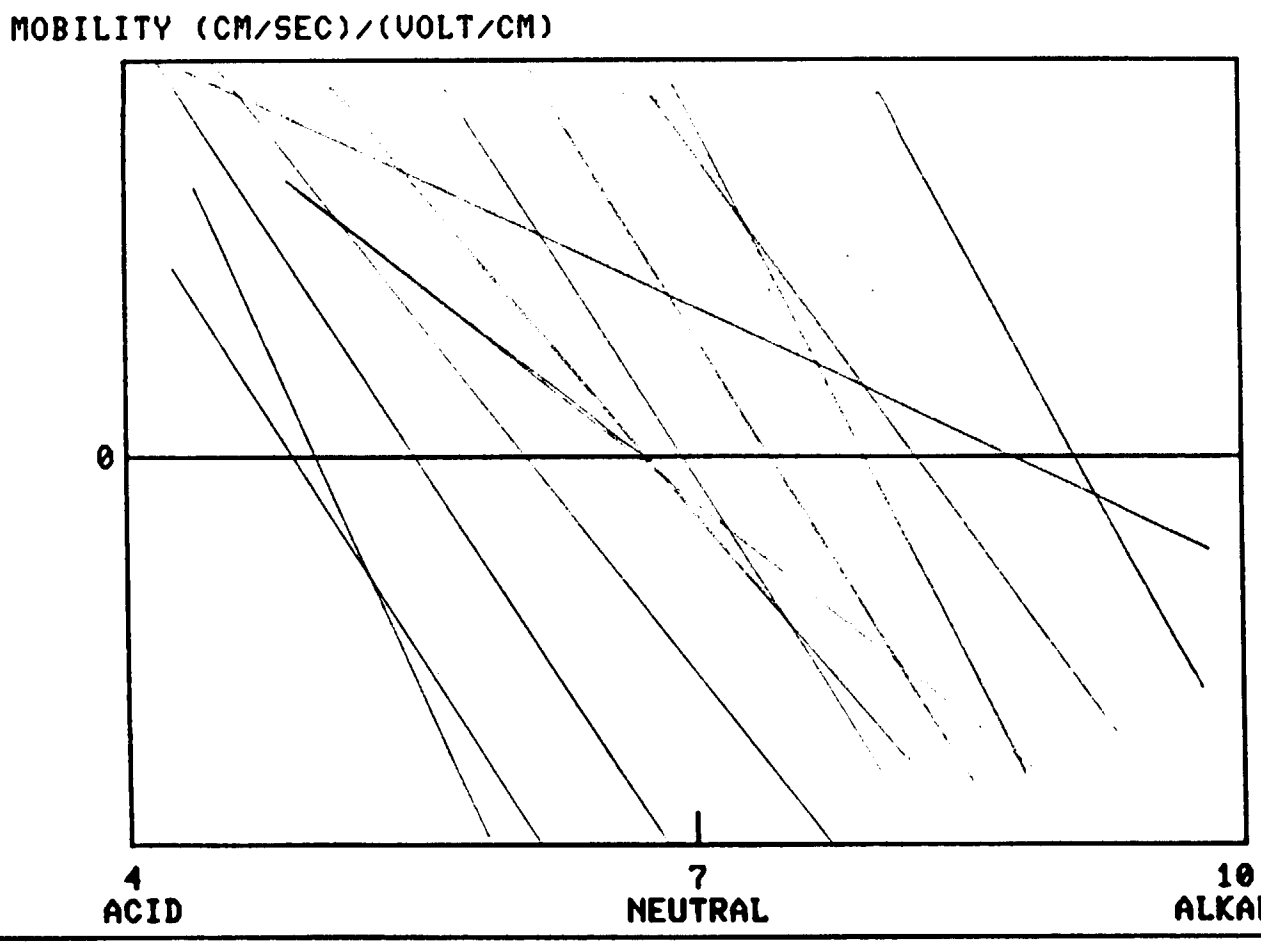

7-JUL-88 19:15

ORGANIZATION: RAI	MARSHALL SPACE FLIGHT CENTER	NAME: GLYN ROBERTS
CHART NO.: 3	ELECTROPHORESIS PERFORMANCE THE SAMPLE CODE	DATE: JUNE 30, 1988

CONTINUOUS FLOW ELECTROPHORESIS (CFE)

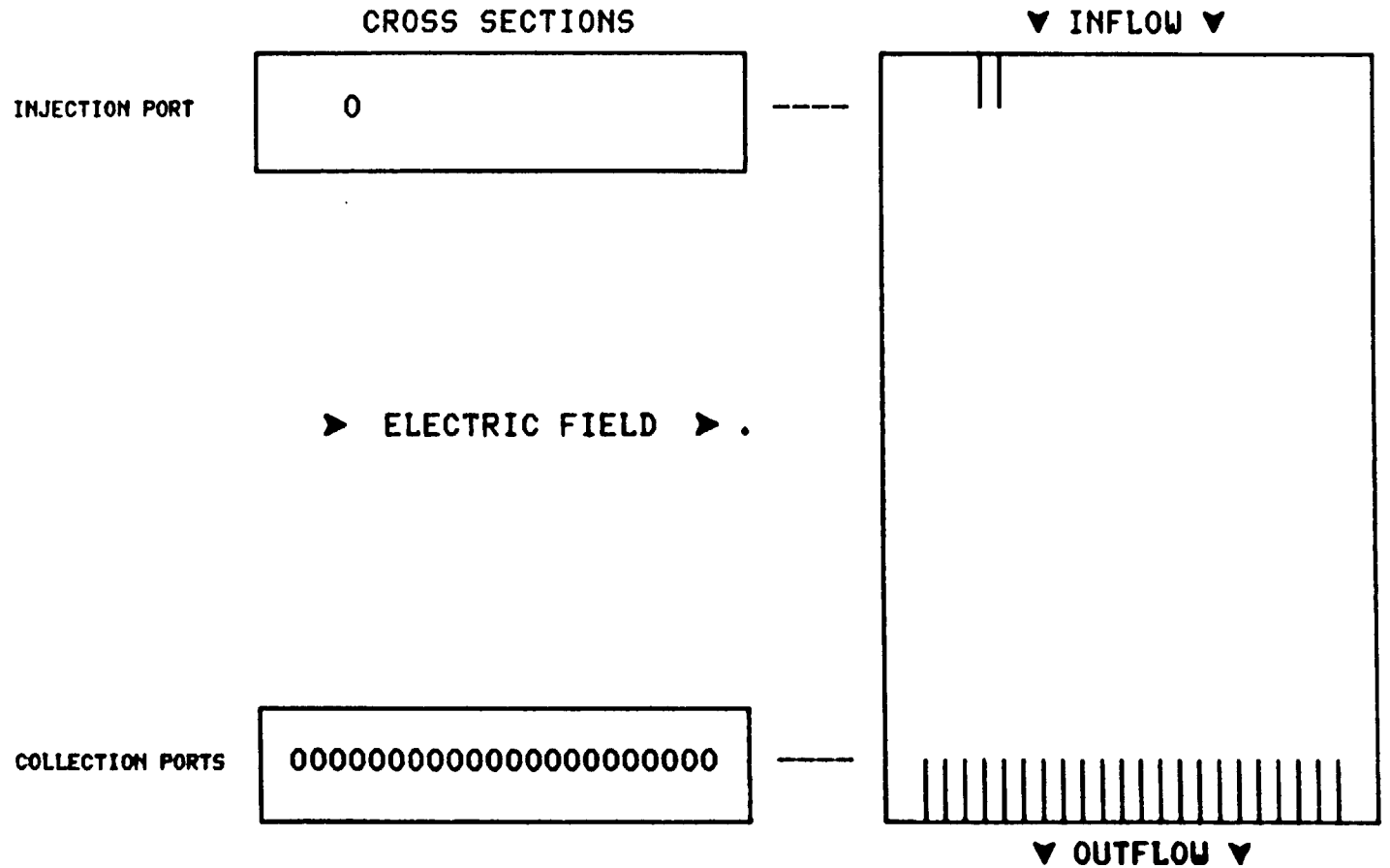

7-JUL-88 19:16

ORGANIZATION: RAI	MARSHALL SPACE FLIGHT CENTER	NAME: GLYN ROBERTS
CHART NO.: 4	ELECTROPHORESIS PERFORMANCE THE SAMPLE CODE	DATE: JUNE 30, 1988

PROBLEMS WITH CFE

- WALL FRICTION AND WALL ELECTRO-OSMOSIS
  - DISTORTS CROSS SECTIONS TO CRESCENTS
  - RESULTING RESTRICTIONS ON RADIUS
  - BUT THIS RESTRICTS THROUGHPUT
  - ALLEVIATED BY PLANNED MOVING-WALL APPARATUS
- NON-UNIFORM ELECTRIC FIELD
  - DISTORTS CROSS SECTION AND OFTEN INCREASES IT
  - AGGRAVATES DISTORTION BY WALL EFFECTS
  - CAUSED BY NON-UNIFORM CONDUCTIVITY DUE TO SAMPLE
  - ALLEVIATED BY LOW CONCENTRATIONS
  - BUT THIS RESTRICTS THROUGHPUT
- NON-UNIFORM FLOW ALONG COLUMN
  - CAUSED BY CHAMBER SHAPE AND DESIGN AND ENTRY FLOW
  - CAUSED BY CONVECTION, DUE TO OHMIC HEATING AND GRAVITY
  - ALLEVIATED BY SMALL CHAMBER DIMENSIONS
  - BUT THIS RESTRICTS THROUGHPUT
- MYSTERY PROBLEMS
  - A/C FIELD TURNS SAMPLE COLUMN TO A RIBBON
  - CERTAIN SAMPLES APPEAR TO BREAK DOWN

7-06-88 19:16

ORGANIZATION: RAI	MARSHALL SPACE FLIGHT CENTER	NAME: GLYN ROBERTS
CHART NO.: 5	ELECTROPHORESIS PERFORMANCE THE SAMPLE CODE	DATE: JUNE 30, 1988

TWO-DIMENSIONAL ELECTROPHORESIS EXPERIMENTS WITH ACETATE FILM

SAMPLE

▼

▶ ELECTRIC FIELD ▶

THIS SYSTEM WAS DESIGNED FOR ONE-DIMENSIONAL ELECTROPHORESIS, WITH LINEAR SAMPLES. WE HAVE USED IT FOR CFE STUDIES, WITH CIRCULAR SAMPLES.

INITIAL SAMPLE

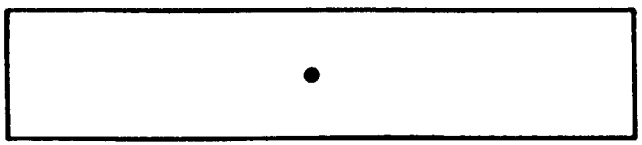

FINAL SAMPLES (TYPICAL)

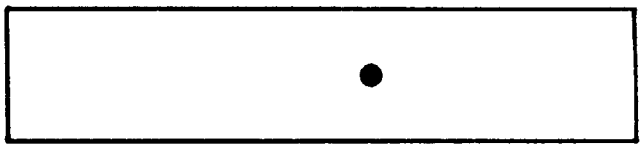

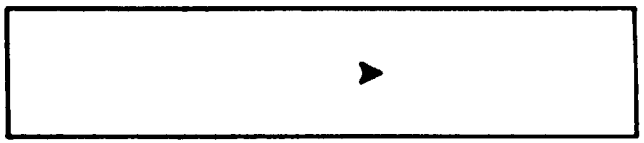

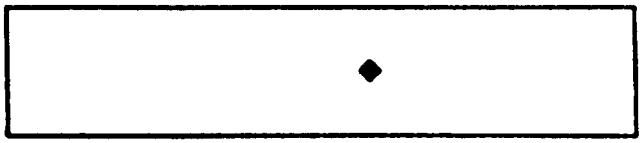

7-JUL-88 19:16

ORGANIZATION: RAI	MARSHALL SPACE FLIGHT CENTER	NAME: GLYN ROBERTS
CHART NO.: 6	ELECTROPHORESIS PERFORMANCE THE SAMPLE CODE	DATE: JUNE 30, 1988

ISOELECTRIC FOCUSING

THIS IS A DIAGNOSTIC METHOD OF WIDE BIOCHEMICAL APPLICATION.

ELECTROLYSIS OF AN AMPHOLYTE MIXTURE IN A GEL BETWEEN IMPERMEABLE ELECTRODES ESTABLISHES A STEADY pH GRADIENT.
AMPHOLYTES, INCLUDING ANY PROTEINS, ARE FOCUSED AT THE pH VALUE AT WHICH THEIR MEAN IONIZATION IS ZERO (ISOELECTRIC POINT).
SMALL AMPHOLYTE MOLECULES HAVE LARGER DIFFUSIVITIES, AND ARE DISTRIBUTED OVER A RANGE SURROUNDING THEIR EQUILIBRIUM POINT, WHILE LARGE PROTEIN MOLECULES ARE SHARPLY FOCUSED, FOR SUFFICIENTLY SMALL CONCENTRATIONS.

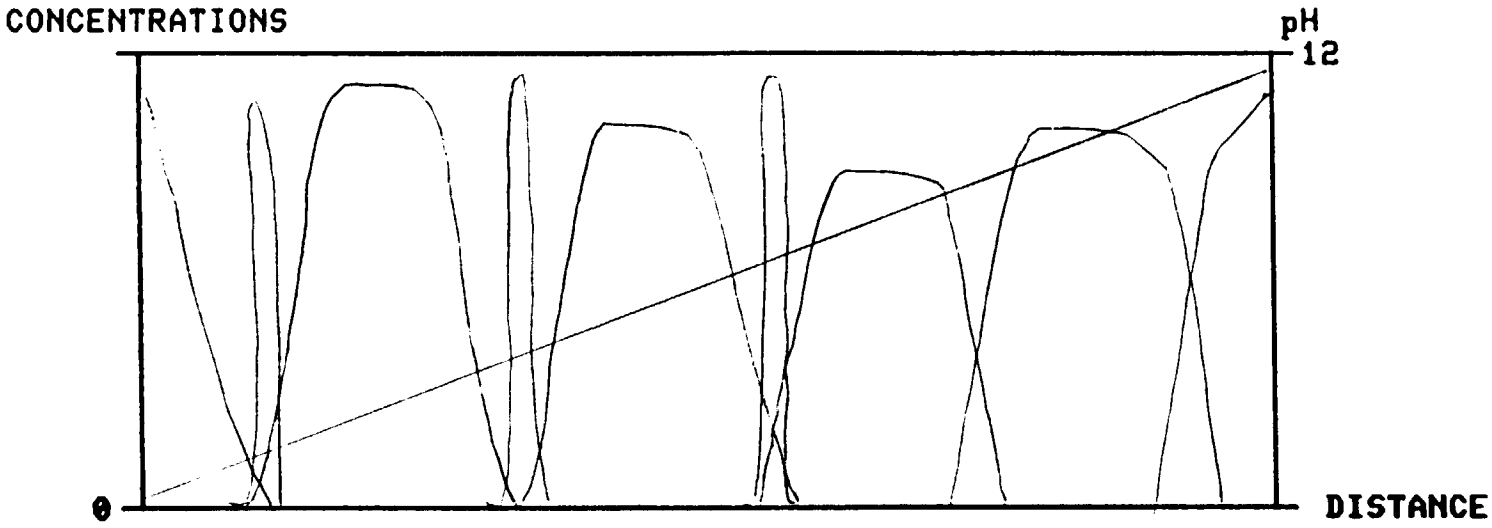

7-JUL-88 19:16

ORGANIZATION: RAI	MARSHALL SPACE FLIGHT CENTER ELECTROPHORESIS PERFORMANCE THE SAMPLE CODE	NAME: GLYN ROBERTS
CHART NO.: 7		DATE: JUNE 30, 1988

CODE SUMMARY

N TWO-DIMENSIONAL RADICAL CONCENTRATION DISTRIBUTIONS ARE EVOLVED IN TIME, OR IN DISTANCE DOWN A CFE CHAMBER.

THE RADICALS MAY BE SODIUM, SULFATE, ACETATE, AMMONIUM, BARBITURATE HISTIDINE, OR HEMOGLOBIN, FOR EXAMPLES.

THERE ARE SIX STAGES FOR EACH INCREMENT OF TIME OR DISTANCE:
- GET THE pH DISTRIBUTION FROM THE LOCAL IONIZATION EQUILIBRIUM;
- GET THE CORRESPONDING MEAN AND MEAN SQUARE DEGREES OF IONIZATION;
- GET THE CORRESPONDING CONDUCTIVITY DISTRIBUTION;
- SOLVE FOR THE ELECTRIC FIELD AND CURRENT DISTRIBUTIONS;
- GET THE FLUXES IN EACH DIRECTION FOR EACH SEPARATE RADICAL;
- UPDATE THE RADICAL CONCENTRATION DISTRIBUTIONS BY APPLYING AN IMPLICIT METHOD TO THE FLUX DIVERGENCES.

ONE-DIMENSIONAL CASES CAN BE DONE AS AN OPTION.

APPLICATIONS INCLUDE:
- STEADY THREE-DIMENSIONAL CFE SOLUTIONS;
- STEADY THREE-DIMENSIONAL MOVING-WALL CFE SOLUTIONS;
- STEADY TWO-DIMENSIONAL MOVING-WALL CFE SOLUTIONS;
- TIME-DEPENDENT TWO-DIMENSIONAL ACETATE FILM EXPERIMENTS;
- TIME-DEPENDENT ONE-DIMENSIONAL ACETATE FILM EXPERIMENTS;
- TIME-DEPENDENT ONE-DIMENSIONAL ISOTACHOPHORESIS;
- TIME-DEPENDENT ONE-DIMENSIONAL MOVING BOUNDARY ELECTROPHORESIS;
- STEADY OR TIME-DEPENDENT ONE-DIMENSIONAL ISOELECTRIC FOCUSING.

7-JUL-88 19:32

ORGANIZATION: RAI	MARSHALL SPACE FLIGHT CENTER ELECTROPHORESIS PERFORMANCE THE SAMPLE CODE	NAME: GLYN ROBERTS
CHART NO.: 8		DATE: JUNE 30, 1988

IONIZATION MODEL

ALL SALTS ARE FULLY IONIZED.

RADICALS IN AQUEOUS SOLUTION HAVE A DEGREE OF IONIZATION DEPENDING ONLY ON THE HYDROGEN ION CONCENTRATION:

$$H = 10^{-pH}.$$

THERE ARE AT PRESENT FOUR IONIZATION MODELS AVAILABLE:

1. STRONG ACIDS AND BASES ARE ASSUMED TO BE FULLY IONIZED, TO AN IMPOSED DEGREE.

2. WEAK ACIDS, WEAK BASES, AND AMPHOLYTES HAVE CONCENTRATIONS OF EACH DEGREE OF IONIZATION IN THE RATIOS

$$\ldots : A^{--} : A^{-} : A : A^{+} : A^{++} : \ldots$$

$$= \ldots : \frac{K_1 K_2}{H^2} : \frac{K_1}{H} : 1 : \frac{H}{C_1} : \frac{H^2}{C_1 C_2} : \ldots$$

$$= \ldots : a_{-2}H^{-2} : a_{-1}H^{-1} : 1 : a_1 H^1 : a_2 H^2 : \ldots$$

WHERE THE CONSTANTS C AND K ARE GIVEN, FROM MEASUREMENTS. FOR A MONOVALENT WEAK ACID THERE IS ONLY ONE CONSTANT, K_1.

THEN $m = \Sigma j a_j H^j / \Sigma a_j H^j$, $M = \Sigma j^2 a_j H^j / \Sigma a_j H^j$.

7-JUL-88 19:33

ORGANIZATION: RAI	MARSHALL SPACE FLIGHT CENTER ELECTROPHORESIS PERFORMANCE THE SAMPLE CODE	NAME: GLYN ROBERTS
CHART NO.: 9		DATE: JUNE 30, 1988

IONIZATION MODEL (continued)

3. WEAK ACIDS, WEAK BASES, AND AMPHOLYTES WITH EACH IONIZATION INDEPENDENT OF THE OTHERS HAVE

$$m = \sum H/(C_J+H) - \sum K_J/(K_J+H) \quad ,$$

4. COMPLEX PROTEINS CAN IONIZE UP 30 OR MORE TIMES. WE THEREFORE USE ANALYTIC FORMULATIONS FOR m AND M :

$$m = a_0 - \sum_1^N a_i \ln\left[\frac{H + t_i}{H + b_i}\right] / \ln(t_i/b_i) \quad ,$$

WITH $N = 1$, m DECREASES SMOOTHLY FROM a_0 TO $a_0 - a_1$ AS pH INCREASES FROM $-\log(t_1)$ TO $-\log(b_1)$.

IN PRACTICE WE USE $N = 4$, AND GET THE 13 COEFFICIENTS BY A LEAST SQUARES FIT TO MEASURED MEAN IONIZATION DATA.

WITH 19 DATA POINTS FOR ONE HEMOGLOBIN TYPE, THIS GIVES A ROOT MEAN SQUARE ERROR OF LESS THAN 0.10.

THE MEAN SQUARE DEGREE OF IONIZATION M, FOR ALL FOUR MODELS, IS

$$M = m^2 + H\, dm/dH \quad .$$

7-JUL-88 19:33

ORGANIZATION: RAI	MARSHALL SPACE FLIGHT CENTER ELECTROPHORESIS PERFORMANCE THE SAMPLE CODE	NAME: GLYN ROBERTS
CHART NO.: 10		DATE: JUNE 30, 1988

IONIZATION MODEL (continued)
MEAN IONIZATION AT VARYING pH

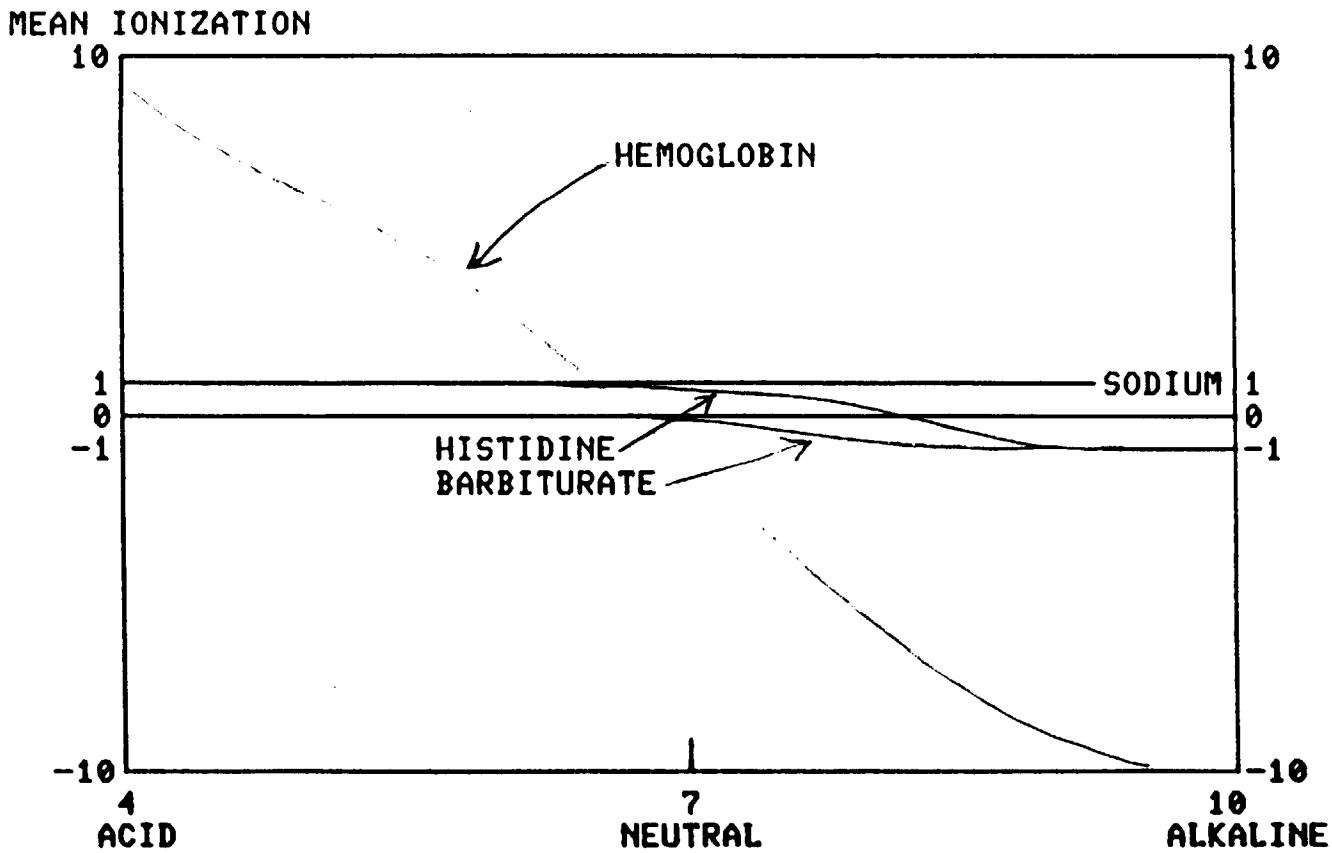

ORGANIZATION: RAI	MARSHALL SPACE FLIGHT CENTER ELECTROPHORESIS PERFORMANCE THE SAMPLE CODE	NAME: GLYN ROBERTS
CHART NO.: 11		DATE: JUNE 30, 1988

pH DISTRIBUTION FROM CHARGE NEUTRALITY

THE CHARGE DENSITY IS NEGLIGIBLE COMPARED WITH ITS COMPONENTS. HENCE

$$\sum_{1}^{N} c_i m_i(H) + H - K_w/H = 0$$

WHERE K_w IS THE IONIZATION CONSTANT FOR WATER, 10^{-14}.

THIS EQUATION DETERMINES H, AS A FUNCTION OF THE LOCAL CONCENTRATIONS c_i.

THE SOLUTION IS UNIQUE, SINCE EVERY TERM IS MONOTONIC.

THE CODE USES NEWTON'S ITERATION, WHICH REQUIRES dm/dH.

ONE ITERATION IS ALWAYS SUFFICIENT EXCEPT AT THE FIRST STEP.

7-JUL-88 19:34

ORGANIZATION: RAI	MARSHALL SPACE FLIGHT CENTER ELECTROPHORESIS PERFORMANCE THE SAMPLE CODE	NAME: GLYN ROBERTS
CHART NO.: 12		DATE: JUNE 30, 1988

ION MOTION AND FLUX AND THE SPECIES CONCENTRATION

ASSUME THAT EACH ION MOVES INDEPENDENTLY THROUGH THE FLUID WITH VELOCITY

$$\underline{E} n U \ ,$$

WHERE n IS THE DEGREE OF IONIZATION,
U IS THE MOBILITY PER UNIT IONIZATION (ASSUMED CONSTANT),
$\underline{E}$ IS THE ELECTRIC FIELD VECTOR.

FROM CONSERVATION, THE CONCENTRATIONS (mmole/cc) OBEY

$$\dot{c}_i = - \nabla \cdot \underline{F}_i \ ,$$

WHERE THE VECTOR FLUX OF RADICAL i IS OBTAINED BY SUMMING OVER THE DEGREES OF IONIZATION AS

$$\underline{F}_i = c_i (\underline{u}_f + \underline{E} m_i U_i) - D_i \nabla c_i \ .$$

HERE $\underline{u}_f$ IS THE FLUID VELOCITY, VARIES WITH THE APPLICATION, AND IS AT PRESENT ZERO EXCEPT FOR CFE,
D_i IS THE EINSTEIN DIFFUSIVITY

$$U_i RT/F \ ,$$

R IS THE GAS CONSTANT (joules/deg/mmole) ,
F IS THE FARAD (cbs/mmole) .

7-JUL-88 19:34

ORGANIZATION: RAI	MARSHALL SPACE FLIGHT CENTER ELECTROPHORESIS PERFORMANCE THE SAMPLE CODE	NAME: GLYN ROBERTS
CHART NO.: 13		DATE: JUNE 30, 1988

ELECTRIC FIELD AND CURRENT DISTRIBUTIONS

WE IMPOSE EITHER THE MEAN ELECTRIC FIELD OR THE MEAN CURRENT DENSITY.

THE ELECTRIC FIELD HAS ZERO CURL, AND IS MINUS THE GRADIENT OF THE POTENTIAL. THE CURRENT VECTOR HAS ZERO DIVERGENCE AND IS THE CURL OF THE CURRENT FUNCTION.

THESE TWO EQUATIONS LEAD TO POISSON-LIKE EQUATIONS FOR EITHER THE POTENTIAL OR THE CURRENT FUNCTION.

EITHER EQUATION IS SOLVED USING FINITE DIFFERENCES AND AN ALTERNATING DIRECTION IMPLICIT (ADI) ITERATIVE METHOD.

THE CURRENT VECTOR IS OBTAINED BY SUMMING OVER IONS AND SPECIES AS

$$\underline{\perp} = \sigma \underline{E} - \nabla P ,$$

WHERE THE CONDUCTIVITY AND ION DIFFUSION CURRENT POTENTIAL ARE

$$\sigma = F \left(\sum c_i M_i U_i + H U_H + K_w U_{OH}/H \right) .$$
$$P = RT \left(\sum c_i m_i U_i + H U_H - K_w U_{OH}/H \right) .$$

THERE IS NO CURRENT CONTRIBUTION FROM THE FLUID VELOCITY, BECAUSE THE CHARGE DENSITY IS ZERO.

P IS ZERO IF THE MOBILITIES ARE ALL EQUAL, FROM CHARGE NEUTRALITY.

7-JUL-88 19:34

ORGANIZATION: RAI	MARSHALL SPACE FLIGHT CENTER ELECTROPHORESIS PERFORMANCE THE SAMPLE CODE	NAME: GLYN ROBERTS
CHART NO.: 14		DATE: JUNE 30, 1988

DEBYE-HUCKEL-ONSAGER MODEL FOR RETARDED ION MOTION

EACH ION HAS AN ATMOSPHERE OF MEAN CHARGE WITH THE OPPOSITE SIGN.
FROM BOLTZMAN'S EQUATIONS, THE RADIUS VARIES WITH THE SQUARE ROOT
OF THE CONCENTRATION.

THE ION MOTION IS RETARDED BY TWO EFFECTS:

FIRST, THE FLUID AT THE ION IS MOVING IN THE OPPOSITE
DIRECTION BECAUSE OF THE FORCE ON THE CHARGED CLOUD.

SECONDLY, THE CLOUD ITSELF IS DISPLACED BY THE FIELD.
THIS REDUCES THE FIELD AT THE ION.

THESE EFFECTS CHANGE THE ION VELOCITY THROUGH THE FLUID TO

$$(1-B)n\underline{E}U \ ,$$

WHERE 1-B IS THE ACTIVITY.
APPROXIMATE ANALYTIC FORMULATIONS ARE BEING DEVELOPED FOR B,
OF ORDER THE SQUARE ROOT OF THE CONCENTRATIONS.
THEY WILL BE TESTED AGAINST MEASUREMENTS.

7-JUL-88 19:35

ORGANIZATION: RAI	MARSHALL SPACE FLIGHT CENTER ELECTROPHORESIS PERFORMANCE THE SAMPLE CODE	NAME: GLYN ROBERTS
CHART NO.: 15		DATE: JUNE 30, 1988

APPLICATION TO CONTINUOUS FLOW ELECTROPHORESIS

TAKE THE x AXIS ALONG THE CHAMBER.
TAKE THE y AXIS ACROSS THE CHAMBER.
TAKE THE z AXIS IN THE FIELD DIRECTION.

THEN

$$\underline{u}_f = (3U(1-y^2/Y^2)/2 , 0 , E_z U_w (3y^2/Y^2 - 1)/2) ,$$

WHERE U IS THE MEAN FLOW,
$2Y$ IS THE CHAMBER THICKNESS,
y IS MEASURED FROM THE MID-PLANE,
$E_z U_w$ IS THE CONSTANT ELECTRO-OSMOSIS WALL SLIP VELOCITY.

THE RADICAL CONCENTRATION EQUATION BECOMES

$$u(y)\dot{c}_i = - \nabla . \underline{E}_i ,$$

WHERE THE VECTOR FLUX OF RADICAL i IS NOW ONLY TWO-DIMENSIONAL,
THE NEW TIME VARIABLE IS THE RESIDENCE TIME $t = x/U$,
AND

$$u = 3(1 - y^2/Y^2)/2 .$$

7-JUL-88 19:35

ORGANIZATION: RAI	MARSHALL SPACE FLIGHT CENTER ELECTROPHORESIS PERFORMANCE THE SAMPLE CODE	NAME: GLYN ROBERTS
CHART NO.: 16		DATE: JUNE 30, 1988

OTHER APPLICATIONS

- MOVING-WALL CFE
  - WALL SPEED $E_z U_w$ IS STILL IMPOSED; IT MAY BE ZERO.
  - $u = 1 + (U_b - 1)(3y^2/Y^2 - 1)/2$
  - U_b IS THE RATIO OF THE WALL SPEED TO THE MEAN

- TIME-DEPENDENT ONE- AND TWO-DIMENSIONAL CASES
  - THE FLUID FLOW IS ZERO. USE $U_b = 1$ TO TIME STEP.
  - THE BOUNDARY AND INITIAL CONDITIONS DIFFERENTIATE THE CASES

7-JUL-88 19:35

ORGANIZATION: RAI	MARSHALL SPACE FLIGHT CENTER ELECTROPHORESIS PERFORMANCE THE SAMPLE CODE	NAME: GLYN ROBERTS
CHART NO.: 17		DATE: JUNE 30, 1988

INITIAL CONDITIONS

TWO SETS OF INITIAL CONCENTRATIONS ARE SPECIFIED, FOR THE BUFFER AND SAMPLE RESPECTIVELY.

THE SAMPLE IS CIRCULAR, CENTERED AT $(y_s,0)$, WITH RADIUS r_s .
THE CONCENTRATION DISCONTINUITY IS SMOOTHED USING p_s .

THESE CONDITIONS ARE SUFFICIENTLY GENERAL FOR ALL APPLICATIONS SO FAR.

FOR ISOELECTRIC FOCUSING THE FINAL STEADY STATE IS INDEPENDENT OF THE INITIAL DISTRIBUTION

FOR ISOTACHOPHORESIS AND MOVING-BOUNDARY ELECTROPHORESIS THERE IS NO SAMPLE, THERE ARE TWO BUFFERS WITH A PLANE INTERFACE. THE CODE USES THE z-DOMAIN $[0 , 2r_s]$. THE LEFT BUFFER IS THE SAMPLE.

7-JUL-88 19:35

ORGANIZATION: RAI	MARSHALL SPACE FLIGHT CENTER	NAME: GLYN ROBERTS
VUGRAPH NO.: 18	ELECTROPHORESIS PERFORMANCE THE SAMPLE CODE	DATE: JUNE 30, 1988

COMPUTATIONAL DOMAIN

FOR THE ONE-DIMENSIONAL CASES, THE y-DOMAIN IS ARTIFICIAL.
WE MAKE Y VERY SMALL, AND USE ONE INTERIOR MESH POINT.

EXCEPT FOR ISOELECTRIC FOCUSING, THE z-DOMAIN IS EFFECTIVELY INFINITE.

THE BOUNDARIES OF OUR COMPUTATIONAL DOMAIN CAN BE FIXED AT THEIR
IMPOSED INITIAL VALUES, OR THEY CAN MOVE WITH IMPOSED CONSTANT VELOCITIES.
THIS GIVES OPTIMAL RESOLUTION OF THE EVOLVING SAMPLE SHAPE.

THIS IS ILLUSTRATED IN THE NEXT VIEWGRAPH.

7-JUL-88 19:36

ORGANIZATION: RAI	MARSHALL SPACE FLIGHT CENTER	NAME: GLYN ROBERTS
CHART NO.: 19	ELECTROPHORESIS PERFORMANCE THE SAMPLE CODE	DATE: JUNE 30, 1988

COMPUTATIONAL DOMAIN (continued)

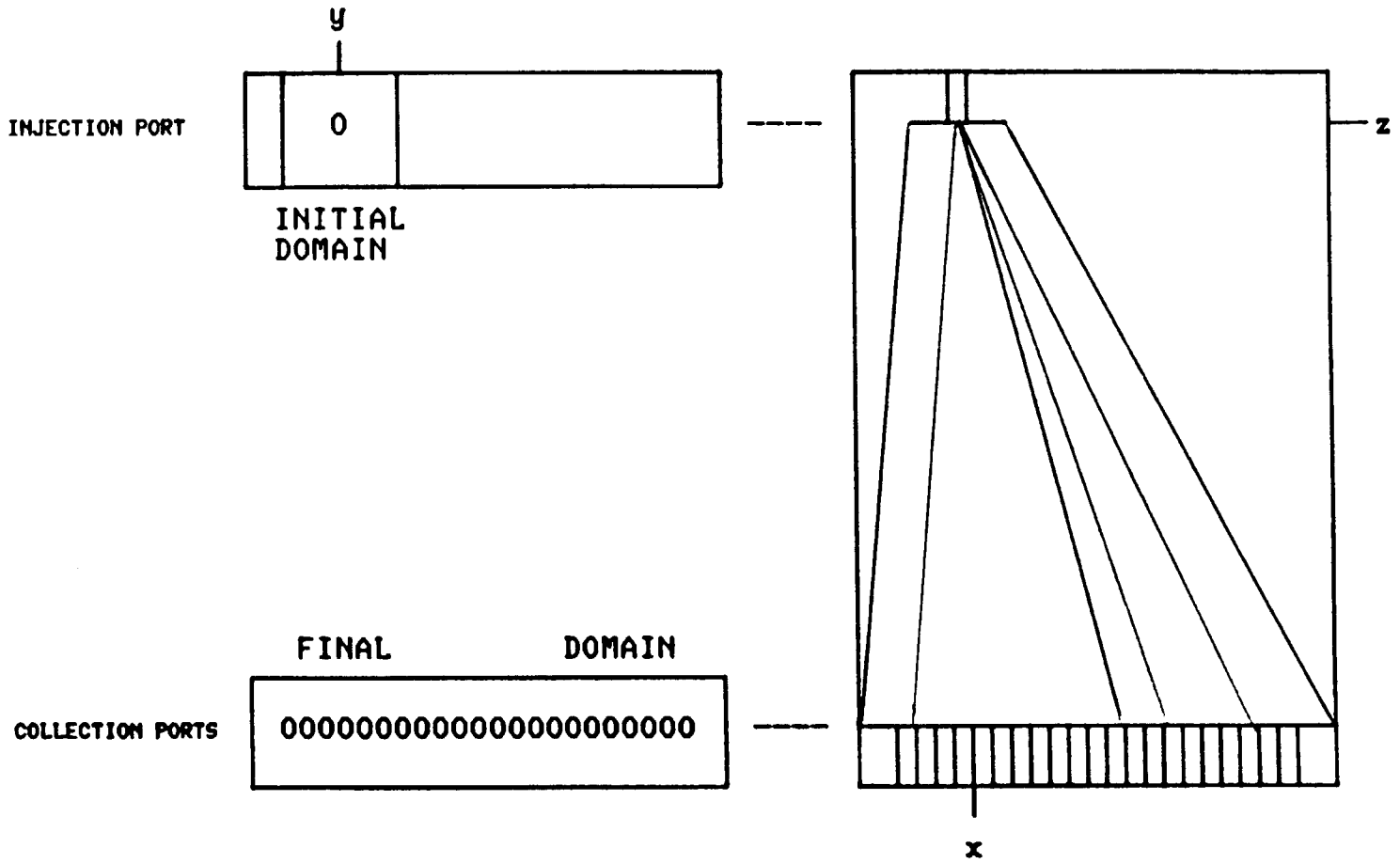

7-JUL-88 19:36

ORGANIZATION: RAI	MARSHALL SPACE FLIGHT CENTER ELECTROPHORESIS PERFORMANCE THE SAMPLE CODE	NAME: GLYN ROBERTS
CHART NO.: 20		DATE: JUNE 30, 1988

BOUNDARY CONDITIONS

- y BOUNDARIES: ZERO FLUX OF EVERY RADICAL
- ISOELECTRIC FOCUSING
  NO FLUX AT EITHER z BOUNDARY
- ALL OTHER CASES
  CONCENTRATIONS IMPOSED WHEN MEAN ION MOTION IS INTO THE DOMAIN
  ZERO DERIVATIVE (PASSIVE) WHEN MEAN ION MOTION IS OUT OF THE DOMAIN

7-JUL-88 19:36

ORGANIZATION: RAI	MARSHALL SPACE FLIGHT CENTER	NAME: GLYN ROBERTS
CHART NO.: 21	ELECTROPHORESIS PERFORMANCE THE SAMPLE CODE	DATE: JUNE 30, 1988

OUTPUT OPTIONS

- NUMERICAL DIAGNOSTICS
- GRAPHICS OUTPUT
  - PRINTER
  - TEKTRONIX (1D AND 2D)
  - (MOVIES)
- GRAPHICS PLOTS ARE AVAILABLE FOR THE FOLLOWING VARIABLES
  - GENERAL VARIABLES
    - pH = - log(H)
    - CONDUCTIVITY (MHO/CM)
    - DISTURBANCE VOLTAGE
    - CURRENT LINES (AMPS/CM)
    - ELECTRIC FIELD (VOLTS/CM)
    - TRANSVERSE ELECTRIC FIELD (VOLTS/CM)
    - DIFFUSION CURRENT POTENTIAL (AMPS/CM)
  - FOR EACH RADICAL TYPE
    - MOLAR CONCENTRATION
    - MEAN IONISATION
    - MEAN SQUARE IONISATION
    - CHARGE MOLARITY
    - CONDUCTIVITY (MHO/CM)
    - CONCENTRATION CHANGE
    - VELOCITY FUNCTION (CM/SEC)

7-AUG-88 19:36